EFFECT OF NITRIDING AND THERMO-HYDROGEN PROCESSING ON THE FATIGUE BEHAVIOR OF WROUGHT TI-6AL-4V ALLOYS

A THESIS SUBMITTED TO
THE GRADUATE SCHOOL OF NATURAL AND APPLIED SCIENCES
OF
MIDDLE EAST TECHNICAL UNIVERSITY

BY

ELİF AYBÜKE ÖZTÜRK

IN PARTIAL FULFILLMENT OF THE REQUIREMENTS
FOR
THE DEGREE OF MASTER OF SCIENCE
IN
METALLURGICAL AND MATERIALS ENGINEERING

JANUARY 2024

Approval of the thesis:

EFFECT OF NITRIDING AND THERMO-HYDROGEN PROCESSING ON THE FATIGUE BEHAVIOR OF WROUGHT TI-6AL-4V ALLOYS

submitted by **ELİF AYBÜKE ÖZTÜRK** in partial fulfillment of the requirements for the degree of **Master of Science** i**n Metallurgical and Materials Engineering, Middle East Technical University** by,

Prof. Dr. Halil Kalıpçılar
Dean, Graduate School of **Natural and Applied Sciences** _____

Prof. Dr. Ali Kalkanlı
Head of the Department, **Met. and Mat. Eng.** _____

Prof. Dr. Arcan Fehmi Dericioğlu
Supervisor, **Met. and Mat. Eng., METU** _____

Prof. Dr. Ziya Esen
Co-Supervisor, **Mechanical Eng., Çankaya University** _____

Examining Committee Members:

Prof. Dr. C. Hakan Gür
Metallurgical and Materials Eng, METU _____

Prof. Dr. Arcan Fehmi Dericioğlu
Metallurgical and Materials Eng, METU _____

Assist. Prof. Dr. Eda Aydoğan Güngör
Metallurgical and Materials Eng, METU _____

Assist. Prof. Dr. Irmak Sargın
Metallurgical and Materials Eng, METU _____

Assist. Prof. Dr. Mehmet Okan Görtan
Mechanical Eng., Hacettepe University _____

Date: 26.01.2024

I hereby declare that all information in this document has been obtained and presented in accordance with academic rules and ethical conduct. I also declare that, as required by these rules and conduct, I have fully cited and referenced all material and results that are not original to this work.

Name Last name : Öztürk, Elif Aybüke

Signature :

ABSTRACT

EFFECT OF NITRIDING AND THERMO-HYDROGEN PROCESSING ON THE FATIGUE BEHAVIOR OF WROUGHT TI-6AL-4V ALLOYS

Öztürk, Elif Aybüke
Master of Science, Metallurgical and Materials Engineering
Supervisor : Prof. Dr. Arcan Fehmi Dericioğlu
Co-Supervisor: Prof. Dr. Ziya Esen

January 2024, 105 pages

The Ti-6Al-4V alloys have become the preferred materials in the aerospace industry for load-bearing mechanical parts owing to their high mechanical strength, low density, fatigue resistance, and corrosion resilience. Even without specific processing, these alloys inherently possess high fatigue strength. Nonetheless, secondary heat and surface treatments, particularly in critical aerospace applications, are applied to enhance their fatigue resistance. This study employed a 2-step thermal-hydrogenation process (THP) and a gas nitriding process on specimens to augment fatigue resistance by introducing a refined microstructure and increasing surface hardness, respectively. In addition, to enhance fatigue resistance simultaneous intention of increasing surface hardness and delaying crack formation by inducing residual compressive stresses on the surface through concurrent nitriding was aimed. While the nitrided samples exhibited the highest hardness values, they also displayed the coarsest microstructure and the lowest fatigue resistance due to the elevated heat treatment temperature. On the other hand, the 2-step THP treatment refined the microstructure of the samples and marginally increased hardness and tensile strength. However, ductility decreased in THP-treated samples due to oxidation compared to other specimens.

Applied processes also resulted in grain coarsening when applied separately. However, the consecutive application of nitriding and THP processes did not notably alter the ductility compared to the untreated specimen, albeit tensile strength decreased compared to untreated specimen. The 2-step THP process applied after the nitriding process increased the material's ultimate tensile strength (UTS) value compared to that of the only nitrided samples. However, notable differences in fatigue resistance and ductility were not observed after the consecutive application of these two processes. Mechanical tests indicated that thermally treated and surface-treated specimens exhibited tensile and yield strength and ductility values that meet the ASTM standards. However, their fatigue strengths decreased due to grain coarsening in the microstructure and oxidation occurring during the applied processes.

Keywords: Ti-6Al-4V Alloy, Gas Nitriding, Conventional Production, Thermo-hydrogen Processing, Fatigue

ÖZ

NİTRÜRLEME VE TERMO-HİDROJENLEME İŞLEMİNİN İŞLENMİŞ Tİ-6AL-4V ALAŞIMLARININ YORULMA DAVRANIŞI ÜZERİNDEKİ ETKİSİ

Öztürk, Elif Aybüke
Yüksek Lisans, Metalurji ve Malzeme Mühendisliği
Tez Yöneticisi: Prof. Dr. Arcan Fehmi Dericioğlu
Ortak Tez Yöneticisi: Prof. Dr. Ziya Esen

Ocak 2024, 105 sayfa

Ti-6Al-4V alaşımları, öncelikle yüksek mekanik mukavemeti ve düşük yoğunluğu, yorulma mukavemeti ve korozyon direnci nedeniyle havacılık endüstrisinde mekanik yük taşıyan parçalar için en çok tercih edilen malzemeler haline gelmiştir. Herhangi bir işleme tabi tutulmasa bile yorulma mukavemeti yüksek olan bu alaşımların yüzeylerine özellikle havacılık endüstrisindeki kritik uygulamalarda yorulma mukavemetini arttırmak amacıyla ikincil ısıl işlemler ve çeşitli yüzey işlemleri uygulanmaktadır. Bu çalışmada, numunelere gaz nitrürleme ve 2-aşamalı termal-hidrojenleme işlemi uygulanarak ince bir mikroyapı ve parça yüzey sertliği arttırılmış bir katman ile malzemede yorulma dayanımının arttırılması amaçlandı. Artan sertlikle birlikte eş zamanlı olarak nitrürlemenin yüzeyde yarattığı basınç gerilmesinin çatlak oluşumunun geciktirilmesi amaçlandı. Nitrürleme işlemi uygulanan numuneler en yüksek sertlik değerlerine sahip iken, yüksek ısı girdisi nedeniyle en kaba içyapı ve en düşük yorulma dayanımına sahip olduğu görülmüştür. 2-aşamalı THP işlemi ise numunelerde içyapıyı inceltmiş ve sertliği az da olsa arttırmıştır. THP uygulanan numunelerde süneklik diğer numunelere göre oksitlenme yüzünden düşmüş ancak çekme dayancı artış göstermiştir.

Aynı zamanda işlem sonucunda tane kabalaşması meydana gelmiştir. THP ve nitrürleme işlemlerin birbiri ardına uygulanması ise numunenin işlemsiz haline göre sünekliğinde neredeyse bir fark yaratmadı ancak çekme dayanımını işlemsiz numuneye göre düşürdü. Nitrürleme işleminden sonra uygulanan 2 aşamalı THP işlemi, malzemenin nihai çekme mukavemeti (UTS) değerini nitrürlenmiş numunelere göre arttırmıştır. Ancak bu işlem sonrasında yorulma ve süneklik değerlerinde kayda değer farklılıklar gözlenmemiştir. Yapılan mekanik testler sonucunda ısıl işlemli ve yüzey işlemli tüm numunelerin çekme, akma dayanımı ve süneklik değerlerinin ASTM standartlarının üzerinde bir değere sahip olduğu gözlemlenmiştir. Ancak yorulma dayanımları mikroyapıda meydana gelen tane kabalaşması ve işlem sırasında meydana gelen oksidasyon nedeniyle düşmüştür.

Anahtar Kelimeler: Ti-6Al-4V Alaşımı, Gaz Nitrürleme, Konvansiyonel Üretim, Termo-hidrojenleme İşlemi, Yorulma

To My beloved Family

ACKNOWLEDGMENTS

I would like to express my most excellent thanks to my supervisor, Prof. Dr. Arcan Dericioğlu, for his guidance, support, constructive feedback, endless tolerance, and patience from the beginning to the end of this thesis. I am grateful for his contributions to present this research as clearly as possible.

I would additionally like to express sincere gratitude to my remarkable co-supervisor, Prof. Dr. Ziya Esen, for his kind attitude, guidance, endless support, and belief in me. I thank him for being a mentor with his vast knowledge. I could not have written this thesis without his guidance and support.

I want to thank Assist. Prof. Dr. Mehmet Okan Görtan for his precious advice and contribution to my thesis and support.

This study was supported by TÜBİTAK (Project No. 221M812).

I sincerely extend my deepest appreciation to beloved Tunay Ayça Alkan for her neverending support, caring, valuable guidance, and lovely friendship. I would also like to thank Doğukan Narbay for his valuable support and friendship.

I would also like to sincerely thank Ceren Özdemirel and Serap Yılmaz, who contributed to every stage of my thesis for their valuable support, lovely friendship, and endless patience.

Merve Nur Doğu and Seren Özer also deserve special thanks for their endless support and lovely friendship.

I would like to express my special thanks to Ertuğrul Büyükhergül for his support, patience, and lovely friendship.

I owe my precious mom, dad, and beloved brother an outstanding debt for their support and unconditional love throughout this thesis and my life.

Finally, but most importantly, I would like to thank Emre Günay for everything. I am so grateful for his endless support, caring, and understanding during all my stressful days.

TABLE OF CONTENTS

LIST OF TABLES

TABLES

LIST OF FIGURES

FIGURES

LIST OF ABBREVIATIONS

ABBREVIATIONS

XRD	X-Ray Diffraction
SEM	Scanning Electron Microscopy
EDS	Energy-Dispersive X-Ray Spectroscopy
EBDS	Electron Backscatter Diffraction
THP	Thermo-hydrogen Processing
HCP	Hexagonal Closed Packed
BCC	Body Centered Cubic
CP-Ti	Commercially Pure Titanium
HIP	Hot Isostatic Press
SLM	Selective Laser Melting
EBM	Electron-beam additive manufacturing
ASTM	American Society for Testing and Materials
UTS	Ultimate Tensile Strength
CNC	Computer Numerical Control
ISO	International Organization for Standardization
BSD	Backscattered Electron Detector
EDAX	Energy Dispersive X-Ray Spectroscopy

CHAPTER 1

INTRODUCTION

1.1 Effect of Heat Treatments on the Fatigue Behaviour of Wrought Ti-6Al-4V Alloys

Studies have stated that 85 % of mechanical damage in modern machines depends on the surface properties and quality [1]. It is known that most of the damages mentioned are caused by fatigue. It has been shown by Lütjering at al. [2] that the onset of cracks that cause fatigue-related fracture usually begins on the surface and spreads. The reason why fatigue cracks start on the surface is the increase in stress due to the notch effect due to surface roughness and other defects. For this reason, reducing surface roughness positively affects fatigue strength [3]. However, it is known that creating compressive residual stresses in regions close to the part surface slows down crack initiation and propagation [4]. Another method that can improve fatigue strength is heat treatment of surfaces. This technique aims to increase the strength of the surface and subsurface region by impregnating different elements into the metallic matrix on the part surfaces and, thus, to slow down the formation and propagation of fatigue cracks [5]. As a result, heat treatment techniques come to the fore in terms of improving the fatigue strength of engineering parts, especially by improving the properties in the surface and subsurface regions. The mentioned methods aim to improve the fatigue performance of the parts under different conditions. It has been proven in recent years that the thermal-hydrogenation process, a thermal-chemical method, can refine the rough internal structure that may occur after additive manufacturing (EBM) and cast titanium alloys [6]. More studies on wrought alloys are needed. Hydrogen, which has a high solubility in titanium, is absorbed into titanium either pure or mixed with argon in a controlled manner at certain temperatures and then is removed under vacuum at controlled temperatures

of hydrogen is recovered. During this process, TiH_2 (titanium hydride) is formed by dissolving hydrogen in the structure, especially in the α phase, and α and TiH_2 phase layers are formed in the alpha phase. When the alloy is kept under vacuum, TiH_2 turns into the α phase again, and a fine grained microstructure can be obtained in the final stage. To enhance the fatigue resistance of the Ti-6Al-4V alloy and improve its microstructure, various surface treatments like applying a thin film or utilizing thermal-chemical processes can be implemented. Nitriding stands out as a thermal-chemical method, and the relatively easy-to-apply gas nitriding process is preferred in applications where fatigue resistance comes to the fore [7].

1.2 Structure of the Thesis

This thesis study, wrought Ti-6Al-4V alloys were examined with 2-step THP and surface coating by gas nitriding technique. The study was carried out by implementing a 2-step thermo-hydrogen process and creating a surface coating process using experiments. The characterization of specimens using Scanning Electron Microscopy (SEM), Electron Backscatter Diffraction (EBSD), Energy Dispersive X-ray Spectroscopy (EDS), and other techniques indicates a thorough investigation. The first part of Chapter 2 covers the literature review about titanium alloys, various post processes, thermo-hydrogen, and nitriding process phase structure. Chapter 2 includes brief information and essential properties of Ti-6Al-4V alloys. After that, heat treating, surface processes, critical process parameters, and their effect on the properties and quality of these alloys are discussed. At the end of the chapter, literature studies about similar studies are discussed. Chapter 3 covers the experimental procedure of heat treatment and surface process preparation and implementation of the Ti-6Al-4V specimens. The first part of Chapter 4 covers the microstructural and mechanical characterization of Ti-6Al-4V alloys. Later parts cover gas nitriding and thermo-hydrogen processes and the combination of these two processes. Finally, all of the results are discussed and compared with literature studies. The final chapter of the thesis summarizes the conclusions of this study.

CHAPTER 2

LITERATURE REVIEW

2.1 Titanium and Its Alloys

This thesis chapter will present the literature review to familiarize readers with Titanium and its alloys. Titanium and titanium alloys are rare engineering materials that combine features such as high specific strength, low density (4.5 gr/cm^3), and excellent corrosion and erosion resistance. Today, titanium and its alloys find extensive use across various industries, including surgery, aerospace, automotive, chemical plants, and more, owing to their unique properties. Titanium is available in various grades, with pure titanium being less robust than titanium alloys. The Ti-6Al-4V alloy, in particular, stands out as the most widely utilized, with credible machinability and outstanding mechanical characteristics [8].

2.2 Microstructure Properties of Titanium and Its Alloys

Titanium is capable of forming different crystal structures across a broad temperature range. The transformation from one crystal structure to another in a material is known as an allotropic transformation, and the specific temperature at which this change occurs is termed the "transition temperature." Titanium, a transition metal, exhibits allotropic behavior by presenting two distinct crystal structures at varying temperatures. Pure titanium experiences an allotropic phase transition from its stable form at room temperature, known as the hexagonal close-packed (hcp) α-phase, to a body-centered cubic (bcc) β-phase when the temperature exceeds 882 °C. Figure 2.1 shows the crystal structures and lattice parameters of the α and β phases are given.

In Figure 2.1, the hexagonal unit cell of α titanium is seen together with the lattice parameter (a = 0.295 nm) and the c parameter (c = 0.468 nm) at room temperature. Additionally, the right side of the figure, the crystal structure of the beta phase is shown with the lattice parameter (a = 0.332 nm) at 900 °C [9].

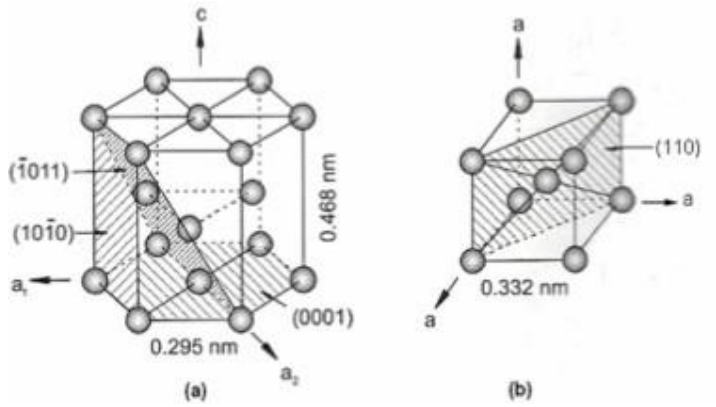

Figure 2.1 Crystal structures, and lattice parameters of α titanium b) β titanium [9].

The transition temperature from the α phase to the β phase for pure titanium is called the β transformation temperature. Among the commonly used titanium alloys containing α -Ti and β -Ti in its microstructure at room temperature is Ti-6Al-4V [9].

2.2.1 Pure Titanium

Commercially pure titanium, containing a percentage of 99.5 - 98.635 % titanium, is in a tightly ordered hexagonal structure, that is, in the α phase at room temperature, and transforms into the phase in the volume-centered cubic structure at 885 °C. However, there is a small temperature range where both phases coexist during this transformation [10]. The microstructure of pure titanium at room temperature consists entirely of the α phase. As the amount of other elements and especially iron increases, small but increasing amounts of β phase are present in the microstructure and grain boundaries.

Annealed unalloyed titanium microstructure can be equiaxed or acicular. The development of the needle-like α phase depends on the cooling applied during the conversion from the β phase to the α phase. As the cooling rate increases, the width of the acicular α plates decreases. Equiaxial α occurs in materials that have undergone recrystallization annealing. The presence of 100 % acicular α phase in the internal structure indicates that the material has been heated up to above the β transformation temperature. Figure 2.2 shows images of the equiaxial and acicular microstructure [9].

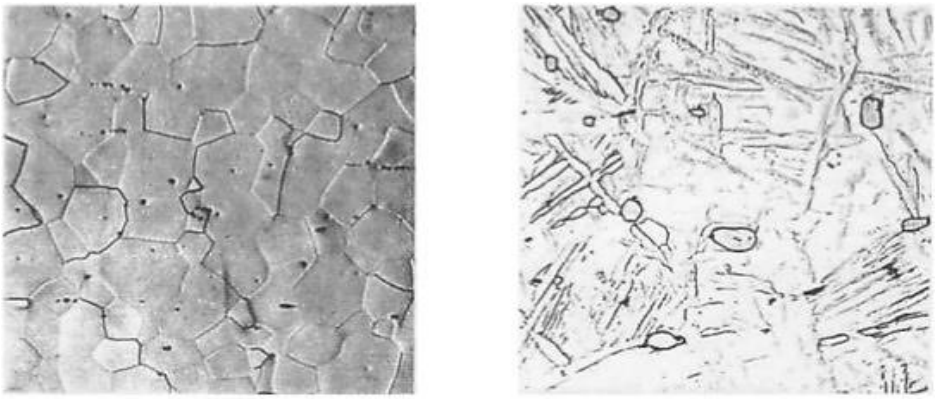

Figure 2.2 Example of equiaxial (a) and acicular (b) microstructure [9].

The most common equiaxial and acicular structure in the microstructure of titanium and its alloys has different characteristics from each other. For example, alloys with equiaxial grain structure; they show high ductility and strength, high forming ability and crack resistance, high resistance to stress corrosion in hot salt baths. Alloys with needle grain structure; It exhibits excellent creep resistance, high fracture toughness, reduced crack formation tendency, excellent resistance to stress corrosion, but a small decrease in strength [11]. Regardless of the cooling rate in pure titanium, it is impossible to prevent the formation of the α phase. While transitioning from the β phase to the α phase, the chemical content does not change, but the crystal structure does. This formation brings along the martensitic transformation, which is a supersaturated structure.

The martensitic structure is an unstable and supersaturated α structure formed through a diffusion less transformation from the β phase called the martensitic α phase. An example of the microstructure of the martensitic α structure is presented in Figure 2.3 [12]. Although there are α phases transformed from the β phase in the microstructure of heat-treated titanium and its alloys, some phases remaining before the heat treatment also exist. These are called "primary α" (primary α). Later transformed α phases can be encountered in different structures. These are called knurled, acicular, plate, Widmanstatten, or martensite structures [13]. The most common microstructure transformed from the β phase during cooling is acicular α. In the β matrix, this structure nucleates in one plane or in many planes, forming α grains that grow. Acicular α formation (Widmanstatten) is seen through one plane in Figure 2.4 (a) and through many planes in Figure 2.4 (b) [14].

Figure 2.3 Martensitic α structure [10].

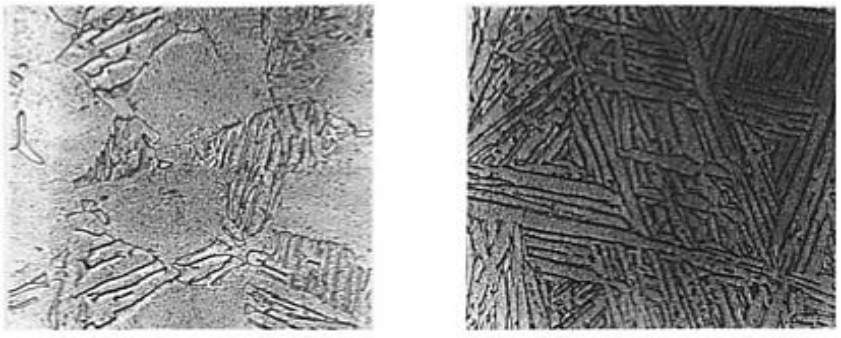

Figure 2.4 Widmanstatten structure formation (a) from a single plane (b) from many planes [15].

2.3 Types of Titanium Alloys According to Phase Structures

Titanium can be alloyed with several elements to improve its mechanical properties. These alloying elements are categorized as either α-Ti and β-Ti stabilizers, based on their impact on the resulting microstructure. The fact that titanium alloys show different properties from each other is mainly due to the properties of the α and β phases and the amount of volume in the structure. Furthermore, the mechanical and physical properties are influenced by the crystal structures of the respective phases [9]. The physical and mechanical properties of titanium alloys in different phases are given in Table 1. Oxygen, nitrogen, and carbon, which are intermediate elements, are the elements that stabilize the α phase. Aluminum is the most essential alloying element that stabilizes the α phase and increases the transformation temperature. α-Ti stabilizers such as nitrogen, aluminum, carbon, and oxygen increase the transition temperature. In contrast, beta-Ti stabilizers such as niobium, vanadium, molybdenum, and tantalum have low solubility in the α phase and reduce the transformation temperature. Additionally, alloying elements like chromium and iron contribute to the formation of lower transition temperatures through eutectoid reactions, resulting in a biphasic microstructure at room temperature. Commercially, titanium and its alloys are commonly categorized as unalloyed titanium, α, α + β, β alloys. Moreover, titanium alloys can be classified into near α (super alpha) and metastable β alloys based on their dominant phase [9].

Table 1 Mechanical properties of some titanium alloys [16].

Alloy	T_β [°C]	Hardness [HV]	E [GPa]	YS [MPa]	TS [MPa]	% El
α Alloys						
high purity Ti	882	100	100-145	140	235	50
Grade 1	890	120		170-310	>240	24
Grade 4	950	260	100-120	480-655	>550	15
Near-α Alloys						
Ti-6-2-4-2-S	995	340	114	990	1010	13
TIMETAL 1100	1010		112	900-950	1010-1050	10-16
TIMETAL 834	1045	350	120	910	1030	6-12
α+β Alloys						
Ti-6-4	995	300-400	110-140	800-1100	900-1200	13-16
Ti-6-6-2	945	300-400	110-117	950-1050	1000-1100	10-19
Ti-6-2-2-2-2			110-120	1000-1200	1100-1300	8-15
Ti-6-2-4-6	940	330-400	114	1000-1100	1100-1200	13-16
Ti-17	890	400	112	1050	1100-1250	8-15
Metastable-β Alloys						
SP700	900	300-500	110	900	960	8-20
Beta III	760	250-450	83-103	800-1200	900-1300	8-20
Beta C	795	300-450	86-115	800-1200	900-1300	6-16
Ti-10-2-3	800	300-470	110	1000-1200	10001400	6-16
Ti-15-3	76	300-450	80-10	800-1000	800-1100	10-20

2.3.1 α Alloys

α titanium alloys typically comprise commercial grade titanium (CP-Ti) and alloys generally alloyed with α stabilizer and/or neutral elements. α alloys have high strength and oxidation resistance at temperatures ranging from 588 to 811 Kelvin, and superior weldability compared to other titanium grades [17]. Unlike $\alpha + \beta$ alloys and β alloys; Since α alloys have a stable α phase, they cannot be hardened by heat treatment. However, recrystallization annealing or just annealing can be done to eliminate the residual stresses after a cold work. α alloys have very low malleability and lower forging temperature tolerances than α + β alloys or beta alloys. The microstructure of alpha alloys differs depending on the cooling rate after annealing [18].

2.3.2 Near α Alloys

The addition of small quantities of β stabilizing elements results in the formation of these alloys from α titanium alloys. They have similar properties to α-phase titanium alloys. They combine both the outstanding creep characteristic of the α alloys and the high strength properties of α + β alloys. In addition, these alloys can also be used in environments with an operating temperature of 500 °C - 550 °C [9].

2.3.3 α + β Alloys

Among the titanium alloys, the most prevalent is the α + β alloys, which have higher strength and can be heat treated. However, their formability is lower than α alloys. After annealing, high ductility, homogeneity, and high strength are provided. In this process, the beta transformation temperature is increased just below in order to form small amounts of α grains and to prevent grain growth in the beta phase. Equiaxial grains with slow cooling; acicular grains are formed with rapid cooling [9]. The volume fraction of β contained in these alloys varies between 5 % and 40 % at room temperature. Ti-6Al-4V, the most extensively utilized titanium alloy, is included in this category. Over 50 % of the currently employed titanium alloys comprise this composition. These low-density materials maintain their strength and corrosion resistance properties up to high temperatures [9].

2.3.4 Beta (β) Alloys

These particular alloys consist of substantial quantities of β stabilizing elements. Compared with other titanium alloys, β alloys exhibit superiority in various aspects, such as their malleability, hardenability, and cold-forming properties. Basically, β alloys exhibit similar room temperature strength to α + β alloys, but their strength values at high temperature are lower than α + β alloys [14]. Beta alloys are unstable alloys and are hardened by precipitation of the α phase in the beta matrix.

They have high fracture toughness. Although they can be processed better than α + β alloys, they are inclined to heat treatment [19].

2.4 Ti-6Al-4V Alloys

The Ti-6Al-4V alloy is the most extensively utilized α + β alloy, finding applications across aircraft components, surgical implants, and pressure vessels. Exceptional characteristics of this alloy include high specific strength, corrosion resistance, low density, and exceptional high cycle fatigue strength. The alloy's properties are intricately tied to its microstructure, which can be finely adjusted through complex thermomechanical processes involving deformation, heat treatment, aging, recrystallization, and stress relief annealing. This manipulation allows for a diverse range of microstructures within α + β titanium alloys [9]. In the Ti-6Al-4V alloy, various microstructures such as lamellar, equiaxed, bimodal, martensite, and Widmanstätten can emerge. These structures are influenced by the arrangement and size of the α and β phases, which result from the cooling rate from the β phase region. These varied microstructures directly dictate the mechanical properties of the Ti-6Al-4V alloy. Figure 2.5 illustrates the microstructural transformations variations observed in an alpha-beta alloy like Ti-6Al-4V [9].

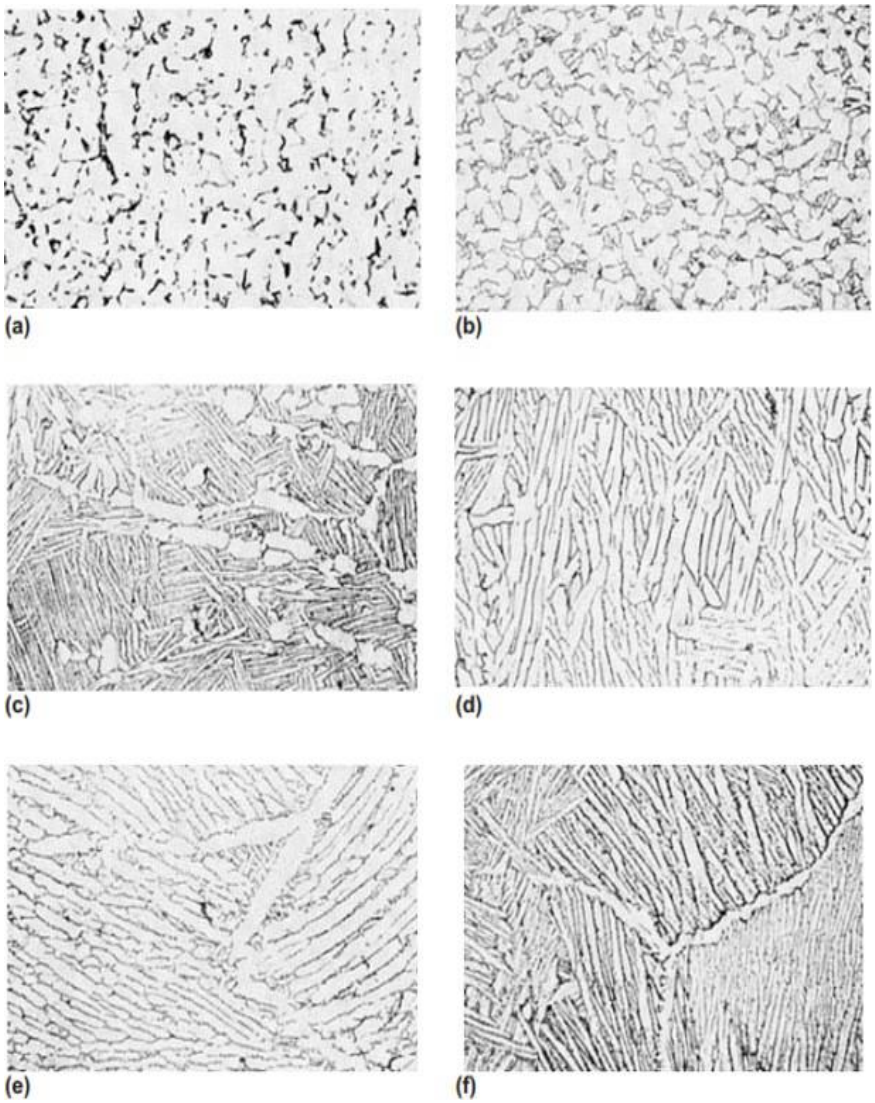

Figure 2.5 The microstructure of a Ti-6Al-4V alpha-beta titanium alloy under typical metallurgical conditions is depicted as follows: (a) Equiaxial α and a small amount of intergranular β, (b) Equiaxial and pointed α and a small amount of intergranular β, (c) Equiaxial α in an acicular α (transformed β) matrix. (d) A small amount of equaxial α in the acicular α (transformed β) matrix. (e) Plate-like acicular α (transformed β) (f) Blocky and plate-like spikes α (transformed β) [9].

2.5 Post Processes for Ti-6Al-4V Alloy Produced by Conventional Techniques

The heat treatments for titanium and its alloys serve distinct purposes. Firstly, stress relief aims to prevent residual stresses during production. Annealing optimizes parameters like ductility, dimensional stability, and machining suitability. Strengthening is achieved through solution and aging processes. Annealing, solution treatment, and aging primarily focus on altering the material's mechanical properties. Moreover, stress relief and annealing techniques can enhance resistance against corrosion, prevent warping, and prepare the material for shaping purposes [13]. Indeed, when heating pure titanium, it is crucial to prevent excessive absorption of oxygen, nitrogen, and hydrogen. Various treatments applied to titanium include cold or hot deformation, stress relief, and soft annealing. While stress relieving and annealing methods can be used for α and super α alloys, none of the processes aimed at increasing strength are effective in these specific alloys [12]. The heat treatment behaviors in α + β alloys vary based on the α and β phases density distribution. Mechanical and microstructural properties can be improved by heat treatments for α and β phases. While aging causes hardening in α + β alloys due to the breakdown of the unstable β phase, their hardening capability is less pronounced than that of β alloys because they possess a lower proportion of unstable β. However, solution and aging processes effectively enable the hardening of α+ β alloys [9]. Ti-6Al-4V alloy is the most widely used α + β alloy. The representative phase diagram of this alloy can be seen in Figure 2.6. According to this diagram, it can be seen that basically two main transformations are important. The first of these is the precipitation of the alpha phase in the beta phase by cooling the material raised above the β transformation temperature to the α + β region. Widmanstatten structure prevails under nearly all cooling rates. The secondary significant transformation occurs when martensite forms in the material cooled with water, originating from the β phase. This transformation is termed as β to α'.

The expression α' represents the highly ordered hexagonal α phase that is supersaturated. Martensite or Widmanstätten alloys are generally not utilized in engineering applications. However, in order to disrupt this structure of the material and distribute the β phase into the α phase uniformly, the α + β region of the phase diagram is examined. Subsequent to this process, annealing the material at 700 °C brings the microstructure to the desired state [20], [17].

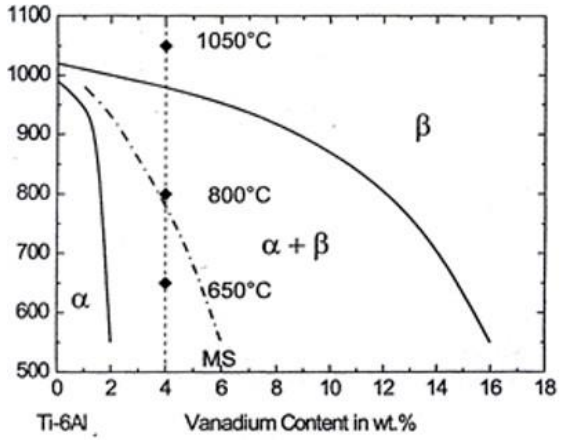

Figure 2.6 Representative binary phase diagram for Ti-6Al-4V [21].

Figure 2.7 shows the microstructure of the Ti-6Al-4V alloy under different cooling conditions. In the figure, lighter areas indicate the α phase and the dark areas indicate the β phase. Distinct heat treatment techniques are applied to enhance specific mechanical properties of titanium alloys, notably improving characteristics like notch strength, fracture toughness, and particularly reducing notch sensitivity. Processes in which titanium alloys are heated to the β phase are generally not used because of the complete transformation of the microstructure and rapid grain growth in the β phase. This situation adversely affects the mechanical properties of the material. Studies have shown that rapid heating of the alloy to the β phase produces better mechanical properties than an isothermal heating. The increase in heating rate, on the other hand, prevents grain growth in the β phase, causing the beginning of a fine-grained structure.

This is not only the result of the material reaching high temperatures in a short time, but also that chemically inhomogeneous regions play a barrier role in grain growth [22].

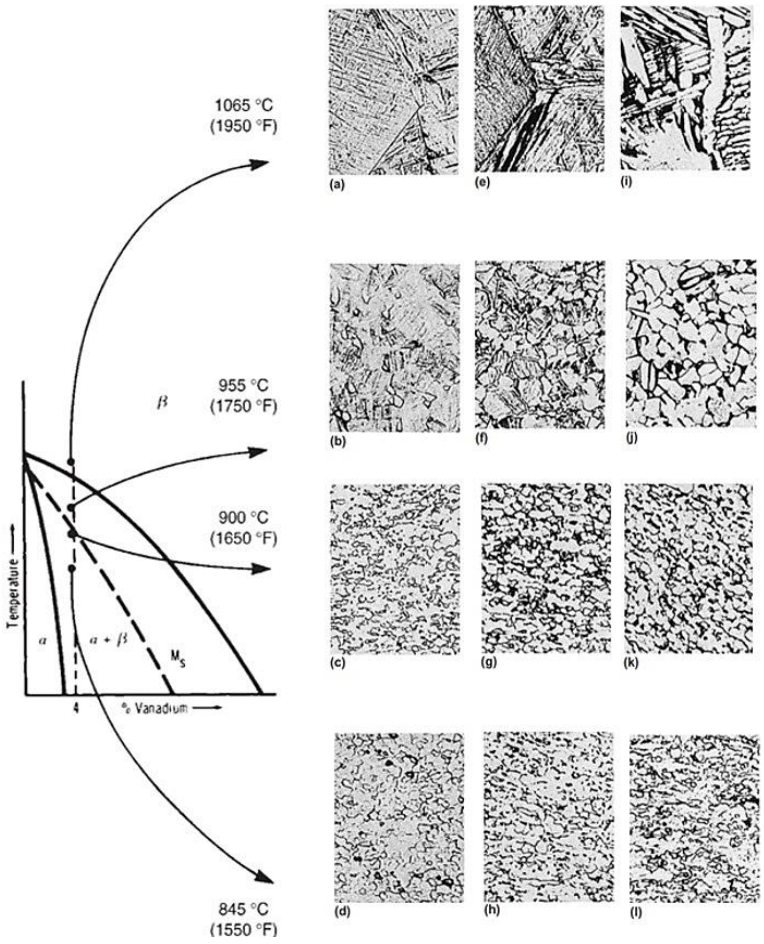

Figure 2.7 The influence of cooling rate on the microstructural formation in an alpha-beta alloy (Ti-6Al-4V) [23].

Research has indicated that rapid heating processes positively affect mechanical properties of all types of titanium alloys. Rapid heating of the β phase followed by air cooling has a positive effect on tensile strength of the titanium alloys. The reason for this is that after the process, the microstructure of the material is formed by completely transformed fine β grains.

Although it is known that rapid heating process is always positive for equiaxial structures, it has been understood that this process is not effective in alloys with coarse grain and lamellar microstructure formed after processes such as casting, welding and β annealing [23]. Various heat treatments are used for conventionally produced Ti-6Al-4V parts to refine their unstable microstructure in the literature. Hot Isostatic Press (HIP) and annealing are the most common heat treatments applied to parts [24]. Bilgin et al. introduced an innovative approach to heat treatment for Ti-6Al-4V fabricated via SLM. They employed a method known as thermo-hydrogen processing (THP), traditionally used for Ti-6Al-4V alloys produced via conventional techniques. Remarkably, Bilgin et al. successfully applied this heat treatment to additively produced Ti-6Al-4V alloys, notable advancement in the process [6].

2.5.1 Thermo-Hydrogen Process (THP)

Hydrogen has a crucial role as an alloying element in titanium alloys. Unlike other elements, hydrogen can be introduced into or removed from the material without melting. When added to the microstructure as an alloying element, hydrogen reduces the strength of titanium alloys at elevated temperatures while enhancing their ductility. It provides convenience in hot forming processes (forging, hot pressing, superplastic shaping, powder metallurgy). The temporary addition of hydrogen to the alloy positively affects the material's machinability and mechanical properties. For this reason, the heat treatment applied to titanium and its alloys is called the "Thermo-hydrogen process." Hydrogen is added to the titanium material in a controlled manner from the hydrogen environment at 500-600 °C and then it is recovered under vacuum with controlled annealing at 700-800 °C [25]. Thermal hydrogenation positively impacts the hardenability of titanium alloys by transforming their coarse-grained microstructure into a much finer-grained structure. For example, cast titanium alloys have a coarse-grained and layered microstructure. With the thermal hydrogenation process applied to this low-strength material, the microstructure is transformed into a equiaxial and fine-grained structure without

deformation and recrystallization. While the porous structure of the material is improved, the tensile and fatigue strength of the material also increases. Furthermore, it has been discovered that the thermal hydrogenation process enhances the hot-forming capability of titanium alloys. This process enables the attainment of the desired microstructure by reducing the hot forming temperature without decreasing the strength of titanium alloys. This observation broadly applies to α and α + β alloys. However, hydrogen addition does not improve the hot-forming capability of β alloys and even makes it difficult [26]. Hydrogen serves as an interstitial element that stabilizes the β phase in titanium alloys. As the concentration of hydrogen increases, the transition temperature to the β phase decreases, facilitating heat treatment at lower temperatures. Moreover, heightened hydrogen content expands the α+ β phase range, particularly beneficial for working with α titanium alloys. The addition of hydrogen to titanium alloys results in softening of the α phase while strengthening the β phase [27]. Studies have noted that the introduction of hydrogen decreases the cooling rate required to obtain martensite, thereby enhancing the hardenability of titanium alloys. Moreover, hydrogen content serves as a means to regulate phase components and their respective volumes in these alloys [28]. The thermo-hydrogen process primarily comprises two main stages: hydrogenation and dehydrogenation. Hydrogenation aims to increase the hydrogen content within the alloy, facilitating the formation of finer grains and new phases in the microstrucure. The introduction of hydrogen triggers alterations in the concentrations of other alloying elements within the pre-existing phases. Once the desired new microstructure is achieved, reducing the hydrogen content becomes essential to prevent hydrogen embrittlement. This process is referred to as dehydrogenation [29]. Given that hydrogen alloying in titanium alloys is a reversible process, dehydrogenation can be accomplished by subjecting the alloy to a high-temperature vacuum or inert gas environment. This dehydrogenation process ensures the preservation of the newly formed microstructure and results in enhanced mechanical properties of the alloy [30].

When the Ti-6Al-4V alloy is exposed to a specific temperature within a hydrogen atmosphere, hydrogen atoms commence diffusing until they reach a solubility limit at that temperature. Notably, solubility of the hydrogen in the Ti-6Al-4V alloy is significantly influenced by hydrogenation pressure. The alloy's equilibrium hydrogen content hinges on the hydrogenation temperature and the pressure within the hydrogen environment [31].

In the currently widely used thermo-hydrogen (THP) methods shown in Figure 2.8, hydrogen is absorbed into the Ti-6Al-4V alloy as a first step, usually at temperatures between 500-800 °C below the β transition temperature. In the subsequent step, heating is conducted above the β transition temperature to achieve the beta phase and dissolve all hydrogen within this phase. The method used to extract hydrogen from the alloy can vary based on the cooling process from the β phase region. difference between the techniques depicted in Figure 2. 8 (a) and (b) is the cooling regime from the β phase region.

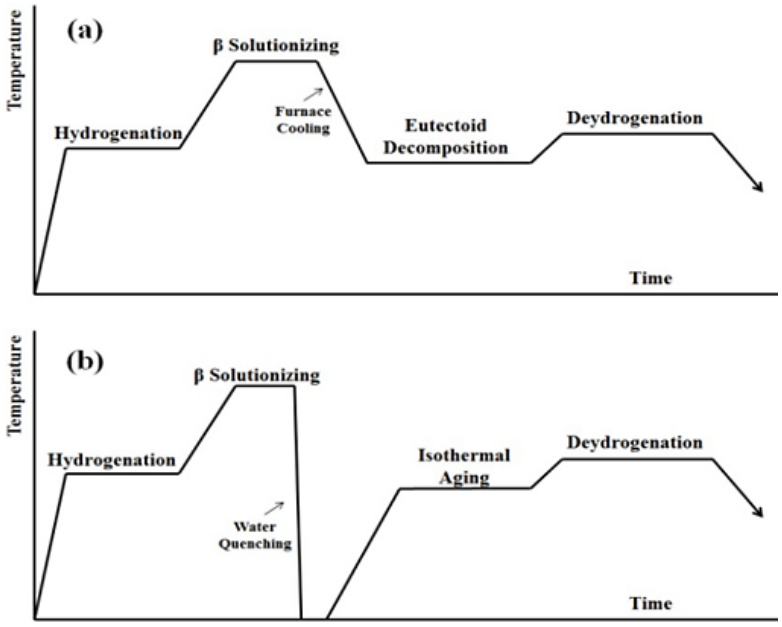

Figure 2.8 Thermally hydrogenated after (a) eutectoid decomposition, (b) martensitic de-composition [32].

In the thermal hydrogen treatment shown in Figure 2.8 (a), in addition to the β phase, the alloy is cooled slowly to the isothermal eutectoid decomposition temperature to obtain fine α and β precipitates in the primary β phase matrix. However, the second process shown in Figure 2.8 (b) involves quenching to convert the entire microstructure to both hcp (α') and orthorhombic (α") martensite prior to the aging step. In both methodologies, a final dehydrogenation phase is executed to diminish the hydrogen content in the alloy, enabling the hydride α phase transformation and subsequent refinement of the structure [9], [21]. Recently, Bilgin et al. introduced a 2-step thermal-hydrogenation treatment specifically designed for Ti-6Al-4V alloy fabricated via SLM. This treatment involved hydrogenation for 1 hour at 650 °C followed by dehydrogenation at 700 °C for 18 hours. To mitigate potential grain coarsening during the β-solution treatment and eutectoid decomposition stages, they adapted the 4-step THP approach. The modified method utilized a 2-step process (hydrogenation and dehydrogenation stages below the β -transus temperature), shown in Figure 2.9 was used as in the study. They found that, in addition to microstructural improvement, 2-step thermal-hydrogenation treatment prevented the formation of α-phase at the grain boundaries, which caused excessive grain growth and reduced tensile strength. In the study, hydrogenation was applied at different temperatures (550, 600, 650, 700, 750, 800, 850 °C) for the Ti-6Al-4V alloy produced by SLM technique and the maximum hydrogen solubility (1.19 % by weight) was 650 °C after 1 hour of treatment. It was observed that the solubility of hydrogen decreased above this temperature.

In the literature, UTS and ductility values for surface and non-surface treated Ti-6Al-4V alloys produced at different orientations have been presented as 811-1116 MPa and 2.1-17 %, respectively [33].

Table 2 Minimum tensile properties of wrought, cast and AM Ti-6Al-4V alloys [6].

Standard	**YS (MPa)**	**UTS (MPa)**	**Elongation (%)**	**Reduction in Area (%)**
ASTM F11108-14 (Cast)	758	860	8	14
ASTM F2924-14 (AM)	825	895	10	15
ASTM F136-13 (Wrought)	795	860	10	25

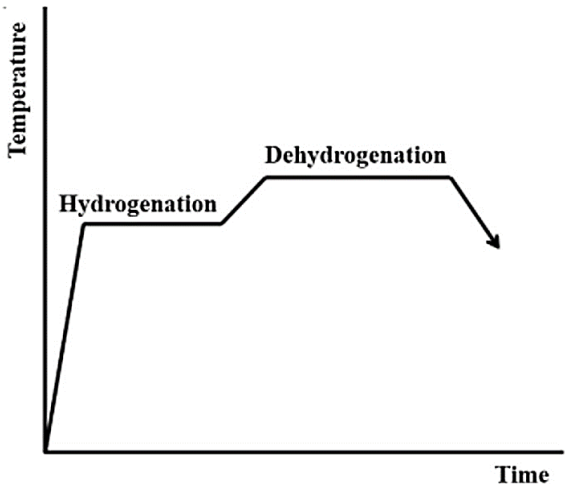

Figure 2.9 2-Step THP [34].

Bilgin et al. [6] applied thermos-hydrogenation treatment (THP) to Ti-6Al-4V alloys produced with SLM to increase ductility and improve microstructure. In conventionally applied 4-step THP, the mechanical properties (Table 3) have decreased despite the improved microstructure due to the accumulation of α phase at the grain boundaries during the β solution and eutectoid decomposition processes.

In addition, another disadvantage of 4-step THP method was found as the excessive growth of β grains during the β dissolution. It was found that 2-step modified THP performed below the α / β transition temperature increased ductility without reducing strength. A similar microstructure was observed in samples subjected to both 4 and 2-step THP. However, in the 2-step THP samples, grain growth and accumulation of the α phase were absent at the grain boundaries. While the initial hydrogen absorption of the alloy remained relatively unchanged across different initial microstructures, the final properties were found to depend on the initial microstructure. THP notably enhanced ductility by converting α' martensite into refined α and β phases. The microstructure, originally containing α'-martensitic phases in the as-received samples, transformed into slender α and β phases upon THP application. Consequently, for the 4-step and 2-step THP-treated samples, the yield strength of the heat-hydrogenated samples decreased by approximately 5% and 10%, respectively [6]. Doğu et al. [34], surface polishing process with HF solution was applied to Titanium alloys that produced at 0 °, 45 ° to 90 ° angles. On the other hand, annealing with a 2-step thermo-hydrogenation process (THP) was applied as a secondary heat treatment to enhance mechanical properties such as hardness and tensile strength and to increase fatigue life [34]. Table 3 presents that mechanical properties of Ti-6Al-4V alloy produced by EBM method and processed by 2-step THP along with their comparison with SLM produced alloy.

There are three different microstructure types in the Ti-6Al-4V alloy. Among these, the α and β layer thicknesses in the bimodal and layered structure change the alloy's fatigue strength, and the alloy's fatigue strength increases with the thinning layer thickness. Therefore, it is essential to obtain a Ti-6Al-4V thin-structured microstructure. The thermal-hydrogenation process, a thermal-chemical method, has recently been used to refine the coarse internal structure of titanium alloys. In this way, a thermal- hydrogenation treatment applied to the surface can thin the material's microstructure and thus increase the fatigue strength.

Table 3 Mechanical properties of Ti-6Al-4V alloy produced by different additive manufacturing methods and 2-step THP process [6], [34].

Specimen	Ultimate Tensile Strength [MPa]	Strain at Fracture [%]
As-produced (EBM)	878.0	10.2
2-step THP (EBM)	895.0	7.6
As-produced (SLM)	1246.7	4.7
2- step THP (SLM)	1110.2	9.8
4- step THP (SLM)	1110.9	3.5
ASTM F2924-14	895.0	10.0

2.5.2 Titanium Nitriding Methods

Nitriding is commonly used to enhance mechanical attributes, metals' hardness, corrosion and wear resistance. Nitriding, an extensive utilized thermochemical surface treatment, involves diffusion of the nitrogen into the metal's surface at elevated temperatures. Nitrogen exhibits significant solubility in solid α-Ti (Figure 10), and the presence of interstitial nitrogen leads to a substantial increase in strength, as illustrated in Figure 2.11 [35]. Referring to the titanium-nitrogen equilibrium phase diagram illustrated in Figure 2.10, the solubility of nitrogen in the α-phase is quite high, as can be seen from Figure 2.10. For instance, at T = 950 °C, it can reach to 17.5 at.% compared to 0.75 at.% in the β-phase. The nitriding process results in a thin compound layer of TiN on the surface, situated above a thicker compound layer of Ti_2N [35],[36].

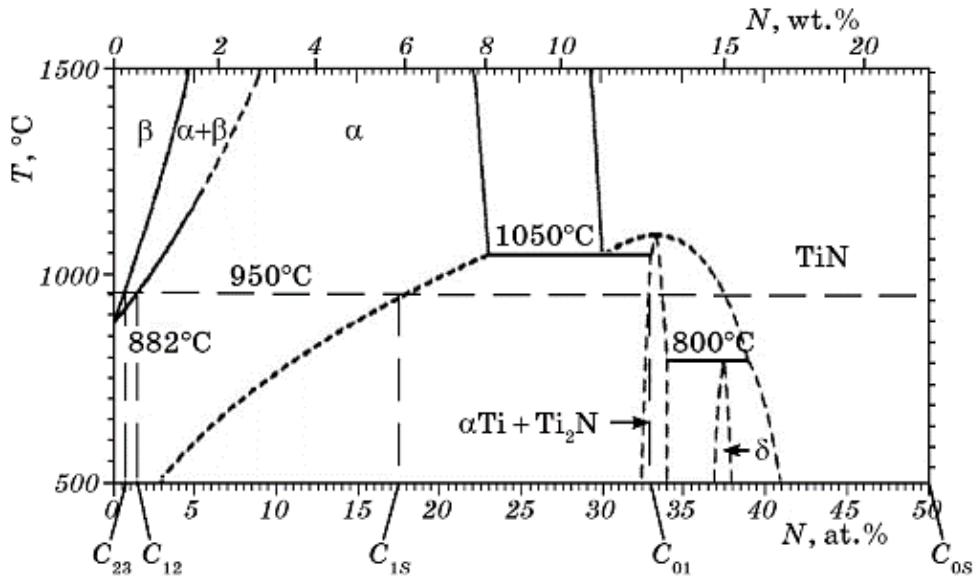

Figure 2.10 Ti-N Phase Diagram [37].

Diffusion coefficient of nitrogen in titanium is relatively low. Therefore, the nitriding process is conducted at relatively high temperatures (800 to 950 °C) [38]. The typical nitriding microstructure consists of a "compound layer" composed of TiN and Ti_2N on the surface, followed by a nitrogen-stabilized α-titanium layer(α-Case) and a nitrogen diffusion zone [39], [40], [41]. When the surface comes into contact with atomic nitrogen, it results in the creation of a compound layer consisting of TiN and Ti_2N nitrides. Since these nitrides do not dissolve aluminum, the aluminum is pushed towards the diffusion zone, where the alpha phase is more prevalent. As the temperature decreases, dispersed nitrides in this zone may precipitate, thereby increasing the hardness. The expansion of the diffusion layer is mainly influenced by the temperature and duration of the process, regardless of whether it is a gas or plasma nitriding process. However, the composition of the process atmosphere can influence the growth of the compound layer. H_2 content increases in the plasma process, and NH_3 in the gas process accelerates the growth of the nitride zone [42].

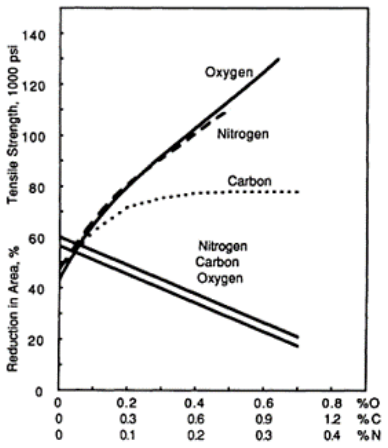

Figure 2.11 The impact of interstitial alloying elements on strength and reduction in area [35].

The primary goals of nitriding are to achieve heightened surface hardness, improved wear and corrosion resistance, and enhanced fatigue life while generally causing negligible alterations to the dimensions and inherent properties of the material itself. In order to increase the fatigue strength of the Ti-6Al-4V alloy and optimize the microstructure, different surface treatments, such as coating the surface with a thin film or thermal-chemical processes, can be applied. Nitriding is a thermal-chemical method applied as gas, laser, or plasma nitriding. A variety of surface engineering techniques, including gas nitriding, laser nitriding, and ion implantation, have been successfully applied to enhance tribological properties in the literature; of these techniques, gas nitriding is considered the most promising method available for engineering applications because it can quickly form a harder nitrided layer on the surface of the materials. This method demonstrates significant improvements in wear resistance. Although plasma nitriding does not require a long process time, the surface of the cathode arcs formed during the process can be damaged. Therefore, the gas nitriding process is preferred where fatigue resistance is essential. Conversely, such surface treatments have been reported to result in a reduction in the fatigue strength of titanium alloys. However, the reason for decreasing in fatigue strength and the fracture mechanisms has yet to be studied in detail [43], [44], [45], [46], [47], [7],[48].

2.5.2.1 Plasma Nitriding

Plasma nitriding is a sophisticated surface modification method involving the introduction of nitrogen into a metal's surface through a glow discharge. This process offers several advantages and considerations [45], [49], [50], [51], [52], [53]:

1. **Temperature Dependence:** The thickness and hardness of the modified layer significantly depend on the temperature used during the process. Temperatures above 850 °C provide the most significant layer thickness and hardness.
2. **Complexity and Equipment Requirements:** Plasma nitriding demands sophisticated equipment and controlled conditions, making reproducing in standard manufacturing setups challenging.
3. **Uniform Treatment:** A notable advantage is its ability to uniformly treat surfaces, regardless of the complexity of the geometry. This facilitates the treatment of intricate components within a feasible timeframe.
4. **Corrosion Resistance Improvement:** Plasma nitriding significantly enhances a material's corrosion resistance, creating a protective barrier that can prevent or reduce corrosion.
5. **Effects on Wear Resistance:** The process temperature affects wear resistance differently. Higher temperatures can enhance wear resistance in some materials, while reducing the temperature may improve corrosion resistance by creating a protective barrier.
6. **Surface Roughness and Friction Coefficient:** Lower process temperatures generally reduce surface roughness and friction coefficients, improving wear resistance.

Farokhzadeh and Edrisy [54] studied at 600 °C to enhance the fatigue performance of plasma-nitrided Ti–6Al–4V alloy by optimizing its microstructure. The assessment of fatigue properties involved rotation bending tests, construction of S–N curves, and comparison of outcomes with those obtained from an elevated temperature treatment (900 °C) and conventional gas/plasma nitriding treatments documented in the literature.

As a result of the nitriding process at 600 °C, the microstructure of the nitride samples consisted of a thin compound layer (1.9 µm) on top of a deep diffusion zone (45 µm). Additionally, the sample subjected to nitriding at 900 °C exhibited a thick compound layer (6 µm) on the surface, followed by a thick (20 µm) α-case and a diffusion zone with a depth of 110 µm. According to their study, the plasma-nitrided alloy at 600 °C exhibited an endurance limit of 552 MPa, surpassing those attained by conventional nitriding treatments performed at 750–1100 °C (Figure 2.14). Conversely, plasma nitriding at 900 °C led to a reduction in fatigue life by at least two orders of magnitude compared to the 600 °C treatment. This was coupled with a 13% reduction in tensile strength and a 78% decrease in ductility (Table 4). The decrease in mechanical properties following the elevated temperature treatment was attributed to several factors. These include formation of a thick compound layer (approximately 6 mm) on the surface, followed by an α-case layer (approximately 20 mm) and phase transformation within the bulk microstructure—transitioning from fully equiaxed to bimodal with coarser grains (The average grain size value increased by approximately five times). The morphology of the compound layer in this study (600 °C) constrain premature crack initiation from the surface. Furthermore, the presence of a deep diffusion zone with a well-bonded interface reduced the likelihood of fatigue initiation at or below the compound layer interface [54]. Figure 2.12 shows that nitriding result of 600 °C condition. Specimen has the diffusion zone and a well-bonded interface between the compound layer. An α-Case layer is not present beneath the compound layer, nor are there any observed microstructural transformations

Figure 2.13 shows the microstructure of Ti–6Al–4V alloy plasma nitrided at 900 °C. It was observed that a thick compound layer and α-Case were present. The microstructure transformed equiaxed α + β intergranular β particles into a bimodal structure [54].

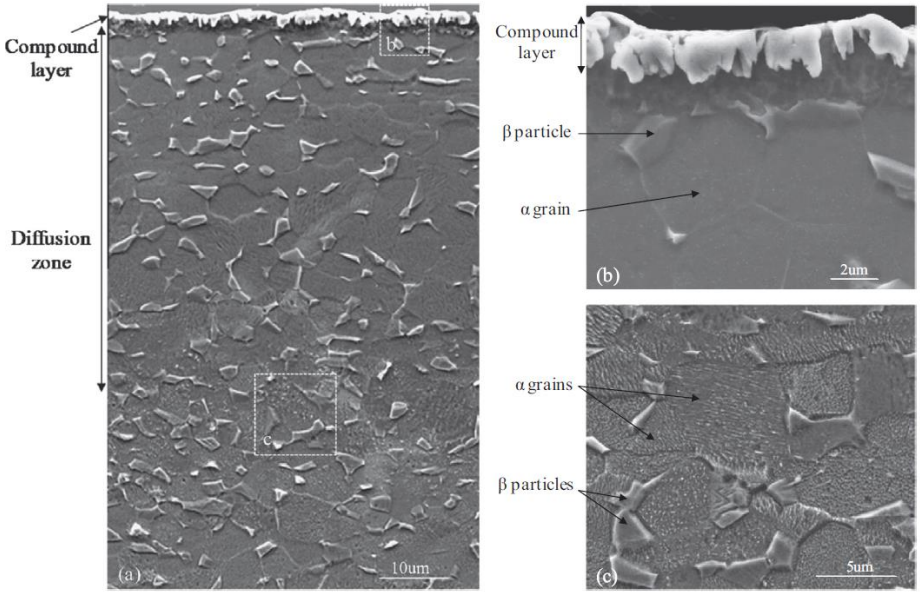

Figure 2.12 SEM image of plasma nitrided Ti–6Al–4V alloy at 600 °C [54].

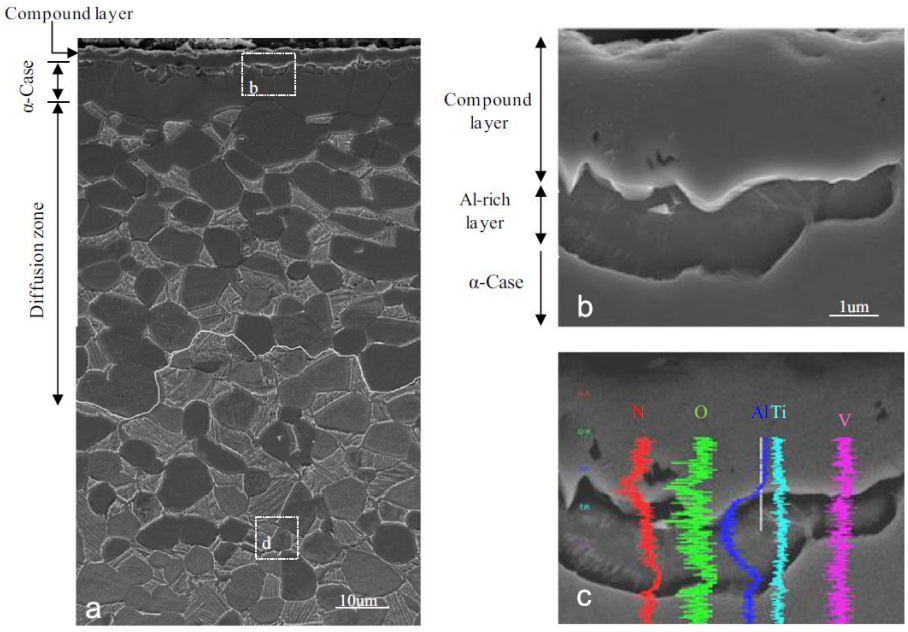

Figure 2.13 SEM image of plasma nitrided Ti–6Al–4V alloy at 900 °C [54].

Table 4 Tensile test data obtained from uniaxial tensile test conducted on as-received Ti-6Al-4V alloy and plasma nitrided alloy at temperatures 600 °C and 900 °C [54].

Sample	Tensile Strength (MPa)	Yield Strength (MPa)	Elongation (%)
As-received Ti64 alloy	1045 ± 9.9	940 ± 3.5	13.9 ± 0.2
Plasma nitrided at 600 °C	1050 ± 4.6	908 ± 3.0	7.8 ± 0.2
Plasma nitrided at 900 °C	913 ± 18.9	847 ± 2.0	1.9 ± 0.2

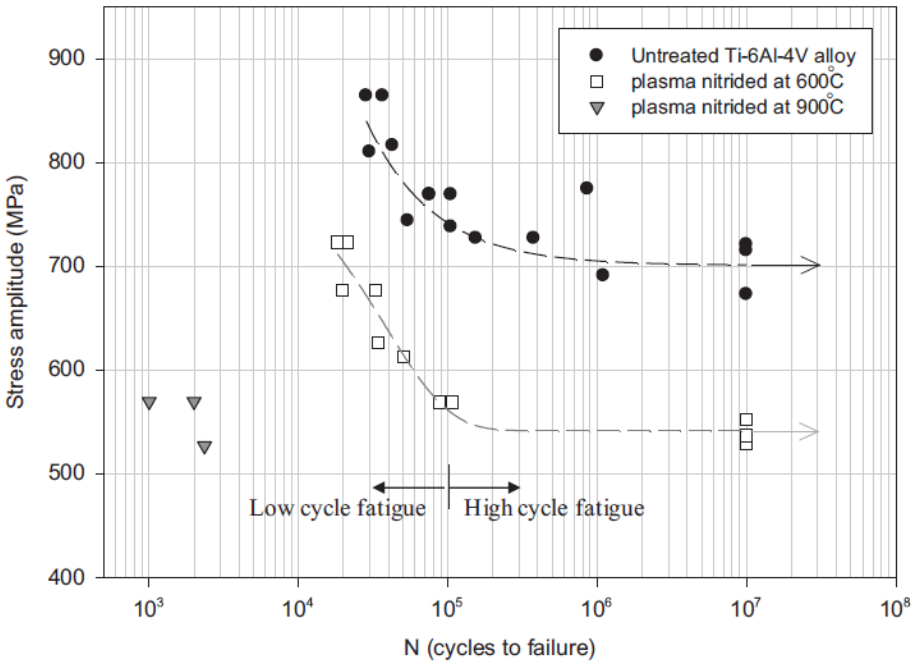

Figure 2.14 The S–N curves depict the fatigue response of the Ti–6Al–4V alloy pre- and post-plasma nitriding treatment at distinct temperatures, namely 600 °C and 900 °C.

2.5.2.2 Laser Nitriding

Utilizing short laser pulses offers numerous advantages over traditional nitriding methods. Laser nitriding has a significant impact on the heat-affected zone, affecting both its depth and lateral dimensions. Consequently, this technique allows for the modification of intricately shaped and heat-sensitive components [55]. While laser nitriding includes remelting of the surface and requires precise control of the parameters. Obtaining a thick coating is not always possible, but effective production with laser nitriding has been reported [56].

2.5.2.3 Gas Nitriding

Gas nitriding is more straightforward than complex methods like plasma or laser nitriding. The process typically involves a furnace operating within specified temperature ranges with reasonable pressure control [57]. Gas nitriding is a process involving diffusion and occurs when nitrogen gas dissolves from the alloy surface and diffuses into the alloy matrix, depending on temperature and time. The optimization of nitriding parameters, including temperature, treatment duration, and gas composition, is crucial for achieving desired material properties. Despite its advantageous properties, this method's complexity and dependency on controlled conditions can challenge its widespread implementation in standard manufacturing setups. Therefore, the gas nitriding process is classified as a thermal-chemical method in which nitrogen dissolves in titanium or forms different nitride layers rather than creating a different layer on the surface than in the subsurface region, as in traditional coating processes. The amount of nitrogen gradually decreases from the alloy surface to the inside. Therefore, unlike coatings created with techniques such as physical vapor storage, there are no problems such as peeling or coating separation from the surface [58]. As a result of nitriding, a TiN phase with a FCC structure is formed on the external surface of the alloy.

Just below the TiN phase is the Ti_2N phase with a tetragonal structure, and below that is the solid solution in which nitrogen is dissolved in the α titanium phase [59]. The formation of TiN and TiN phases on the alloy surface as a result of nitriding increases the hardness of the Ti-6Al-4V alloy and these phases contribute to delay crack formation by inducing compressive stresses on the surface. Therefore, the fatigue life of the alloy increases [60]. The thickness of the phase layers formed on the surface due to the gas nitriding process is directly related to the nitriding temperature and time. Although the gas nitriding process applied at relatively high temperatures, such as 900 °C, constitutes a thick nitride layer with high hardness, it causes grain coarsening in the alloy. Therefore, fatigue strength and fatigue life decrease in titanium alloys subjected to nitriding at high temperatures. Nitriding processes performed at 600 °C and lower temperatures prevent grain coarsening in the titanium alloy and form a solid solution layer on the alloy surface instead of a nitride layer. Accordingly, significant improvements occur in the fatigue strength and life of the alloy [61].

Tokaji et al. [62] studied the effect of gas nitriding on fatigue behavior and fracture mechanisms. They observed that the hardness and depth of the nitriding layer enhanced with higher nitriding temperatures and extended periods. Their findings indicated varying effects on fatigue strength based on the specific titanium material. Fatigue strength was increased by nitriding in pure titanium, while in the Ti-6Al-4V and Ti-15Mo-5Zr-3Al alloys, nitriding generally resulted in a reduction in overall fatigue strength. According to their findings, the influence of the nitrided layer on fatigue behavior exhibited variability depending on the material's strength. The increased fatigue strength due to nitriding was associated with improved resistance against crack initiation in materials with lower strength, such as pure titanium. Conversely, fatigue strength decreased primarily due to premature crack initiation in materials with higher strength, like the Ti-6Al-4V and Ti-15Mo-5Zr-3Al alloys, following the nitriding process [63]. In addition to titanium alloys produced by traditional methods, similar studies have been conducted in the literature on samples produced by additive manufacturing methods.

Mukhtar et al. [64] investigated the fatigue life of AM Ti64 with and without nitriding following identical thermal treatments. Their findings revealed that nitriding reduced the fatigue life of AM Ti64 compared to its counterpart, which underwent the same thermal treatment but without nitriding. This observation was associated with a brittle nitrided layer, facilitating early crack initiation and swift crack propagation within the bulk material, thereby accelerating the growth rate of these cracks [64].

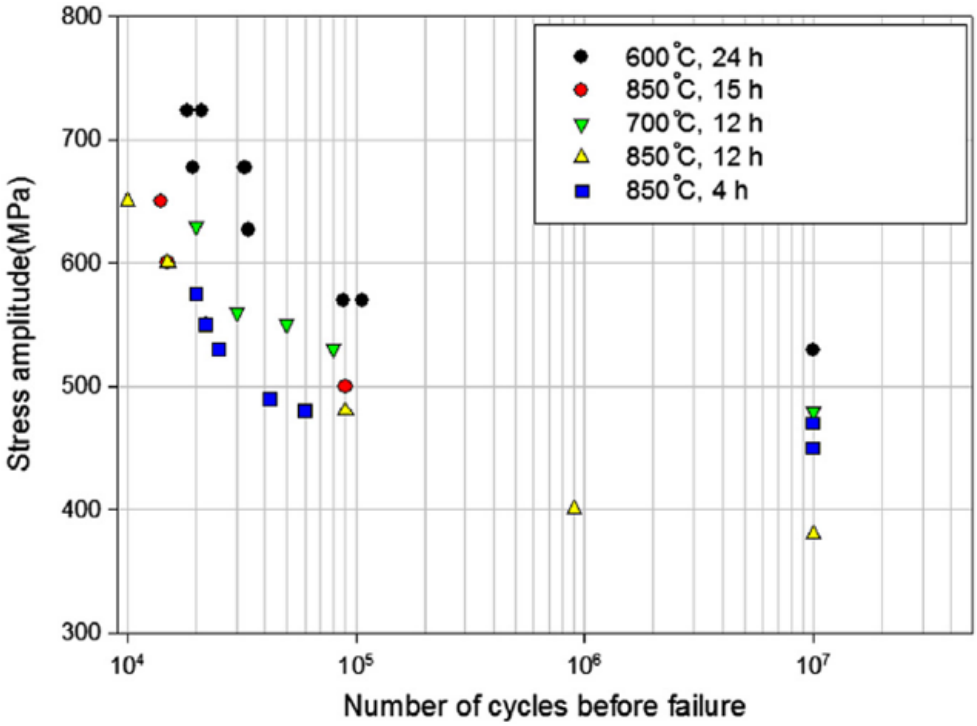

Figure 2.15 A comparison of fatigue data obtained for plasma nitrided Ti-6Al-4V alloy compared to the conventional gas and plasma nitriding of the alloy as investigated by various researchers. [43],[65],[63].

Figure 2.15 illustrates the S-N curve obtained from a study conducted on Ti-6Al-4V alloys subjected to similar nitriding processes. Based on this graph, there is a noticeable decrease in the fatigue strength of the alloys as the nitriding temperature increases. Furthermore, in alloys processed at the same temperatures for varying durations, an increase in processing time has resulted in a decrease in fatigue strength.

CHAPTER 3

EXPERIMENTAL PROCEDURE

3.1 Introduction

In this thesis, the surface morphology, microstructure, and mechanical properties of Ti-6Al-4V alloys were investigated. Samples were manufactured to examine the characterization of the materials in terms of mechanical and fatigue strength. Fatigue test specimens were produced in a dog bone shape, and cylindrical bars were manufactured to optimize the heat treatment applied post-production. First, the microstructure and mechanical properties of samples without any secondary treatment were examined as received. It was aimed to simultaneously obtain a nitrogen-rich surface layer to prevent fatigue crack initiation and a fine-structured $\alpha+\beta$ phase mixture to slow down crack propagation in the Ti-6Al-4V alloy in this study. For this purpose, the nitriding process was first applied to the as-received cylindrical samples, and then a modified 2-step THP was applied. To evaluate the impact of these applied processes, the microstructure and mechanical properties of these samples were analyzed.

3.2 Starting Materials

In this study, commercially available wrought Ti-6Al-4V bars 12 mm in diameter (as-received) were machined using the CNC available in the Department of Mechanical Engineering at Hacettepe University, following ISO 6892-1 standards. Samples were produced with the identical parameters for various tests. Cylindrical bars were manufactured to optimize post-production heat treatments, while tensile and fatigue test samples were designed in dog bone shape.

Table 5 presents the elemental composition of the Ti6Al-4V alloy used in the current study as defined by ASTM F136-13.

Table 5 The analysis of composition was conducted on the wrought Ti-6Al-4V alloy in comparison to the ASTM F2136-13 standard specifications [6].

Chemical Composition (%)	
Element	**ASTM F136-13 (wrought)**
Al	5.50 to 6.50
V	3.50 to 4.50
Fe	0.25 max
O	0.13 max
C	0.08 max
N	0.05 max
H	0.015
Titanium	Balance

3.2.1 Surface Roughness Measurement

One of the most influential factors on the fatigue life of machine elements shaped by traditional manufacturing techniques is known to be surface conditions. Considering that factors such as stress accumulation arising from surface roughness structure and defects that can create a notch effect, as well as oxidation, contribute to the initiation of microscopic cracks acknowledged as the beginning of fatigue, surface roughness has been measured to determine the most suitable machining parameters. According to the literature, it has been understood that fatigue may start at lower stress values as surface roughness increases. As surface roughness decreases, fatigue damage may begin at higher stresses. Surface roughness measurements were conducted in the direction of progression on samples produced using different machining parameters according to ISO 4287:1997 standard.

Mitutoyo Surftest SJ-210 equipment has been utilized for the surface roughness measurements. As can be observed in Table 6, parts produced with a feed rate of 0.1 mm/rev exhibit significantly smoother surface quality compared to those produced at 0.2 mm/rev. For instance, at the same cutting depths, the sample produced at 0.1 mm/rev showed a Ra value of 0.62 µm, whereas when the feed rate was increased to 0.2 mm/rev, the same value rose to 1.03 µm. However, there was no notable difference in surface quality was observed between the rough and final cutting depth values specified in the table. The susceptibility of titanium to form alloys with elements in the cutting tools is high. Hence, it is crucial to accurately select processing parameters and ensure adequate heat dissipation during chip removal. Therefore, in this study, selecting parameters that provide the highest possible cutting depth and feed rate while offering the lowest high roughness was of great importance. Therefore, the parameters highlighted in red in Table 6 namely, a feed rate of 0.1 mm/rev, a rough cutting depth of 0.5 mm, and a final cutting depth of 0.2 mm have been selected.

Table 6 Surface roughness measurement results.

Feed Speed [mm/dev]	**Depth of cut [mm]**	**Final Pass Cutting Depth [mm]**	**R_a [µm]**	**R_z [µm]**
0.1	0.25	0.1	0.60	2.68
0.1	**0.5**	**0.2**	**0.62**	**2.74**
0.2	0.25	0.1	0.97	4.69
0.2	0.5	0.2	1.03	4.83

3.3 Experimental Methods

The details of the applied post processes, and characterization techniques are summarized in Figure 3.1.

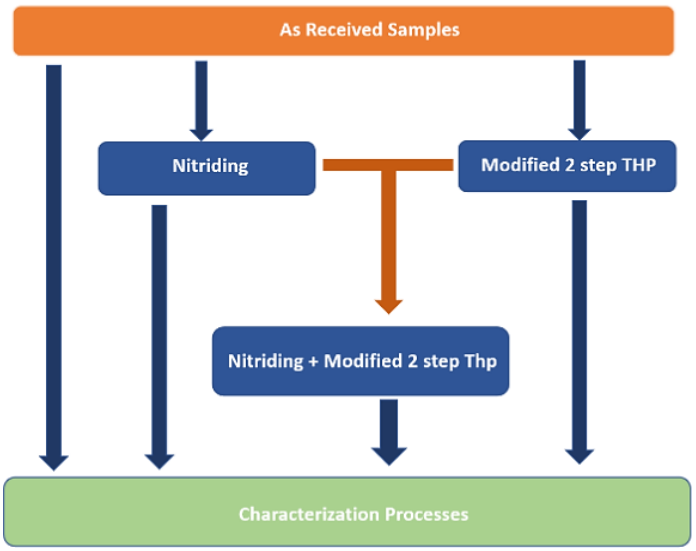

Figure 3.1 Route of applied methods.

3.3.1 Thermo-Hydrogen Process

The thermo-hydrogen process (THP) offers an effective way of altering the microstructure and enhancing the mechanical properties of titanium alloys without necessitating deformation or conventional heat treatments involving recovery and recrystallization. Various forms of THP (hydrogenation + dehydrogenation) have been employed, commonly employing a 4-step sequence (hydrogenation, β solution treatment, eutectoid decomposition, and dehydrogenation) for treating titanium alloys. In the current study, modified 2-step THP was used as in the study of Bilgin et al. This adapted process involves hydrogenation and dehydrogenation steps conducted below the β-transus temperature. The purpose of this modification is to prevent potential grain coarsening during the β-solution process and eutectoid decomposition stages.

3.3.1.1 Sample Preparation for 2-step THP

Wrought Ti-6Al-4V alloy samples (cylindrical bars, tensile, and fatigue test samples) prepared for various tests were cleaned using an ultrasonic bath by soaking them with ethanol for 10 minutes before the THP (hydrogenation + dehydrogenation) process. Following cleaning, the samples were dried with the help of a dryer.

3.3.1.2 Hydrogenation Process

During the initial phase of THP, specimens were loaded with hydrogen to enable the formation of δ (TiH_2) phase, which constitutes the foundation for microstructural enhancement in the THP (hydrogenation + dehydrogenation) process. Initially, cleaned and dried samples placed in an aluminum boat were introduced into a horizontal tube furnace at room temperature. Subsequently, the furnace was vacuumed using a turbo-molecular vacuum pump, achieving a vacuum level of about $3x10^{-5}$ torr. Following this, the furnace was purged with high-purity argon gas through two cycles of de-gassing and purging. Then, the furnace was heated under high-purity hydrogen flow (0.6 l /min) up to 650 °C, a temperature previously established as the optimal hydrogenation temperature for Ti-6Al-4V alloy according to the findings of Bilgin et al. [6]. Upon reaching 650 °C, the specimens were soaked for one hour in hydrogen atmosphere. In the case of the first set of samples, after soaking the samples at the hydrogenation temperature for 1 hour in the presence of hydrogen atmosphere, the furnace was turned off to gradually cool it down to room temperature at a cooling rate of 10 °C per minute again under high purity hydrogen flow. Hydrogenated samples were cooled down to room temperature to examine the impact of hydrogen incorporation on the microstructural changes and mechanical properties. The second set of samples were hydrogenated using identical conditions described above, yet after hydrogenation instead of cooling to room temperature they were directly heated to the dehydrogenation temperature, as detailed below.

3.3.1.3 Dehydrogenation Process

The dehydrogenation process involves reversing the hydrogen reaction with titanium, allowing the removal of hydrogen from the alloy with increased diffusion rate at elevated temperatures [66], [6]. The aim of this step was to extract hydrogen from previously hydrogenated samples, eliminating hydrogen embrittlement. This extraction facilitated the phase transformation from the δ phase (formed during hydrogenation) to a refined α phase, contributing to a finer microstructure composed of α + β phases. Following hydrogenation, as mentioned earlier, for dehydrogenation samples were directly heated to 700 °C under hydrogen gas flow. Subsequently, they were subjected to high vacuum (approximately $3x10^{-5}$ torr) for 18 h, a duration also determined through optimization in the work of Bilgin et al. [6]. The final step involved shutting down the furnace, allowing the samples to cool to room temperature within the high vacuum environment.

3.3.2 Nitriding Process

Gas nitriding, a thermochemical surface treatment method, involves nitrogen diffusion into the metal's surface to create a nitrided layer. This process relies on nitrogen's capacity to dissolve into the metallic structure, facilitating the formation of a hardened layer on the material's surface. Upon gas nitriding, a thin layer of TiN, a nitrided compound, can develop at the surface layer of the Ti-6Al-4V alloy sample. This technique enhances several aspects, including surface hardness, corrosion and wear resistance together with fatigue, and fracture properties [67]. In this study, the nitriding process was conducted in a furnace with inert gas atmosphere control. Pure nitrogen was used as the nitriding gas resource. Nitrogen was supplied to the chamber at a constant flow rate (0.5 l/min) and a specific temperature (850 and 950 °C).

Firstly, the furnace was evacuated, and a gas flow was introduced to reach atmospheric pressure. The thickness of the TiN surface layer and the microhardness value depends on two parameters: time and temperature. Therefore, samples were processed under different environmental conditions (vacuum or nitrogen) and at different temperatures (1, 5, and 10 hours) and time combinations to determine the optimum variables. In the final stage of the process, the samples were cooled in the furnace under high-purity nitrogen. The detailed experimental parameter set is given below in Table 7.

Table 7 Nitriding parameters applied in this study.

Temp. (°C)	Time (h)	Heating Condition	Cooling Condition	Applied Gas
850	5	Vacuum	Nitrogen	Nitrogen
950	5	Vacuum	Nitrogen	Nitrogen
950	1	Vacuum	Nitrogen	Nitrogen
950	1	Nitrogen	Nitrogen	Nitrogen
950	10	Nitrogen	Nitrogen	Nitrogen

In this step, the same cleaning and drying procedures were implemented for the samples used in the hydrogenation-dehydrogenation steps. After cleaning, the samples were placed into the horizontal tube furnace at room temperature. As shown in Table 3, the furnace was heated to different temperatures in different environmental conditions (vacuum or nitrogen) while other parameters were kept constant. During cooling, the samples were held under a flowing nitrogen atmosphere (0.5 l/min) for different time periods. Following this, the furnace was powered off, allowing the samples to gradually cool down to room temperature at a rate of 10 °C per minute while under the nitrogen gas atmosphere.

3.3.3 THP Process After Nitriding

It is aimed to simultaneously obtain a nitrided surface layer that will prevent fatigue crack initiation and a fine-structured $\alpha + \beta$ phase mixture that will slow down crack propagation in the Ti-6Al-4V alloy with the THP heat treatment applied after the nitriding process. Additionally, the developed process aims to increase the hardness of the surface and subsurface regions of the Ti-6Al-4V alloy. For this process route of the study, the samples were first subjected to the nitriding process, and then the THP process was applied. Based on initial studies, the parameter set involving heating of samples under nitrogen flow followed by nitriding at 950 °C for 1 h was selected as the optimum parameter for nitriding. Therefore, in this part of the study, the nitriding process was applied to the samples with this parameter set, and then the 2-step THP process was applied after the samples were completely cooled to room temperature.

3.4 Experimental Set-Up

All heat and surface treatments (THP and nitriding) were conducted using the experimental setup shown in Figure 3.2. To execute successful heat treatment experiments, a 1000 mm long quartz tube with internal and external diameters of 45 and 48 mm, respectively, was utilized in the furnace, and the samples were put in an alumina crucible placed inside this quartz tube. Temperature measurement within the horizontal tube furnace was accomplished using a K-type thermocouple. Hydrogen, nitrogen, and argon gas flow rates were regulated using digital and manual flow meters. The high vacuum level within the furnace is sustained through a turbo-molecular vacuum pump (Nano-Vak, Turkey).

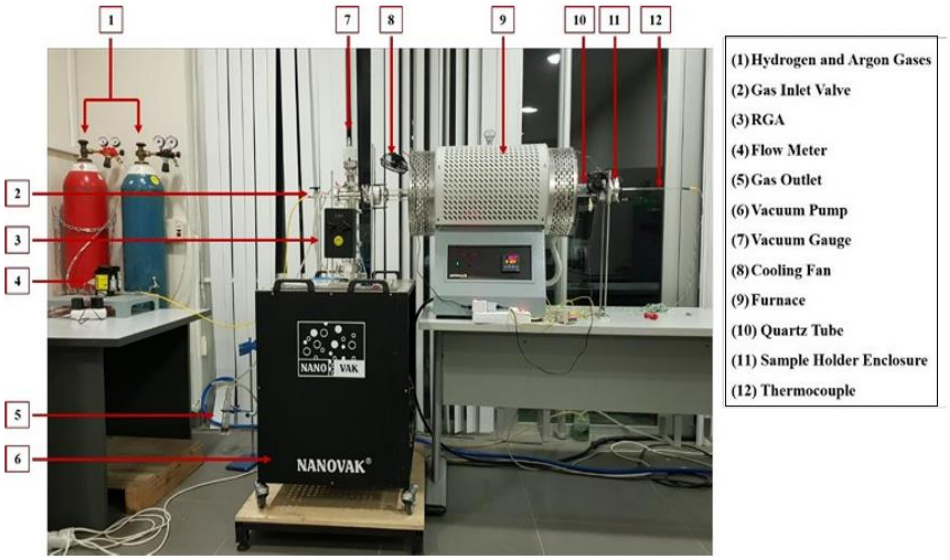

Figure 3.2 Experimental set-up for the heat treatments applied in this study [34].

3.5 Characterization Techniques

3.5.1 X-Ray Diffraction Analysis (XRD)

XRD analysis was performed on the cross-section of the samples to detect possible nitride phases formed on the surface after the nitriding and THP (hydrogenation + dehydrogenation) processes and to determine the phase content of the Ti-6Al-4V alloy. The phase constituents of the as-received, hydrogenated and dehydrogenated, as well as nitrided materials were determined through XRD analysis conducted using a standard X-ray diffractometer (Rigaku D/Max 2200/PC, Rigaku Corporation, Tokyo, Japan) employing Cu-Kα radiation at 40 kV. The analysis involved continuous scanning over the 2θ range between 20 ° and 80 °, with a scanning speed set at 0.5 ° per minute.

3.5.2 Hidrogen Content Determination

As-received and post-processed Ti-6Al-4V alloy samples were analyzed using LECO TCN 600 and LECO CS230 to determine hydrogen contents. Three measurements were taken from each sample.

3.5.3 Microstructural Analysis

The samples were cut into cylindrical specimens for microstructural analysis using a table-top abrasive cutting machine (Struers Labotom-15). The extracted specimens were embedded in conductive bakelite using Struers CitoPress-1 hot mounting device. Coarse and fine sanding was performed with SiC sandpaper (320, 500, and 800 grit). Sample surfaces were polished using Struers Tegramin-25 device, following 3-stage polishing with diamond polishing suspensions of 9 µm, 3 µm, and 1 µm. The following sample preparation procedure complies with ASTM E3 standards. Finally, the samples were etched for 40–50 seconds using Kroll's reagent (2 ml HF+8 ml HNO_3+92 ml H_2O). The sample surfaces were examined under a Zeiss Merlin field emission gun scanning electron microscope (FEG-SEM) with a backscattered electron detector (BSD) using 20 kV acceleration voltage and 1.0 nA probe current. Spatial micro-chemical analyses were performed on the sample surfaces with the EDAX Pegasus EDS (Energy Dispersive X-ray Spectroscopy) system. Additionally, electron backscattered diffraction (EBSD) analyses were done using the same FEG-SEM.

3.5.4 Mechanical Testing

3.5.4.1 Microhardness Test

Microhardness tests were conducted using ZWICK/ROELL microhardness device (200 g load for 20 seconds) to determine Vickers hardness values of the samples. 5 measurements were performed on the cross-sections of each sample.

3.5.4.2 Tensile Test

The stress-strain behaviors of both as-received as well as heat-treated Ti-6Al-4V alloy samples were analyzed using the Instron 5582 Universal Testing Machine, which had 100 kN loading capacity. Tensile tests were performed according to ISO 6892-1:2019 standard. The testing was conducted at a constant crosshead speed of 1 mm/min. The geometry of the test specimen is shown in Figure 3.3.

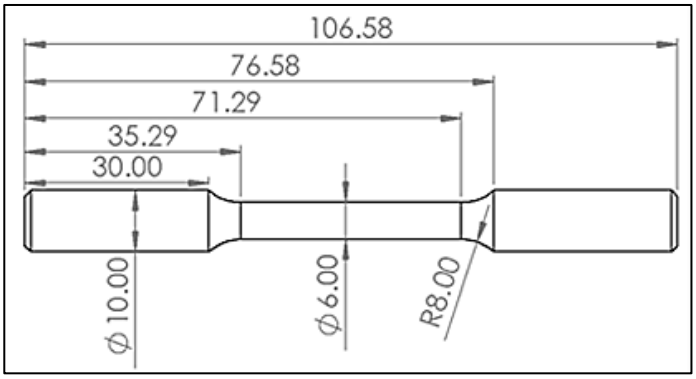

Figure 3.3 Tensile test specimen geometry.

3.5.4.3 Fatigue Test

Fatigue testing machine (BEMAK, Turkey) was used to conduct axial fatigue tests at different stresses (610-650 MPa) (f= 4 Hz, R= -1) for the as-received, THPed, nitrided and nitrided + THPed Ti-6Al-4V alloy samples. Fatigue tests were performed according to ASTM E466-07 standards. The test specimen geometry is shown in Figure 3.4. The fatigue test device had a servo-hydraulic structure. A maximum frequency of 20 Hz could be reached during tests performed in the tensile or compression direction. However, in the case of fully reversible loading (R = -1), which was desired to be applied in the current study, the loading frequency capacity of the machine was lower. In the initial tests performed with the servo-hydraulic device, it was determined that it could operate with a maximum frequency of 4 Hz in case of fully reversible loading. Therefore, fatigue tests were performed under fully reversible loading conditions at 4 Hz of loading frequency.

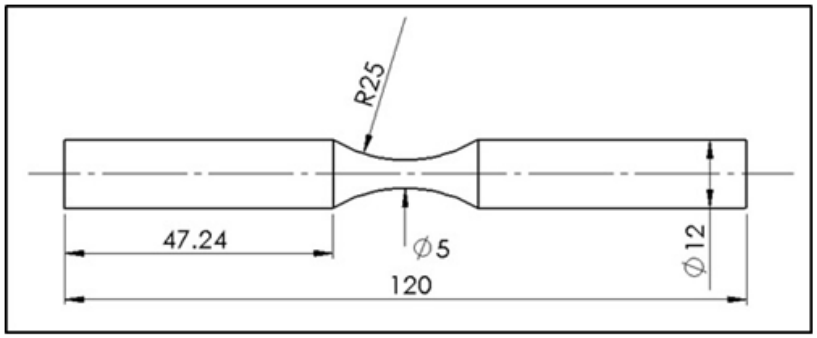

Figure 3.4 Fatigue test specimen geometry.

CHAPTER 4

RESULTS AND DISCUSSION

In this study, the microstructure and mechanical properties of the Ti-6Al-4V alloy have been examined, keeping all production variables constant. First, as-received samples were analyzed in terms of their mechanical and microstructural characteristics. Then, 2-step THP, nitriding, and nitriding + 2-step THP, a combination of these two processes, were applied to the as-received samples separately, and changes in their mechanical and microstructural properties were investigated.

4.1 Microstructural and Chemical Analysis

The microstructure of Ti-6Al-4V alloys was examined using cylindrical samples under different conditions. These conditions are as-received, heat-treated (THP), surface-treated (nitrided), and finally, both heat and surface treated. The examinations were conducted in both transverse and longitudinal directions. To investigate the microstructure, chemical composition, and phase content of the specimens, optical microscopy, Scanning Electron Microscopy (SEM), Electron Back Scatter Diffraction (EBSD), Energy-dispersive X-ray Spectroscopy (EDS), and X-ray Diffraction (XRD) techniques have been utilized.

4.1.1 As-received Ti-6Al-4V Alloy

In this section, the microstructures of the samples were examined in detail, and the chemical composition of the observed areas was analyzed using EDS. The optical and SEM images of as-received specimens taken from the transverse direction are given in Figure 4.1 and Figure 4.2, respectively. It can be seen from the optical microscope images in Figure 4.1 that the used starting alloy consists of an equiaxed α phase (light-colored regions) and an intergranular β phase (dark-colored regions). In the SEM images in Figure 4.2, the dark equiaxed regions represent the α phase, and the white regions represent the β phase. In addition, the dark-colored regions represent the aluminum-rich α-phase, and the white-colored regions represent the vanadium-rich β-phase, which were also verified by EDS (Figure 4.3) and XRD (Figure 4.4) analysis. The two-dimensional distributions of the main elements identified by EDS analysis confirmed the presence and distribution of aluminum, which helps stabilize the α (hcp) phase, and vanadium, which acts as a stabilizer for the β (bcc) phase, in the as-received Ti-6Al-4V alloy. According to the analysis, the amount of aluminum is 6.27 %, and titanium is 89.03 %. As previously stated in Section 3.2, EDS analysis results of the wrought alloy specimen, given in Figure 4.3, are consistent with the values given in ASTM F136-13. In addition, XRD analysis was done to elucidate the phase constituents present in the as-received alloy. According to the XRD results (Figure 4.4), it is clear that the as-received alloy contains equilibrium phases, hcp-α, and bcc-β, formed at relatively slower cooling rates.

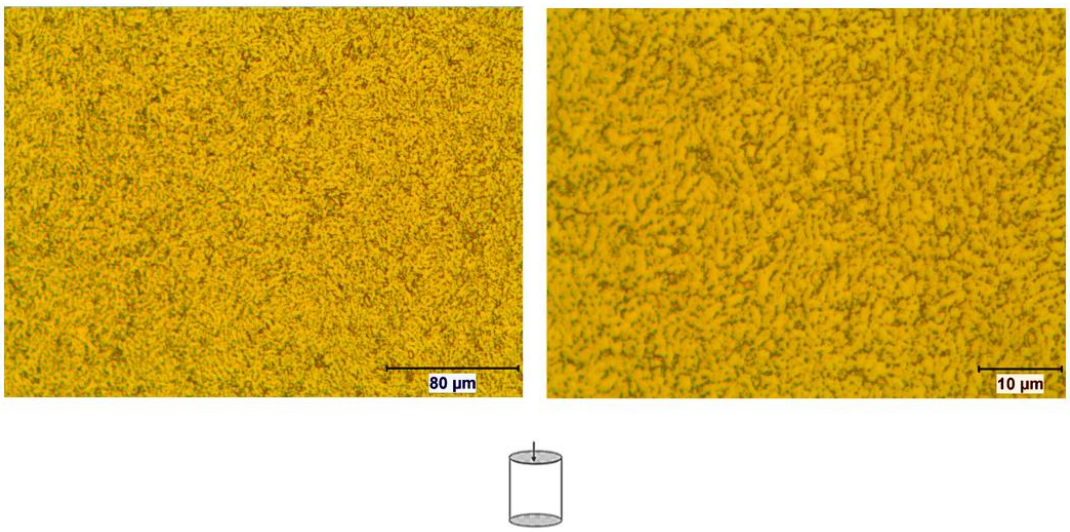

Figure 4.1 Optical microscope images of the examined as-received Ti-6Al-4V alloy (transverse direction).

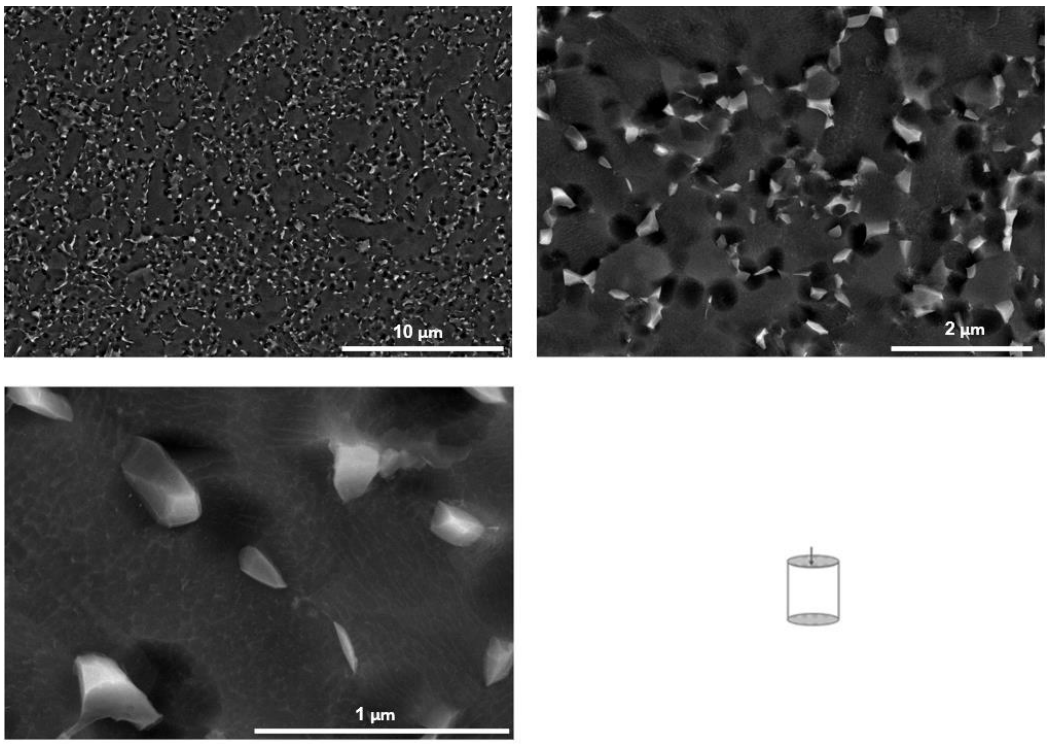

Figure 4.2 SEM images of the examined as-received Ti-6Al-4V alloy (transverse direction).

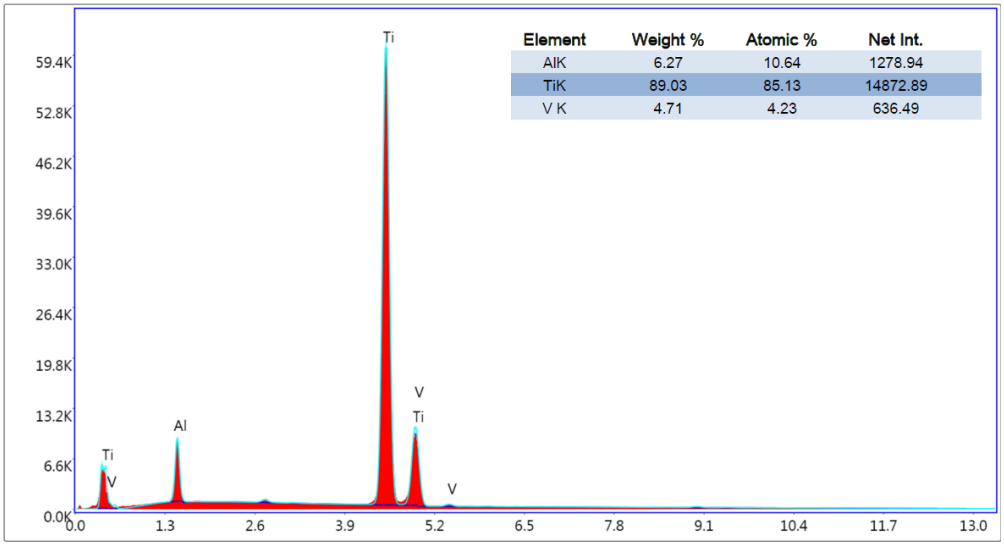

Figure 4.3 EDS analysis result of the as-received alloy.

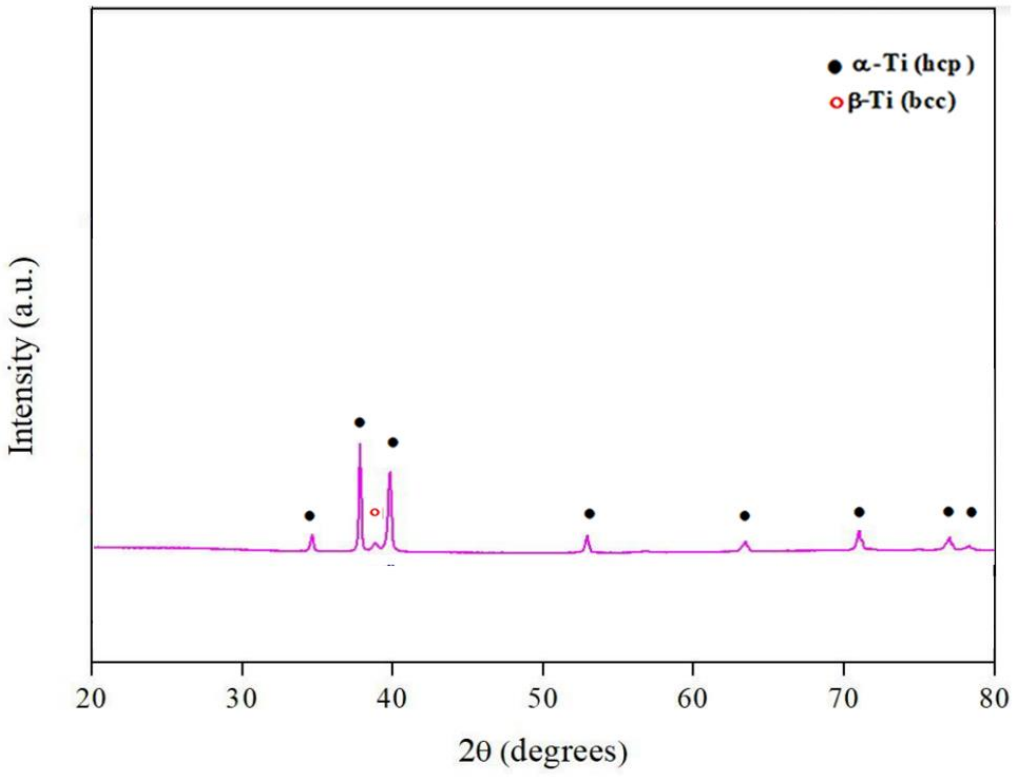

Figure 4.4 The XRD pattern of as-received alloy.

4.1.2 THPed Ti-6Al-4V Alloy

In this study, the modified 2-step thermal-hydrogenation process has been applied to wrought titanium alloys composed of hydrogenation and dehydrogenation steps. The Ti-6Al-4V alloy underwent thermochemical treatments of hydrogenation and dehydrogenation to refine its microstructure without any mechanical process involved. The hydrogenation process was carried out in a high-purity hydrogen atmosphere at 650 °C for 1 hour, while dehydrogenation was conducted under a high vacuum condition (approximately $3x10^{-5}$ torr) at 700 °C for 18 hours. The initial hydrogen content of the as-received alloy (0.0030 wt.%) increased to 0.22 wt.% following the hydrogenation process. Dehydrogenation under a high vacuum environment reduced the hydrogen content significantly, down to 0.0012 wt.%, well below the maximum value defined by ASTM F136-13 (Table 5). Obtaining the highest hydrogen level during the hydrogenation process for the alloy plays a crucial role in enhancing the microstructure by forming the δ-phase (TiH_2).

Bilgin et al. [6] conducted experiments at various temperatures to determine the optimal hydrogenation process. Based on their findings, it was observed that the hydrogen concentration remained relatively stable below 650 °C, and the maximum hydrogen level was observed to be achieved by holding at 650 °C for 1 hour. This increase was noted to be 1.19 wt.%. Similarly, Doğu et al. [34] chose 650 °C for hydrogenation and reported loading the alloy with approximately 1.97 wt.% hydrogen in their study. Therefore, in this thesis study, the hydrogenation process was conducted for 1 hour at 650 °C. As a result, the alloy's hydrogen concentration was determined to reach 1.81 wt.% (Table 8).

Table 8 Hydrogen concentration of the as-received, hydrogenated, and dehydrogenated samples of the current study.

Sample	**Hydrogen Concentration (wt.%)**
As-received	0.0030
Hydrogenated	1.81
Dehydrogenated	0.0012

XRD analysis was applied to detect the δ-phase expected to occur after hydrogenation. According to the XRD analysis result (Figure 4.5), δ-phase was confirmed to be present in the structure following hydrogenation. However, in order to fully detect the formation of this phase, the hydrogenated microstructure should be examined with High Resolution Transmission Microscope (HR-TEM) to conclusively verify the existence of the δ-phase. The hydrogenation process resulted in the anticipated formation of the δ-phase (TiH_2). The emergence of the peak of the δ-phase induces an expansion of the α phase peaks due to the overlap of the peaks of α and δ-phases [68]. Furthermore, the diffraction peaks of the hydrogenated sample are slightly shifted towards higher 2θ angles compared to as-received specimen. After the hydrogenation process, the dehydrogenation process (at 700 °C for 18 h under $3x10^{-5}$ torr), which is the last step of the 2-step thermal-hydrogenation process, has been applied to the samples, and microstructural and chemical analyses of the samples were conducted after the process.

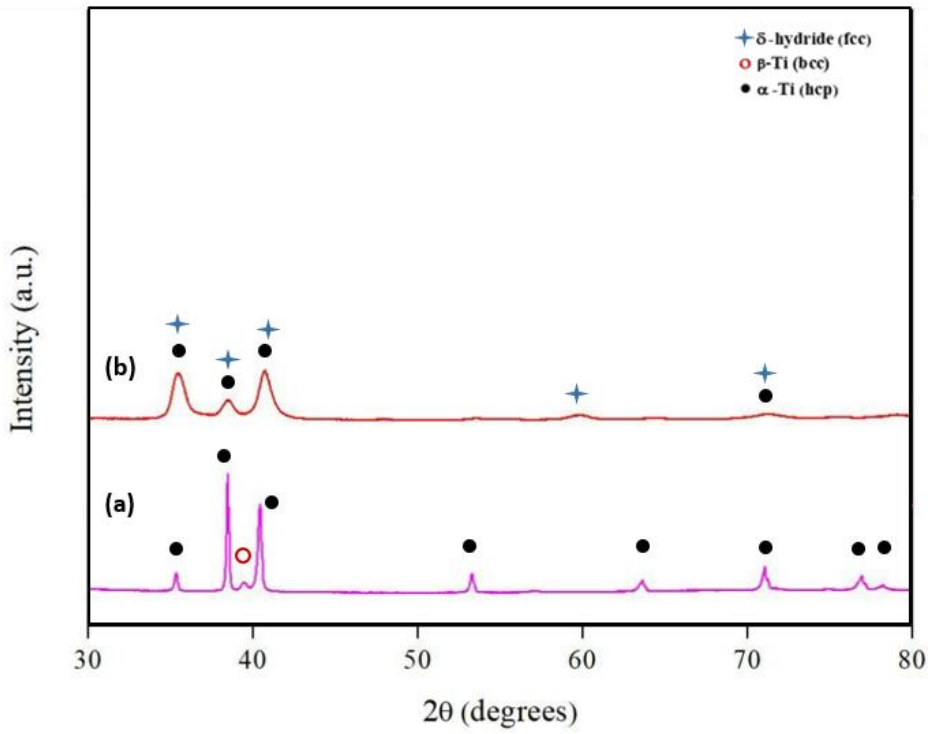

Figure 4.5 XRD patterns of (a) as-received, (b) hydrogenated Ti-6Al-4V alloy.

Bilgin et al. [6] stated that enhanced hydrogen desorption proved to be more efficient during dehydrogenation at elevated temperatures for extended periods. Nevertheless, prolonged exposure to higher temperatures increased the amount of α precipitates along grain boundaries. The formation of grain boundary α and growth of primary α is unfavorable in Ti-6Al-4V due to the resultant reduction in both ductility and strength. Thus, it is crucial to establish an optimal dehydrogenation temperature and duration to mitigate the adverse effects of high-temperature dehydrogenation. Loading of the Ti-alloy with maximum hydrogen content during hydrogenation is crucial for inducing the TiH_2 phase formation. This phase transforms to fine α phase during dehydrogenation, significantly contributing to microstructural refinement. It is established that the minimum necessary hydrogen content for TiH_2 phase formation is 0.38 wt.% [69].

Below this threshold, the formation of the TiH_2 phase does not occur. After the hydrogenation process, the dehydrogenation process was applied to the specimens to analyze the effect of the THP process. In this study, a 2-step THP (hydrogenation and dehydrogenation below β-transus temperature) has been applied instead of a 4-step THP to prevent grain coarsening during the β-solutionizing and eutectoid decomposition stages. The purpose of the dehydrogenation step in THP is to refine the microstructure by retrieving hydrogen from the sample, allowing the transformation of the thin α phase from the hydrogen-rich δ hydride phase at equilibrium. Transverse optical microscope and SEM images of the post-processed samples after dehydrogenation were depicted in Figure 4.6 and Figure 4.7, respectively. It was observed that a finer α phase was obtained in the samples subjected to dehydrogenation (Figure 4.6) when compared to the as-received sample (Figure 4.4). During the dehydrogenation step, the δ-hydride phase lost its hydrogen and transformed into a thin α phase (Figure 4.5). The hydrogen levels of the α and β phases in hydrogenated samples decreased after hydrogen withdrawal.

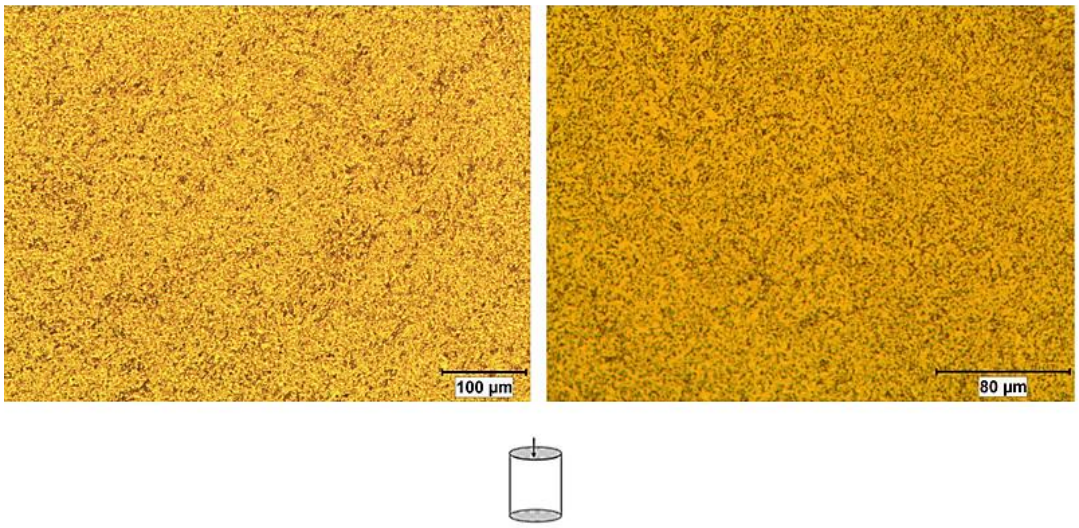

Figure 4.6 Optical microscope images of the Ti-6Al-4V alloy following the application of 2-step THP (transverse direction).

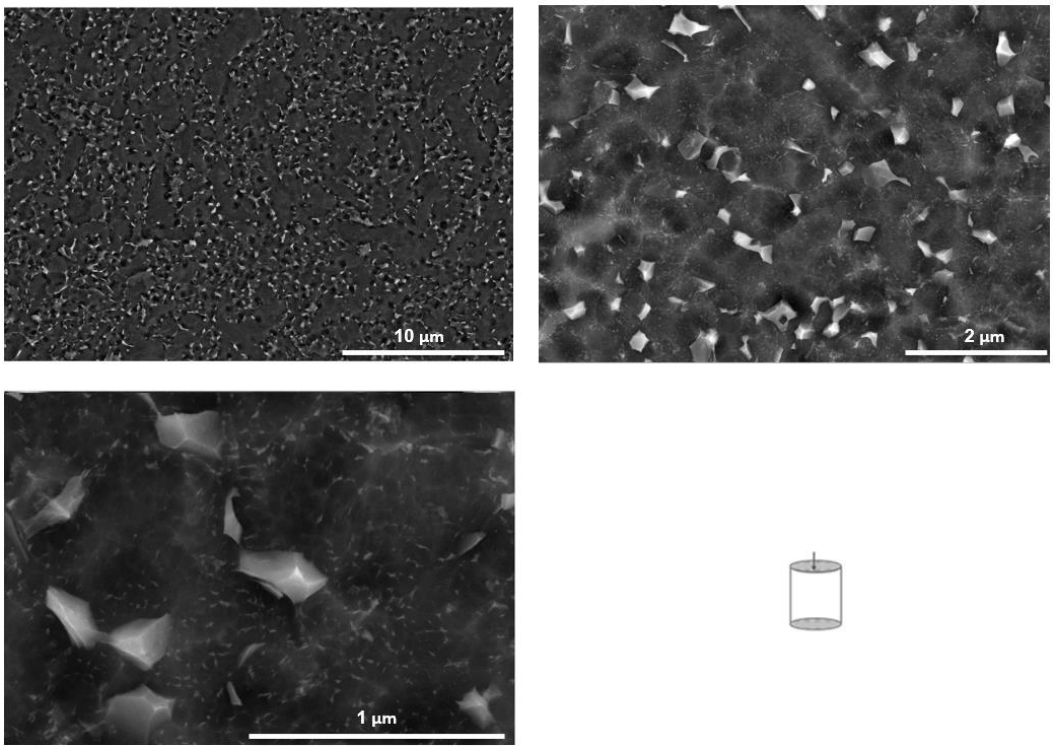

Figure 4.7 SEM images of the Ti-6Al-4V alloy following the application of 2-step THP (transverse direction).

Microchemical analysis has been conducted after the dehydrogenation process. The analysis result of the sample subjected to EDS area analysis is shown in Figure 4.8. The result of the analysis meets ASTM F136-13 requirements similar to the as-received specimens. The XRD patterns displayed in Figure 4.9 present the as-received and THPed Ti-6Al-4V alloy specimens. The as-received specimen exclusively exhibited hcp-α and bcc-β phases. Following hydrogenation, the sample contained hcp-α and δ-hydride phases. However, after the dehydrogenation process, the XRD pattern of the alloy displayed peaks corresponding to hcp-α and bcc-β phases similar to as-received samples. It is apparent that the δ-phase ceased to appear, potentially due to its transformation into the hcp-α phase, as hydrogen levels dropped below certain levels during exposure to high vacuum conditions.

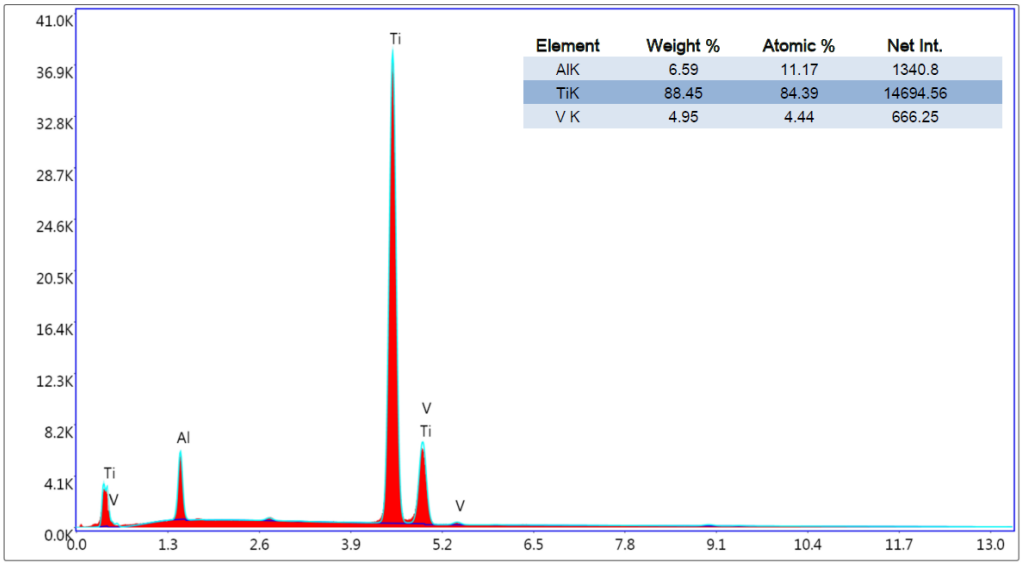

Figure 4.8 Microchemical analysis result of the THPed specimen obtained by SEM-EDS.

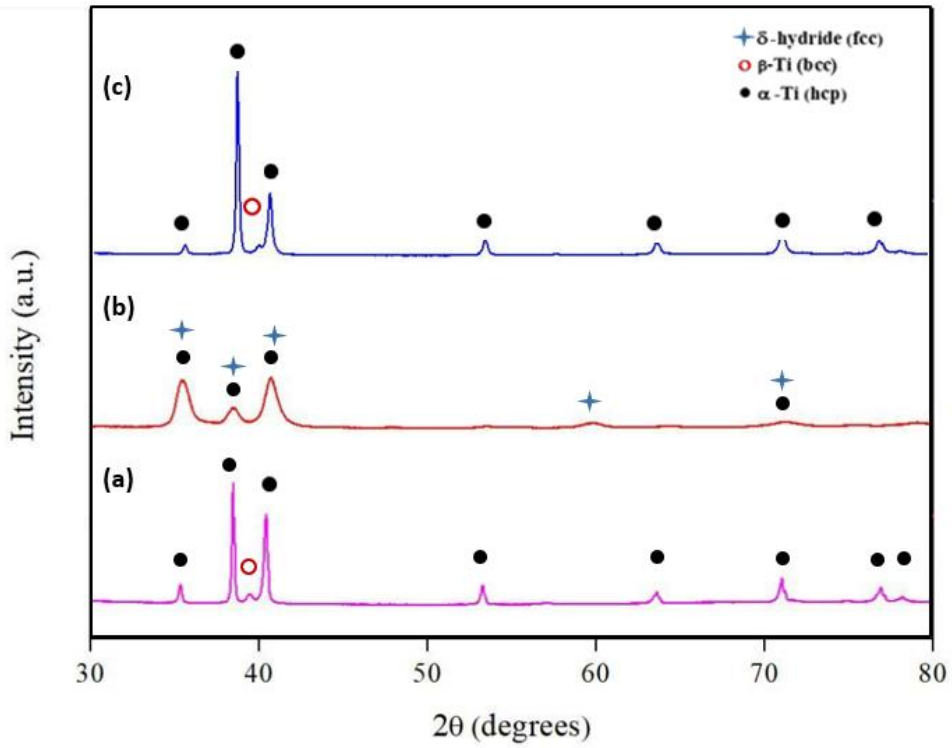

Figure 4.9 XRD patterns of the Ti-6Al-4V alloy specimens in (a) as-received, (b) hydrogenated at 650 °C for 1 h, and (c) dehydrogenated at 700 °C for 18 h conditions.

4.1.3 Nitrided Ti-6Al-4V Alloy

In this study, Ti-6Al-4V alloy nitrided at different conditions have been examined. The thickness of the surface layer and the microhardness value depends on two parameters in nitriding: time and temperature. Samples were tested under different environmental conditions (vacuum or nitrogen) and at different temperature and time combinations to determine the optimum variables. In the final stage of the process, the samples were cooled in the furnace under high-purity nitrogen. EDS line analysis was performed to analyze the diffusion of nitrogen into the specimen from the surface to the inner regions using the EDAX Pegasus EDS system connected to the scanning electron microscope. The change in element content was examined, and microchemical analyses were performed on the material.

The following section summarizes the microstructural evolution and chemical compositional changes that occurred in the Ti-6Al-4V alloy subjected to nitriding under different conditions. It is known that temperature and time directly affect nitriding. Therefore, in this study, the effect of temperature and time was investigated in order to determine the optimum parameters. The primary factor that influences diffusion is temperature. The formula for the diffusion coefficient D for mass transport is typically expressed as:

$$D = Do\ exp\left(-\frac{Qd}{RT}\right) \qquad \text{(Equation 4.1)}$$

This equation illustrates how the diffusion coefficient changes with temperature. The diffusion coefficient increases with increasing temperature. The equation for D reveals an exponential dependence on T. Do is the pre-exponential constant, Qd is the activation energy, and R is the gas constant.

The diffusion layer thickness ($\bar{\Delta}$) refers to the distance over which a concentration gradient exists in a material due to the process of diffusion. Diffusion layer thickness depends on time and diffusion coefficient according to equation 4.2.

$$\bar{\Delta} = \sqrt{2Dt} \qquad \text{(Equation 4.2)}$$

Table 9 Summary of compound layer thickness and EDS results depending on the nitriding conditions.

Nitriding Conditions	**Compound Layer Thickness (µm)**	**Nitrogen Content (wt.%)**
850 °C 5h (vacuum)	7.21 ± 1.18	8.37
950 °C 5h (vacuum)	4.36 ± 0.56	7.99
950 °C 1h (vacuum)	6.92 ± 1.04	7.67
950 °C 1h (nitrogen)	5.19 ± 0.98	12.99
950 °C 10 h (vacuum)	28.04 ± 1.55	7.40

The first specimen was heated under vacuum at 850 °C for 5 h and then cooled under nitrogen gas, and the surface layer thickness was measured. According to the thickness results taken from 10 different locations, the compound layer thickness was 7.21 µm (Figure 4.10 (a)). EDS analysis (Figure 4.10 (a)) was applied using the line scan method from the compound layer to the parent material interface. Nitrogen content was 8.37 wt.% in this sample. It was observed that oxidation could not be prevented. The other sample, where all other conditions were kept constant except for temperature, was heated under vacuum at 950 °C for 5 h, then cooled under nitrogen, and the compound layer thickness was measured. According to the thickness results taken from 10 different locations, this sample's compound layer thickness was 4.36 µm (Figure 4.10 (b)). EDS analysis (Figure 4.10 (b)) was applied using the line scan method from the external layer surface to the parent material interface. According to the analysis results, the nitrogen content of this sample was 7.99 wt.%. In the nitriding process, the diffusion coefficient reveals an exponential dependence on T. Therefore, as the nitriding temperature increases, the layer thickness is expected to increase substantially (Equation 4.1), yet in this case, as temperature increased, oxidation could not be prevented, so the compound layer could not adhere well to the surface due to elastic mismatch and nitrided layer was separated from the parent material. When the two samples nitrided at two different temperatures under vacuum were compared, it was seen that even though all other conditions were the same, the temperature increase affected the compound layer structure. Although oxygen pickup could not be prevented completely, the layer thickness was higher at lower temperatures due to better adhesion.

Compared to similar studies in the literature, the layer thickness is expected to increase as temperature increases [54]. Although there is not a remarkable difference between the thickness of the compound layers at different temperatures, this can be attributed to the fact that nitrogen diffusion was not provided equally for both samples during the experiment because of the improper adhesion to the surface under both applied conditions combinations. In other words, a homogeneous and well-adhered non-porous layer could not be obtained on the surface in both cases.

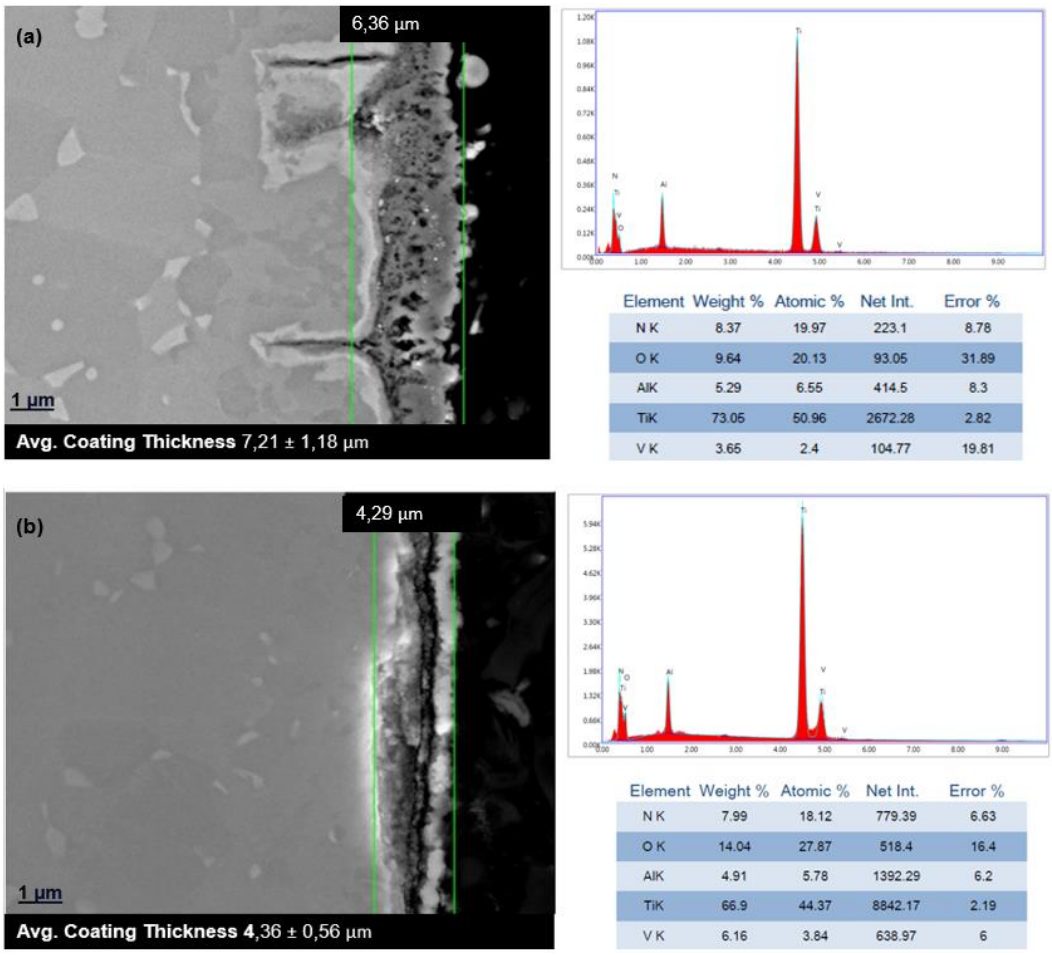

Figure 4.10 (a) FEG-SEM image and microchemical analysis of the sample surface heated under vacuum at 850 °C for 5 h and then cooled under nitrogen gas (b) FEG-SEM image and microchemical analysis of the sample surface heated under vacuum at 950 °C for 5 h and then cooled under nitrogen gas.

As seen in Figure 4.10, the temperature difference did not make a considerable difference in the structure and thickness of the compound layer. In order to prevent oxidation from occurring in the experiment, the heating conditions were changed from vacuum to nitrogen gas environment., and the effect of heating conditions on oxidation was investigated.

As a result of oxidation occurring during the process, heating conditions and nitriding time were changed. Since the temperature effect is more dominant than time in the diffusion process, the processing time was reduced to 1 h to reduce the samples' exposure to the atmosphere where oxidation occurs. However, the higher nitriding temperature of 950 °C has been utilized to reach a certain thickness of the layer.

Firstly, the sample was heated under vacuum at 950 °C for 1 h and then cooled under nitrogen, and the layer thickness was measured. According to the nitrided layer thickness results taken from 10 different locations, this sample's layer thickness was 6.92 µm (Figure 4.11 (a)). EDS analysis (Figure 4.11 (a)) was applied using the line scan method from the external layer surface to the parent material interface. It was determined that there was a considerable amount of oxygen pickup in the sample. Nitrogen content was 7.67 % in this sample. It was observed that the compound layer separated from the parent material at several points, and also oxidation could not be prevented. Then, the sample was heated under nitrogen gas atmosphere at 950 °C for 1 h and then cooled under nitrogen gas, and the layer thickness was measured. This sample's layer thickness taken from 10 different areas was 5.19 µm (Figure 4.11 (b)). EDS analysis (Figure 4.11 (b)) was applied using the same method from the external layer surface to the parent material interface. However, the average layer thickness decreased only slightly. As a result, it was observed that oxidation could not be prevented entirely in the samples heated in vacuum, but when the same experiment was repeated in nitrogen environment, well adhered non-porous compound layer was obtained.

In this study, the time-dependent change of the thickness of the diffusion layer during the nitriding process at a constant temperature was also investigated. Tests were continued at 950 °C to investigate the effect of time on the gas nitriding process, where all other conditions were kept constant. The diffusion layer thickness ($\overline{\Delta}$) refers to the distance over which a concentration gradient exists in a material due to diffusion. According to Equation 4.2, as time increases at a constant temperature, the thickness of the diffusion layer is expected to increase.

In order to fully observe the effect of nitriding duration on the material, the nitriding duration was increased to 10 h compared to the previous sample for comparative analysis. The sample was heated under vacuum at 950 °C for 10 h and then cooled under nitrogen, and the compound layer thickness was measured.

The thickness of the diffusion layers was derived for samples nitrided at 950 °C for 1 and 10 h, respectively, using the below equations.

$$\bar{\Delta} = \sqrt{2D(1)} \qquad \text{(Equation 4.3)}$$

$$\bar{\Delta} = \sqrt{2D(10)} \qquad \text{(Equation 4.4)}$$

When the nitriding time increases from 1h to 10 h, the diffusion layer thickness is expected to increase by a factor of $\sqrt{10}$ due to the square root relationship between time and diffusion distance. According to the layer thickness results taken from 10 different locations in the sample treated under nitrogen gas under the same conditions, this sample's layer thickness was 28.04 µm (Figure 4.12 (b)). EDS analysis (Figure 4.12 (b)) was applied using the line scan method from the external layer surface to the parent material interface. According to the analysis results, it was determined that there was a high amount of oxygen pickup in the sample. Nitrogen content was 7.4 wt.% in this sample. It was observed that an undesirable porous layer was formed, and oxidation could not be prevented. As time increased, the porous structure in the coating became more pronounced. In addition, when the sample that was subjected to nitriding for 1 at 950 °C, where all other conditions were the same except for the processing time, was compared with the sample that was subjected to nitriding for 10 h at 950 °C, there was a considerable increase in the coating layer thickness as the processing time increased. The compound layer thickness of the 1 h nitrided sample was 4.36 µm; when the processing time was increased to 10 h, the compound layer thickness increased to 28.04 µm. As the processing time increased, the coating layer thickness increased by almost a factor of √(10), as expected from Equations 4.3 and 4.4.

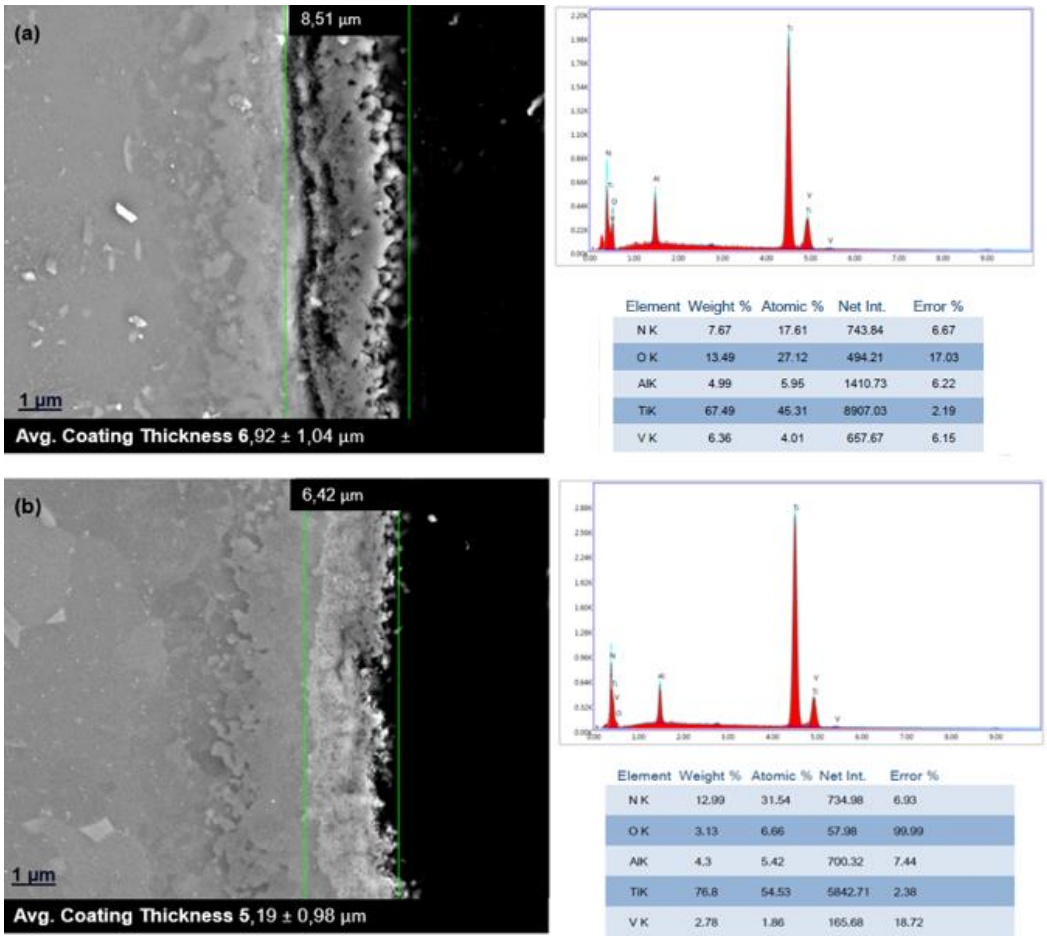

Figure 4.11 FEG-SEM image and microchemical analysis of the sample surface heated under vacuum at 950 °C for 1 hour and then cooled under nitrogen gas (b) FEG-SEM image and microchemical analysis of the sample surface heated under nitrogen gas at 950 °C for 1 hours and then cooled under nitrogen gas.

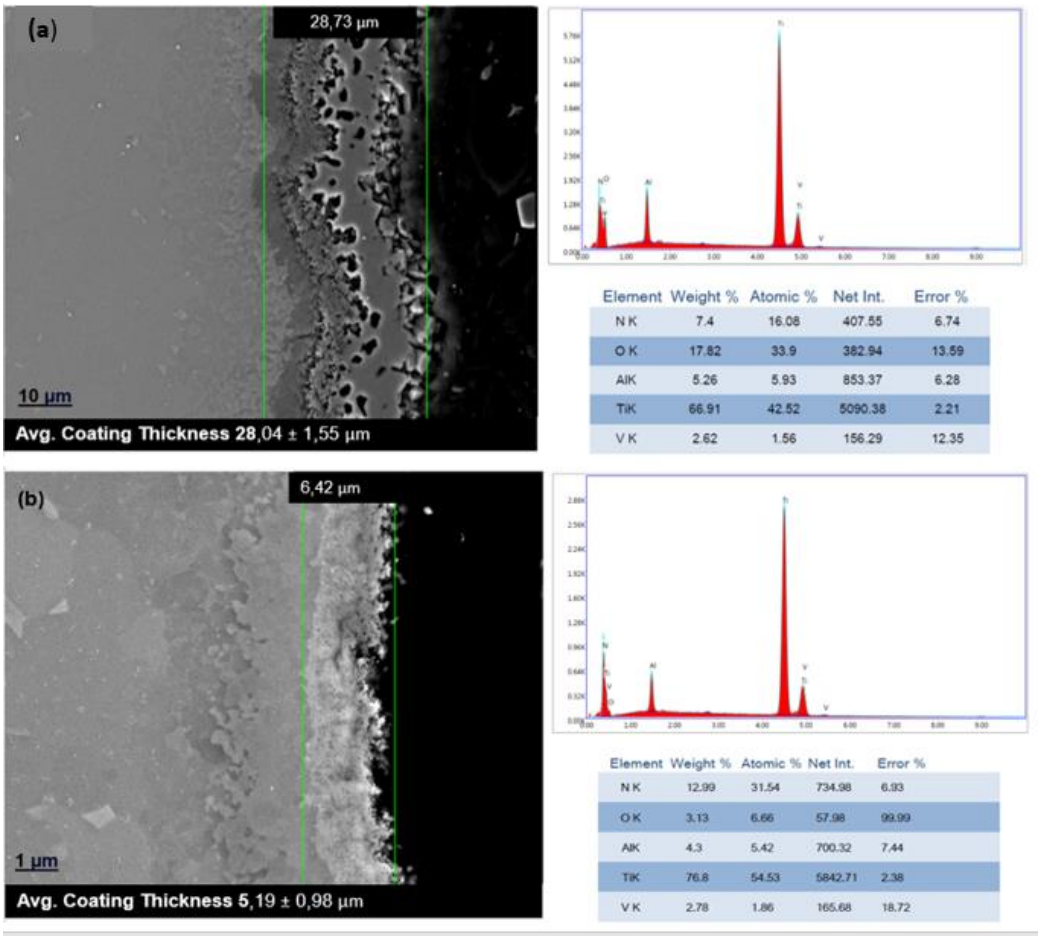

Figure 4.12 (a) FEG-SEM image and microchemical analysis of the sample surface heated under vacuum at 950 °C for 10 h and then cooled under nitrogen gas (b) FEG-SEM image and microchemical analysis of the sample surface heated under nitrogen gas at 950 °C for 1 h.

In the samples, which were nitrided at 950 °C for 10 h, the effect of the atmosphere used during heating didn't yield reproducible results in terms of oxygen content and compound layer possibly due to prolonged exposure to high temperature. On the other hand, nitriding at 850 °C did not produce a continuous and thick coating layer. Therefore, heating under a nitrogen atmosphere and nitriding at 950 °C for 1 h was chosen as the optimum process condition because of the reproducibility. Although there was some oxidation in the optimum parameter set, as in all other parameters, the expected non-porous nitride layer formation was observed.

In addition, it was observed that the layer thickness was higher in this study compared to similar studies in the literature. In the study by Lee et al. [70], a compound layer with a thickness of approximately 2.5 µm was formed in Ti-6Al-4V alloys subjected to gas nitriding at 850 °C for 1 h. When the time was increased to 12 h at the same temperature, a 5 µm thick compound layer consisting of Ti_2N and TiN was formed after nitriding. In this study, a compound layer with an average thickness of 7.21 µm was formed in the sample that was nitrided at 850 °C for 5 h. As mentioned in Section 2.5.2, the increase in gas permeation in the gas nitriding process may have accelerated the growth of the nitride zone.

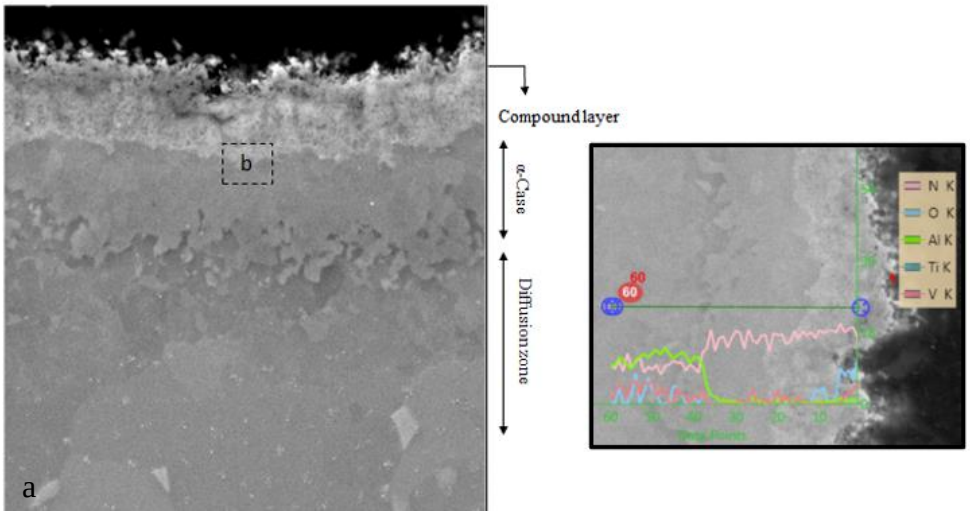

Figure 4.13 α-case formation on the sample nitrided at 950 °C for 1 h heated under nitrogen gas atmosphere.

As mentioned in Section 2.5.2.1, the formation of the α-case (Al-rich) can be observed in samples subjected to high temperatures during nitriding. In this study, since the nitriding process was carried out at relatively high temperatures (850-950 °C), the formation of the α-case was observed in all nitrided samples. This structure was confirmed through microstructural observations and EDS analyses. Figure 4.13 shows that microstructure and chemical analysis of the sample nitrided at 950 °C for 1 h heated under nitrogen gas atmosphere.

In the literature, it has been indicated that, following the nitriding process, the original metallic silver color of the material transforms into shades of blue, golden, and gray. Specifically, at initial lower temperatures (below the β-transus temperature), the silver metallic color of the titanium alloy changed to shades of blue and golden, with the reported increase in the intensity of these colors being associated with the elevated nitriding temperature and duration [71]. In this study, specimens processed at 850 °C and 950 °C exhibited a transformation of the silver metallic color into golden tones.

Microchemical analyses performed with the EDS system showed that the layer formed was composed of nitride phases. After the nitriding process, XRD analysis was conducted on the samples to identify the potential nitride phases on the surface and determine the other phases in the microstructure. Considering the nitriding conditions and the phases determined through XRD analysis, the optimal conditions for nitriding were determined to be heating under nitrogen gas and nitriding at 950 °C for 1 h. In other samples processed under different conditions, a notably higher rate of oxidation was observed, leading to detachment of the nitrided layer from some regions of the alloy surface. Figure 4.14 presents the XRD analysis result of the sample heated to 950 °C under nitrogen gas, followed by a 1 h nitriding process. According to the analysis, simultaneous nitriding and oxidation occurred on the layer surface. The layer consists of $TiVO_4$ along with minor phases of Ti_2N and TiN. Furthermore, the oxidation of the alloy at 950 °C for 1 h led to the formation of a thin TiVO4 layer on the surface. Considering the EDS results, it is evident that oxidation primarily occurred on the layer surface. Nitrogen diffused into the Ti-6Al-4V alloy, where the layer on the surface consisted of TiN as the major phase and Ti_2N as the minor one. Al, V, and O were dissolved in the layer. Considering the energy resolution and tolerances of the EDS system, it was evaluated that the primary material was within the standard composition range of Ti-6Al-4V. However, since a proper vacuum environment could not be created for the samples heated under vacuum, it was observed that more oxidation occurred during the heat treatment stage,

and the layer was separated in some areas. Oxidation at 950 °C and 850 °C for different time intervals formed TiO_2 and $TiVO_4$ layer on the surface. It was observed that oxidation decreased in the samples that were nitrided by heating under nitrogen. In addition, it was observed that in samples heated under nitrogen, the layer became more porous as time increased, and oxidation increased as well, according to EDS results.

According to EDS line scan analysis, it was also observed that oxygen decreased from the outer layer to the inside. Titanium alloys have high strength and low elastic modulus. The elastic modulus of the TiN layer is two to six times higher than the elastic modulus of the core material. Due to this difference between the nitrided layer and the core material, the nitrided layer may have separated from the parent material in some parts. When all the results were considered, it was seen that the sample heated under nitrogen gas and nitrided at 950 °C for 1 h, followed by cooling under nitrogen gas, had the best results.

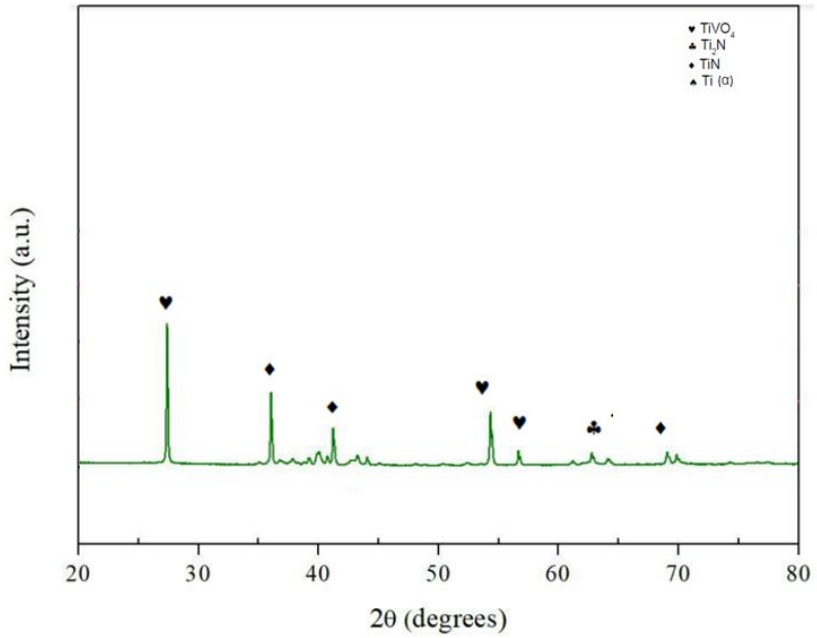

Figure 4.14 XRD analysis of nitrided specimens at 950 °C for 1h (heated and cooled under nitrogen atmosphere).

4.1.4 Nitrided and THPed Specimens

Specimens that were subjected to a 2-step modified THP process after 1 h of nitriding under nitrogen at 950 °C were examined in this section. The sample heated under nitrogen and nitrided at 950 °C for 1 h was determined to contain the best nitrided surface layer, considering the layer thickness and structure together with diffusion into the surface. Two-dimensional distributions of major elements were determined by EDS along the cross-section of the surface layer. Al and V distributions (Figure 4.17) were observed to be compatible with the enrichment of Al and decrease of V in the α microstructure, and the enrichment of V and reduction of Al in the β microstructure. The hydrogen removal step in THP aims to refine the microstructure and reduce residual stresses by transforming the hydrogen-enriched δ-hydride phase into a finer α phase in equilibrium through hydrogen recovery in the sample. As evident from the optical microscope and SEM images (Figure 4.15 and 4.16), the material's microstructure has been refined through the THP process applied after nitriding. Following the hydrogen absorption process, a relatively finer microstructure consisting of a mixture of α and β phases has been formed. The δ-hydride phase lost hydrogen during dehydrogenation and transformed into a finer α phase. Hydrogen levels in the α and β phases of hydrogenated samples decreased after the hydrogen removal. Additionally, the reformation of the α phase along grain boundaries and within grains has been observed as a consequence of the transformation from the δ-hydride phase to the α phase . Since the δ-hydride phase transforms back into the α phase by hydrogen removal, the precursor α phase formed at grain boundaries in the produced samples could not be eliminated after the hydrogen removal process. Additionally, the layer formed due to nitriding is preserved even after THP. However, it was observed that the layer thickness decreased slightly after THP. Figure 4.18 shows the presence of α-case, changing microstructure and compound layer after the consecutive application of nitriding and THP processes.

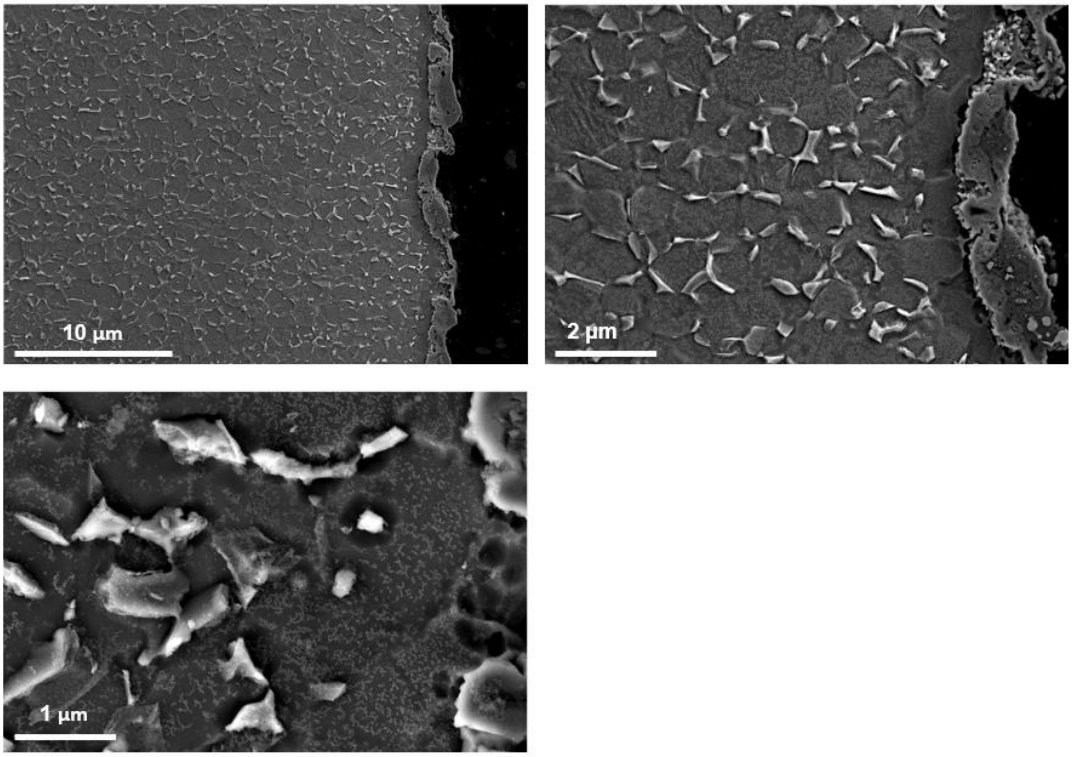

Figure 4.15 FEG-SEM images of the sample subjected to a 2-step modified THP (hydrogenation and dehydrogenation) process after nitriding at 950 °C for 1 h.

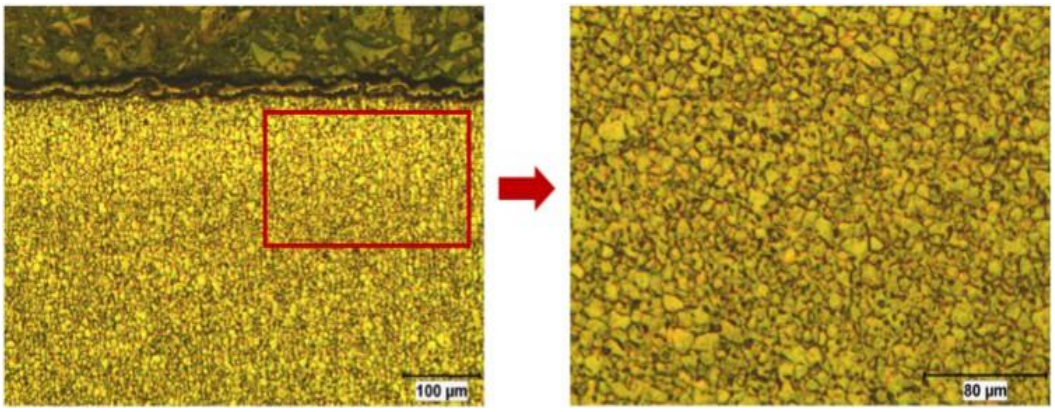

Figure 4.16 Optical images of the sample subjected to a 2-step modified THP (hydrogenation and dehydrogenation) process after nitriding at 950 °C for 1 h.

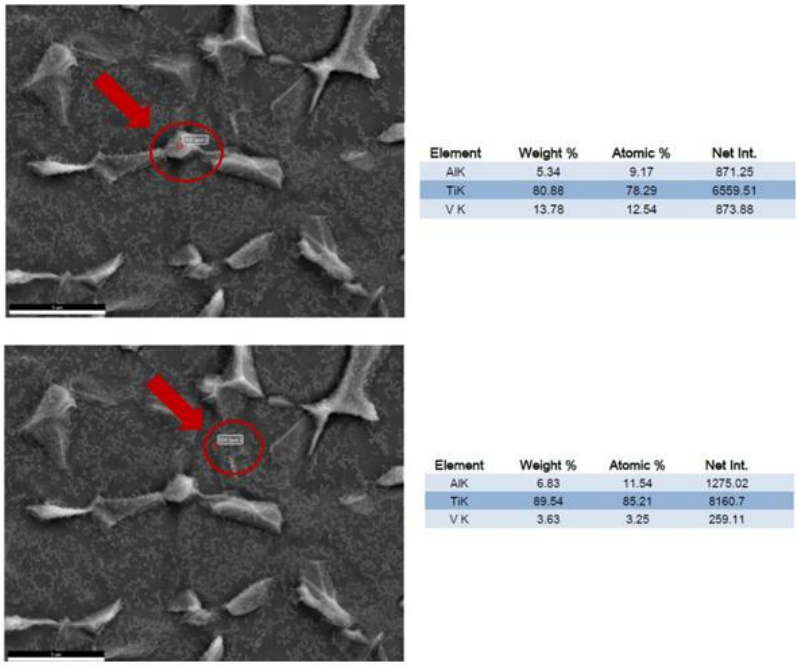

Element	Weight %	Atomic %	Net Int.
AlK	5.34	9.17	871.25
TiK	80.88	78.29	6559.51
V K	13.78	12.54	873.88

Element	Weight %	Atomic %	Net Int.
AlK	6.83	11.54	1275.02
TiK	89.54	85.21	8160.7
V K	3.63	3.25	259.11

Figure 4.17 Microchemical point analysis on the THPed specimen after nitriding for 1 h at 950 °C a) β phase b) α phase.

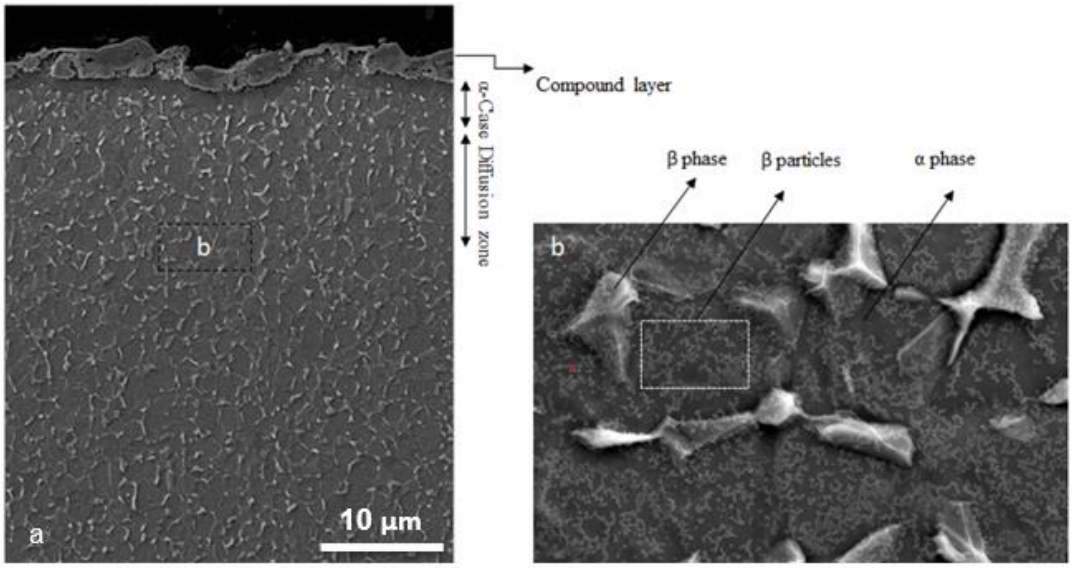

Figure 4.18 Presence of α-case, changing microstructure, and compound layer after the consecutive application of nitriding and THP processes.

4.2 EBSD Analysis

EBSD studies were done to clarify the specimens' microstructural development in the transverse directions. Grain Size, Kernel Average Misorientation (KAM), and Grain Orientation Spread (GOS) maps were analyzed for as-received, THP treated (THPed), nitrided, and THPed after nitriding samples.

Grain size distribution curves of as-received, THPed, nitrided, and THPed after nitriding samples are shown in Fig. 4.19. As-received samples had the finest microstructure compared to heat-treated samples. The coarser grains were obtained after the THP and nitriding processes. According to the EBSD results while the average grain size of the as-received sample was 0.85 ± 0.24 µm, the average grain size after the THP process reached to 2.83 ± 0.93 µm, and after nitriding, it reached to 3.21 ± 1.17 µm. The THP process applied after the nitriding process reduced the grain size relatively. The average grain size of THPed after nitriding sample was 2.88 ± 1.01 µm. Therefore, when the starting materials have a coarser microstructure, THP could considerably improve grain refinement.

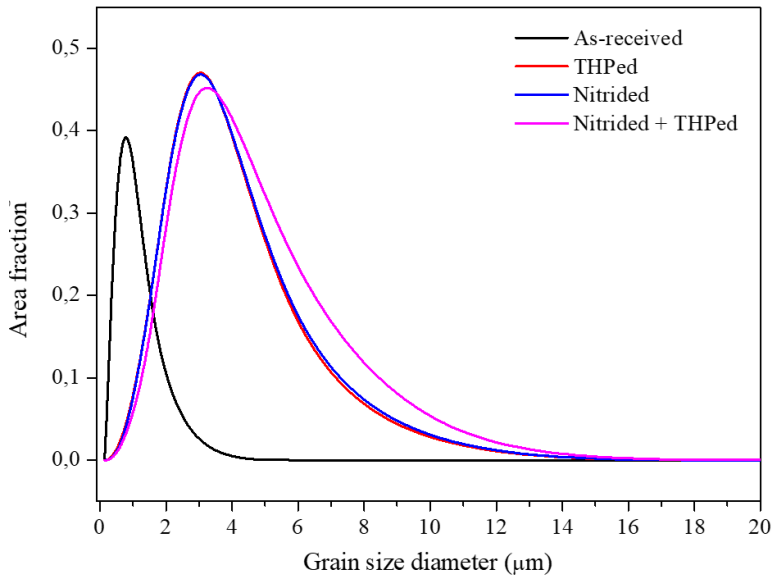

Figure 4.19 Grain size distributions of the as-received, THPed, nitrided, and THPed after nitriding samples.

KAM values give information about average local grain misorientation. GOS values provide information on plastic strain and dislocation density. GOS and KAM are high due to higher dislocation density when a material is highly deformed. KAM and GOS maps are given in Fig. 4.20 and 4.21. Corresponding KAM and GOS distributions of the as-received, THPed, nitrided, and THPed after nitriding samples are shown in Fig. 4.22 and 4.23, respectively. KAM values are 1.41 ± 0.8, 0.50 ± 0.2, 0.39 ± 0.23, and 0.46 for as-received, THPed, nitrided and THPed after nitriding samples, respectively. According to the KAM results, as-received samples had the highest value, and nitrided samples had the lowest KAM value. Both KAM and GOS maps were labeled with a rainbow scale, where blue represents the minimum and red represents the maximum. The blue regions observed on the KAM maps (Fig. 4.20 (a), (b), (c), (d)) of the heat-treated samples can be identified as recrystallized grains. Additionally, as expected, the KAM value decreased with increasing heat treatment temperature. It was noted that the nitrided sample treated at a higher temperature exhibited a greater number of recrystallized grains compared to the THP-treated sample.A similar trend with KAM values was observed for the GOS values. GOS values were 1.25 ± 0.61, 0.43 ± 0.22, 0.37 ± 0.19, and 0.39 ± 0.24 for as-received, THPed, nitrided, and THPed after nitriding samples. The GOS map expresses dislocation density on a grain-by-grain basis, scaling from blue to red. Blue (minimum) represents low dislocation density, while red indicates regions with maximum dislocation density. GOS is also used to distinguish recrystallized grains. Grains with a GOS value below 1.5 represent recrystallized ones [72]. The as-received sample has the highest GOS value according to GOS maps (Figure 4.21 (a)). While the extent of blue regions indicates recrystallization, other colors on the map indicate grains with relatively different orientations in the material. Occurrences of grain growth and recrystallization were observed in the GOS maps of the heat-treated samples (Fig 4.21 (b), (c), (d)). After THP (Figure 4.21 (b)) and nitriding processes (Figure 4.21 (c)), it is observed that the dislocation density has diminished, and nearly complete recrystallization has taken place according to GOS maps.

When the GOS maps and distributions of the THPed samples and those THPed after nitriding were compared, it was observed that the dislocation density and amount of recrystallization in the microstructure were close to each other (Figure 4.21 (b) and (d)).

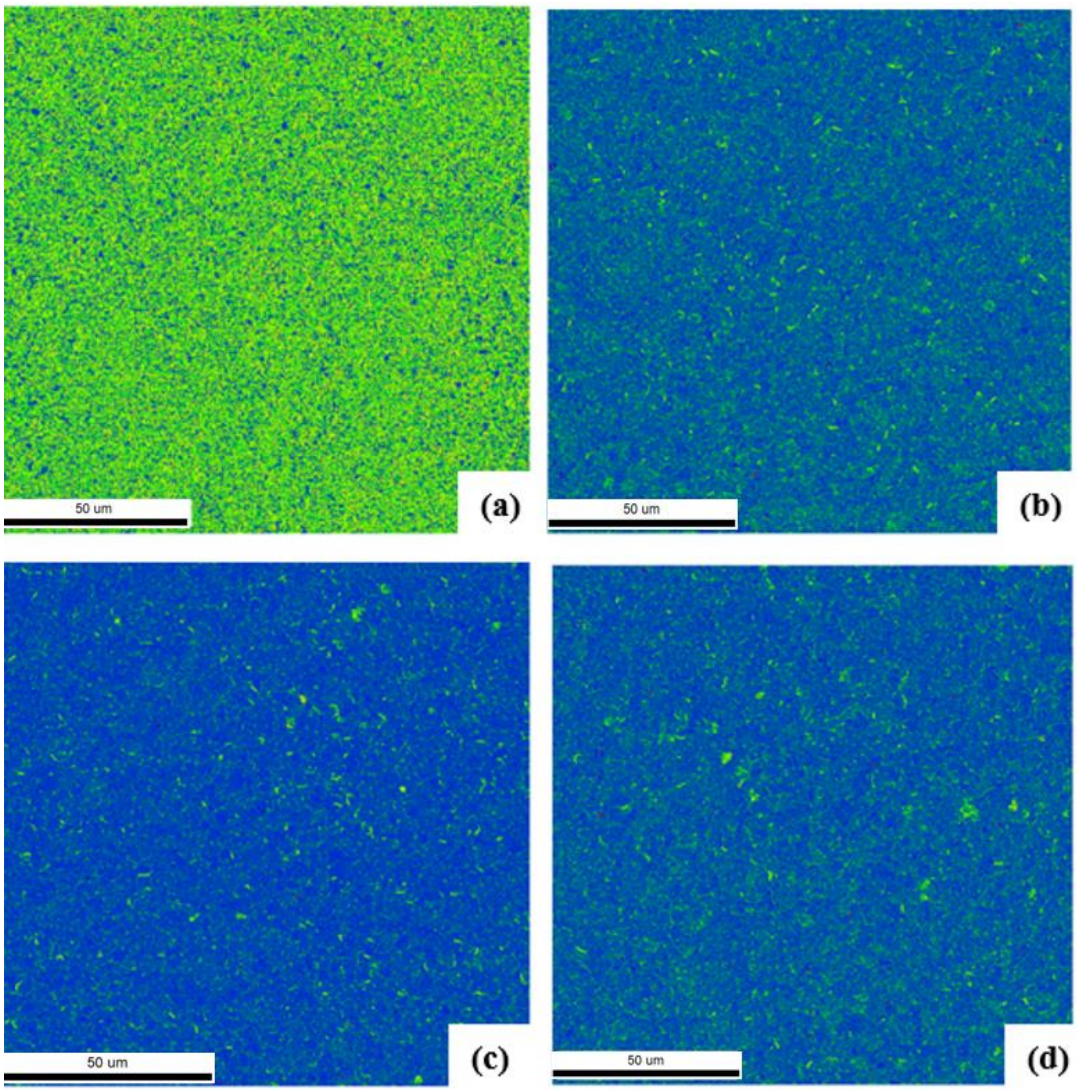

Figure 4.20 KAM maps of (a) as-received, (b) THPed, (c) nitrided, and (d) THPed after nitriding samples (transverse direction).

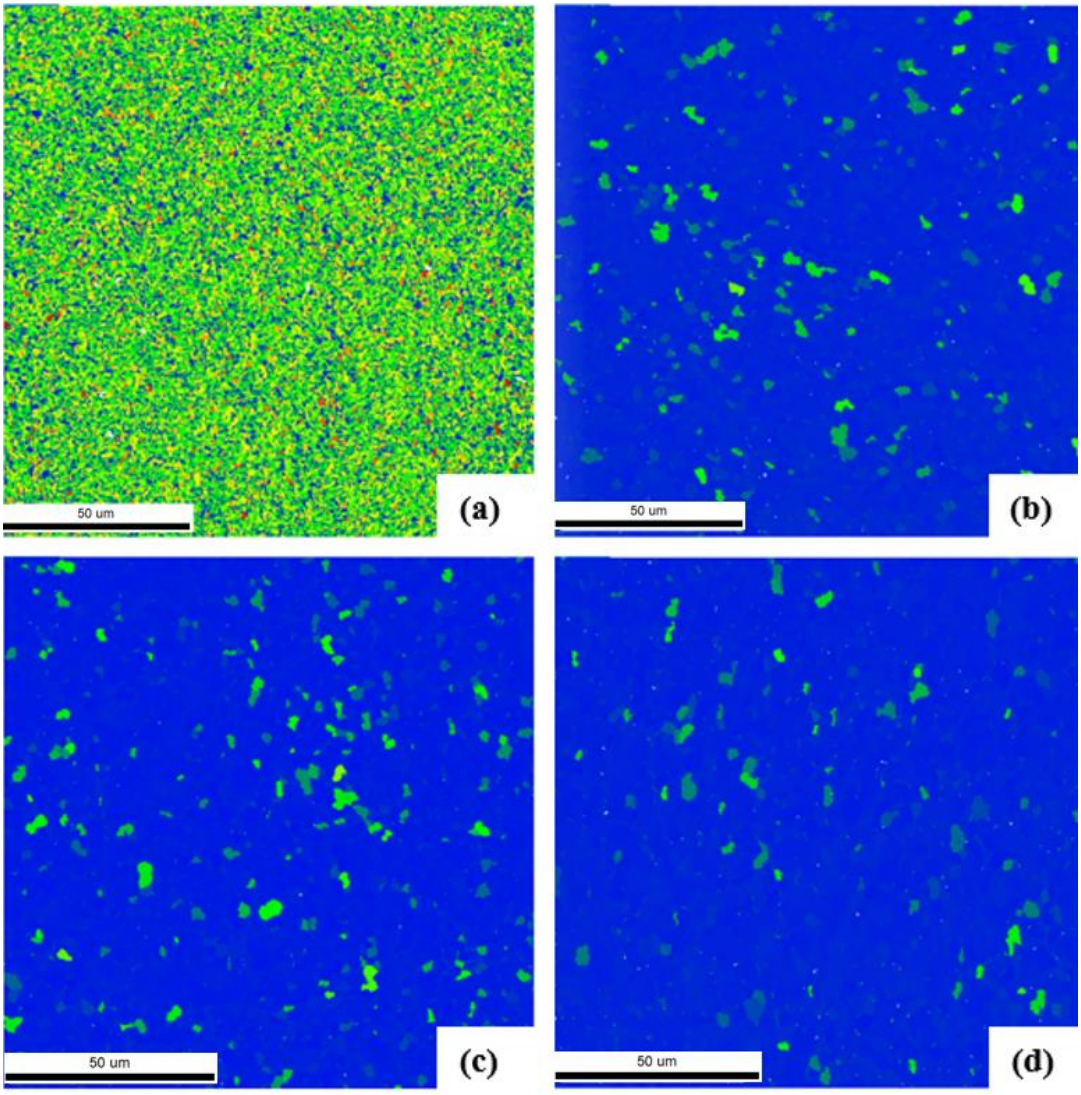

Figure 4.21 GOS maps of (a) as-received, (b) THPed, (c) nitrided, and (d) THPed after nitriding samples (transverse direction).

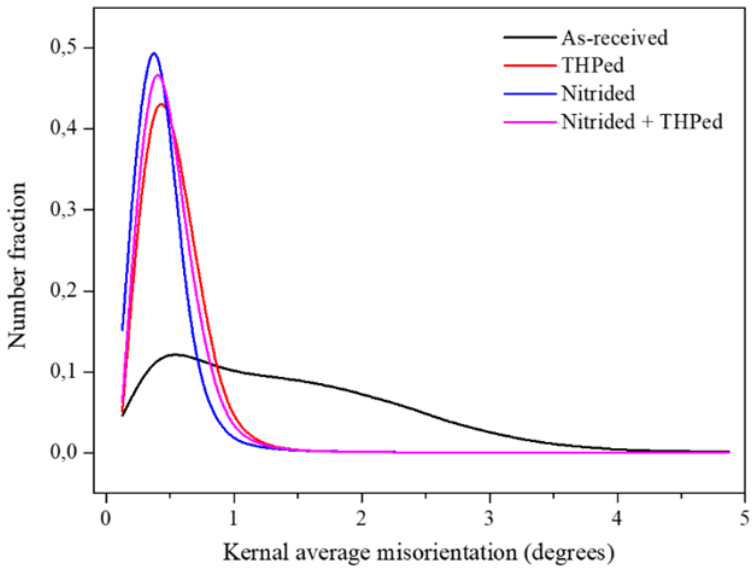

Figure 4.22 KAM distributions of as-received, THPed, nitrided, and THPed after nitriding samples.

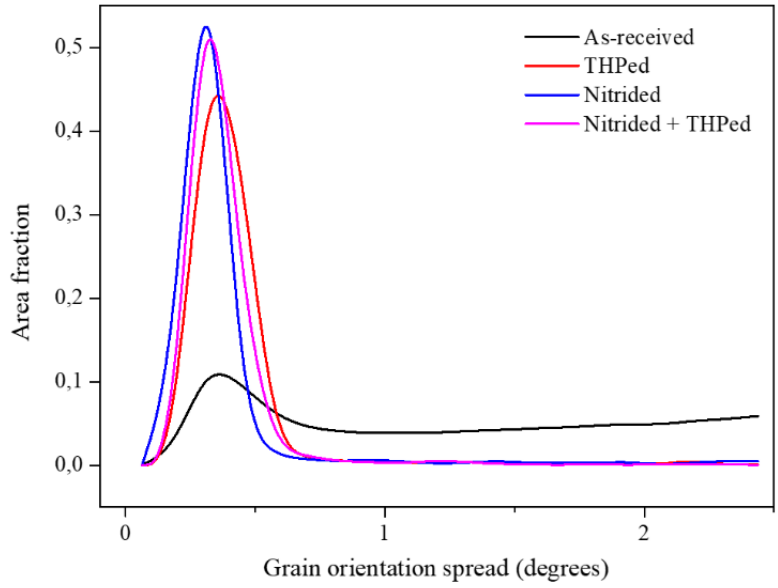

Figure 4.23 GOS distributions of as-received, THPed, nitrided, and THPed after nitriding samples

4.3 Mechanical Properties

4.3.1 Microhardness Measurements

The effect of applied heat treatment and surface processing on the hardness values of surface and subsurface regions was determined according to the ASTM E92-17 standard by Vickers hardness measurements for as-received, hydrogenated, dehydrogenated, nitrided, and THPed samples after nitriding samples. Fig. 4.24 shows the compound layer hardness values of as-received, surface processed and THPed alloys. The initial compound layer hardness of 321 HV seen in as-received samples was increased to ~450 HV due to the formation of a hard δ-phase (Figure 4.5). However, dehydrogenation, simply THP, reduced the alloy hardness down to ~380 HV, which was still above the hardness value of the as-received sample. THP refined the microstructure, while it caused the transformation of -phase back into, which caused a reduction in hardness value. On the other hand, nitriding induced the formation of a hard nitrogen-rich compound layer (containing TiN + TiN2 phases) and -case with the diffusion layer with slight oxide formation on the surface (Figure 4.13), thereby increasing the hardness up to ~620 HV. The highest hardness of ~820 HV was obtained in the sampled which was THPed after being nitride. Both the formation of a nitrogen-rich layer and refined microstructure (Figure 4.15) increased the hardness of the alloy. Oxidation of the surface was thought to be one of the reasons for increased hardness as well due to prolonged exposure to high temperatures during THP.

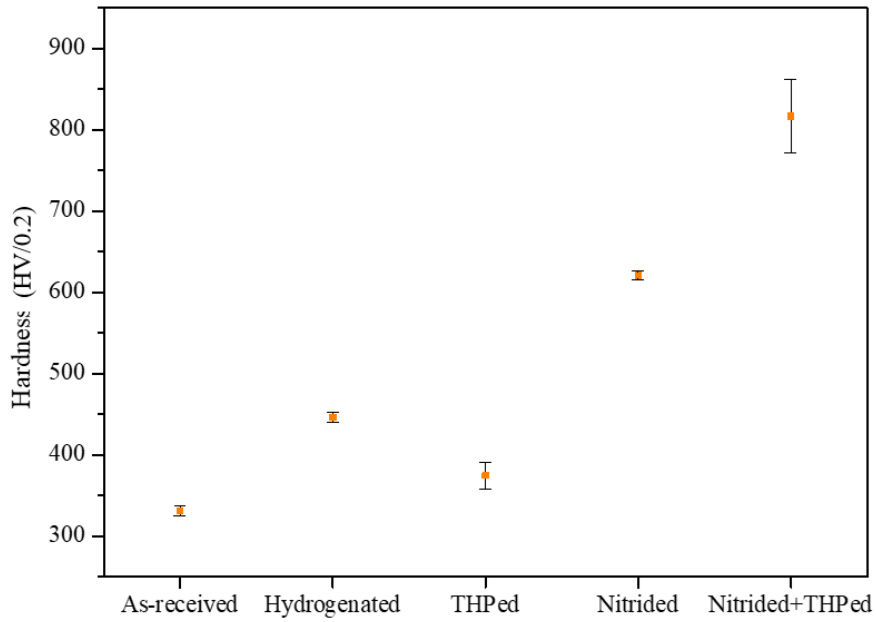

Figure 4.24 Compound layer hardness values of as-received, surface processed and THPed samples.

The second set of hardness measurements were done along the cross-section of the samples, close to surface region of as-received samples and THPed samples, and just beneath the hardened compound layer of nitrided samples (Figure 4.25).

The as-received samples' average hardness value just beneath the surface layer was found to be minimum, around 321 HV. Approximately a 35-40% increase was detected in hardness value as a result of hydrogenation, which was attributed to the formation of δ phase (TiH_2) in the sample (Figure 4.9). Nevertheless, the hardness of the specimen experienced a reduction after the dehydrogenation step, similar to hardness taken from the surface of the samples, owing to the transformation δ phase formation back into α-phase. Despite the observed hardness decrease after the dehydrogenation step, the hardness of the dehydrogenated samples was higher than that of the as-received sample because of the refined microstructure. As mentioned previously, the most suitable nitriding parameters were chosen as 950 °C and 1 h by using a nitrogen atmosphere during the heating and cooling stages of the nitriding process. Gas nitriding of as-received samples using selected process variables caused

an increase in the hardness value of as-received sample from 321 to 447 HV, close to hardness of hydrogenated sample. As shown in 4.13, nitriding results in the formation of nitride compounds on the outermost surface layer, -case, and solid solution of nitrogen dissolved α phase just beneath the compound layer. The average hardness values shown in Figure 4.23 belong to average hardness of α-case and solid solution of nitrogen dissolved α regions since it was difficult to do hardness measurements at compound layer along the cross-section. The sample experienced 2-step THP process (hydrogenation + dehydrogenation) after nitriding under the same nitriding conditions had the highest average hardness value of 544 HV. Although nitriding forms nitride compounds on the surface layer, α-case and solid solution of nitrogen dissolved α, application of THP refines the microstructure as well in addition to the microstructure obtained in nitriding. Therefore, combined effect of refined microstructure and nitriding related microstructure resulted increased hardness. Mukhtar et al. [64], who worked on nitriding of the SLM Ti64 parts at 850 ^{o}C for 4 hours, detected hardness values as high as 550 HV around compound layer. However, in the present study, the hardness measurements were taken at points below the compound layer.

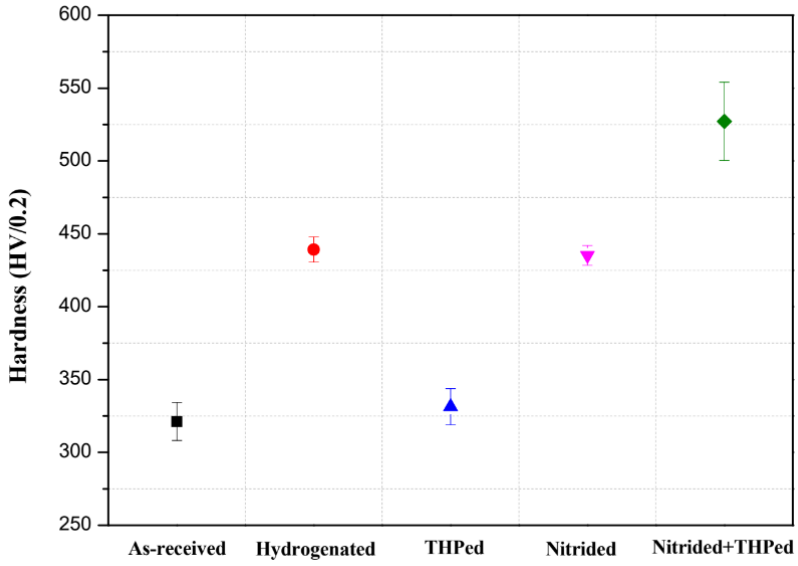

Figure 4.25 Cross-sectional diffusion layer hardness values of as-received, THPed, Nitrided and Nitrided + THPed samples.

The hardness profiles of nitrided samples were observed to be dependent on the atmosphere used during the heating stage. As presented in Table 7, the samples were heated to gas nitriding temperatures either in vacuum or nitrogen gas environments. Figure 4.26 displays the hardness profiles of nitrided samples at 950 °C for 1 h, which were heated under vacuum and nitrogen gas up to nitriding temperatures. The hardness profiles were produced to verify the depth of the hardened layer after nitriding. Since it was difficult to do hardness measurements in the outermost surface compound layer, hardness measurements started from the point just beneath the compound layer. The samples, which were nitrided only, were composed of α-case region and diffusion layers (nitrogen dissolved region) beneath the compound layer (TiVO, Ti_2N and TiN phases (Figure 4.13)). As can be seen in Figure 4.26, hardness decreases from the diffusion layer to interior regions and becomes constant where there is parent material only. However, the alloy heated under a nitrogen atmosphere displayed a higher hardness value throughout the hardness profile compared to the samples heated under a vacuum.

As presented in previous parts, heating under vacuum caused severe oxidation of the surface and resulted in a porous compound layer (Figure 4.11). Additionally, samples heated under vacuum showed less amount of dissolved nitrogen with respect to samples heated under nitrogen gas. Accordingly, the nitriding process (950 °C, 1h) carried out by heating under nitrogen gas resulted in higher hardness. On the other, for both types of samples, hardness layer thickness was found to be around 200 µm.

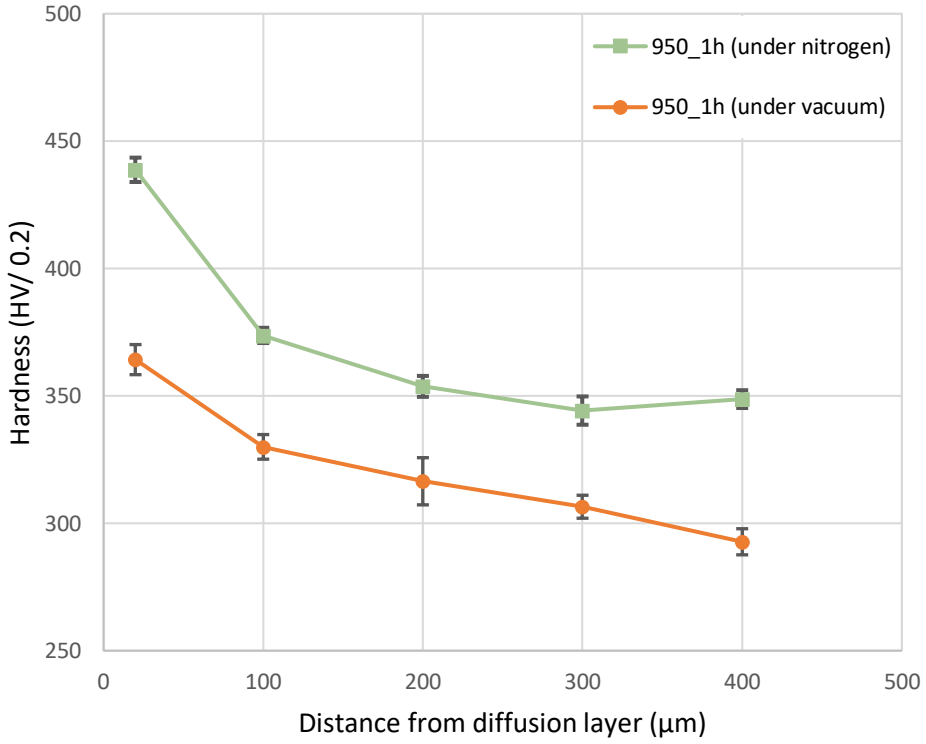

Figure 4.26 Hardness profiles of the cross-section of the diffusion layer on samples nitrided at 950 °C for 1h under vacuum or nitrogen atmosphere.

The comparison of hardness profiles taken from the cross-sections of samples nitrided only and THPed after nitriding are also given in Figure 4.27. Similar to other samples, hardness measurement was started just beneath the outermost compound layer. As can be seen, THPed samples, after nitriding, displayed higher hardness at any depth from the surface.

The depth of the hardened layer in samples nitrided only was around 200 µm, while it was ~400 µm for the samples THPed after nitriding. Similar to nitrided samples, nitrided + THPed samples contained compound layer, α-case and a diffusion layer (Figure 4.18). However, THP treatment after nitriding refined the microstructure, especially α phase, in which small β-platelets formed after THP. Therefore, the hardness value increased compared to nitrided samples. Moreover, the higher degree of oxidation may be one the reason of increased hardness. The application of THP in addition to nitriding increased the time of exposure to high temperatures (> 650 °C) at which titanium alloys are prone to oxidation. Since THP took an additional 19 h (1h for hydrogenation and 18 h for dehydrogenation) with respect to nitriding (1 h), the possibility of oxidation of nitrided + THPed samples was high.

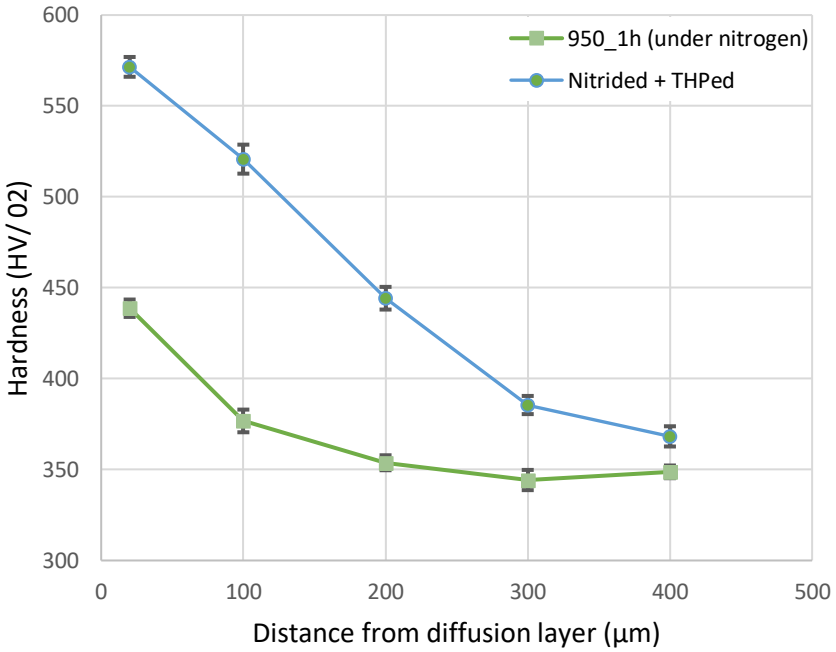

Figure 4.27 Hardness profiles of the cross-section of the diffusion layer of nitrided only and THPed after nitriding samples.

4.3.2 Tensile Testing

The tensile tests were applied to dog-bone-shaped specimens and the stress-strain curves for the samples in as-received and THPed, nitrided, and THPed after nitriding condition were presented in Figures 4.28 and 4.29, respectively. All of the samples displayed engineering stress-strain curves similar to wrought alloys, which include linear elastic region, strain hardening region subsequent to yielding, and fracture point. Based on Figure 4.29 and Table 10, Although THP treatment refined -the phase of the alloy, its effect on yield strength was not remarkable, possibly due to increased grain size. However, THP increased the UTS value, which accompanied the ductility decrease of about 25%. On the other hand, upon nitriding of the as-received sample at 950 ℃ for 1 h resulted about 12 and 10% decrease in yield and UTS values of the sample while the ductility remained almost constant. Although nitriding produced a hardened surface layer, it caused grain growth due to high process temperature of 950 ℃. Upon application of THP after nitriding process increased the yield strength and UTS slightly by 1-1.5% despite refinement of α-phase in nitrided sample. Therefore, grain coarsening encountered in nitrided samples was observed to be more effective in the strength of the samples. On the other hand, all of the samples including as-received one exhibited superior mechanical properties with respect to those defined in ASTM F136-13.

Figure 4.28 Tensile test specimens before testing, (a) as- received, (b) THPed (c) Nitrided + THPed, (d) Nitrided.

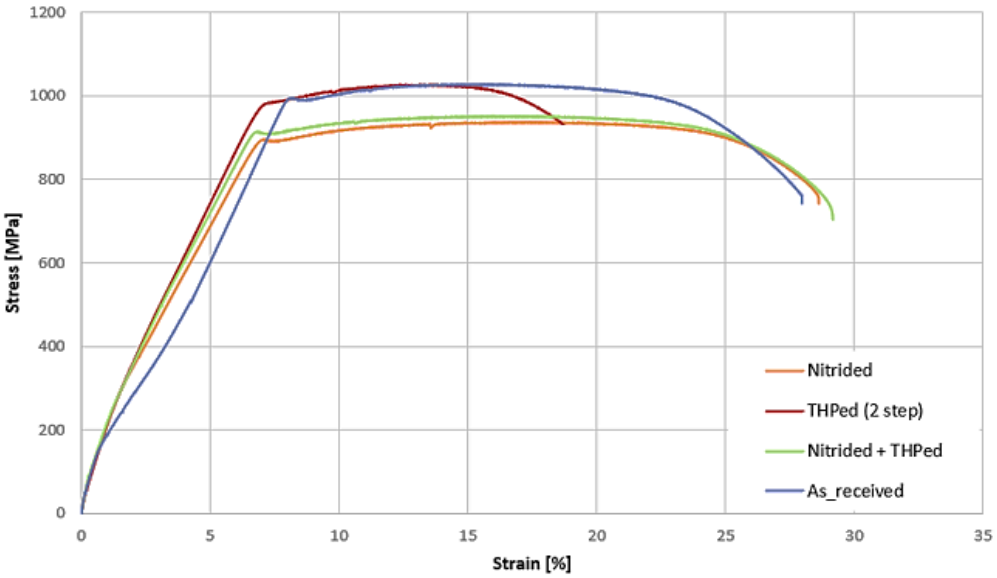

Figure 4.29 Stress-strain diagram of the as-received, THPed, Nitrided, and THPed after nitriding specimens.

Table 10 Tensile test results of the samples.

Sample	**Yield Strength (MPa)**	**Ultimate Tensile Strength (MPa)**	**Strain at Fracture (%)**
As-received	1015 ± 7.1	1035 ± 10.7	28 ± 0.9
THP	1010 ± 10	1050 ± 21.5	21 ± 2.7
Nitrided	893 ± 2.9	936 ± 0.4	27 ±1.1
Nitrided + THP	902 ± 3.2	951 ± 0.2	28 ± 2.8
ASTM F136-13	795	860.0	10.0

All the samples displayed cup-and-cone type fracture, which is seen in moderately ductile materials. As-received Ti-6Al-4V alloy fracture surface contained equiaxed dimples surrounded by shear lips, which is characteristic of ductile failure (Fig. 4.30 (a). The α+β phase containing microstructure in the as-received samples transformed into relatively thinner α phase when THP was applied. Therefore, tensile strength increased slightly, which induced smaller equiaxed dimple formation during fracture (Fig. 4.30 (b)). As presented previously, although nitriding 950 °C at 1 h induced a hard coating layer on the surface, it decreased the strength of the alloy due to increased grain size. The effect of grain growth was also seen in the fracture surfaces of the nitrided alloy by increased size of the equiaxed dimples (Fig. 4.31 (a)). On the other hand, the alloy THPed, after nitriding, exhibited equiaxed dimples with sizes larger than that of nitrided alloy (Fig. 4.31(b)). The prolonged processing time of around 19 h in THP, in addition to 1 h nitriding, resulted in coarser grain, which induced larger dimples in the fracture surfaces.

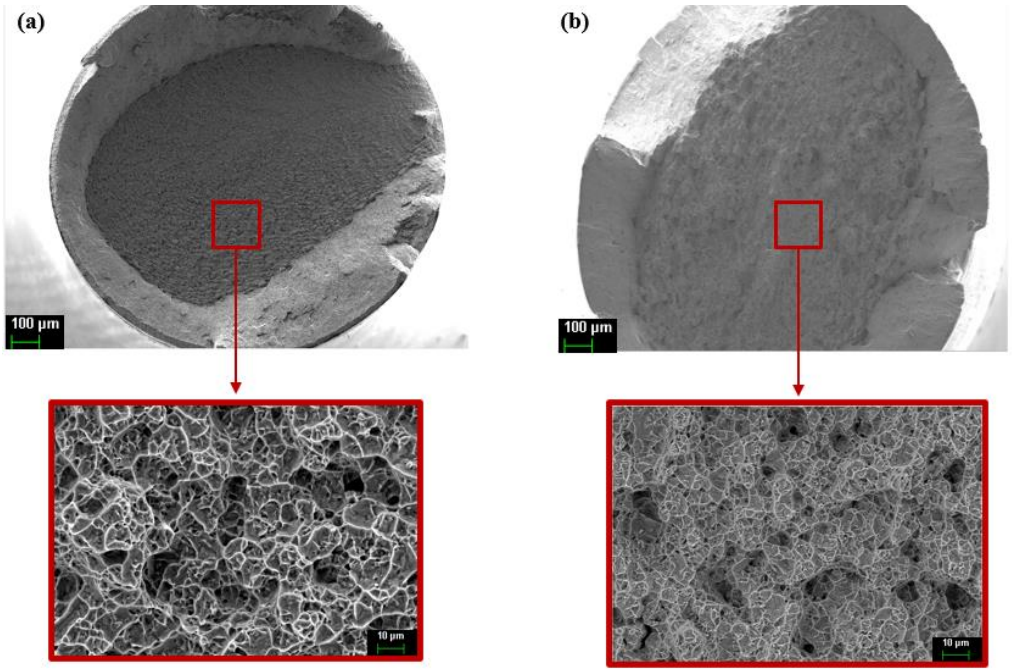

Figure 4.31 SEM images of the tensile fracture surface of Ti–6Al–4V alloy, (a) as-received, (b) THPed.

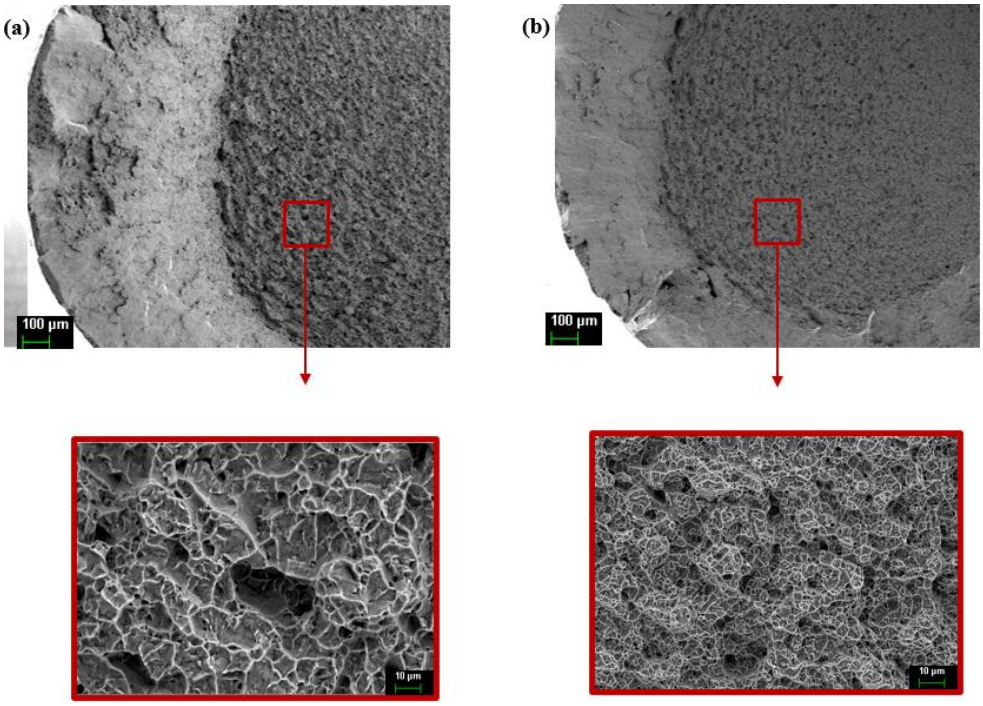

Figure 4.30 SEM images of the tensile fracture surface of Ti–6Al–4V alloy, (a) THPed, (b) THPed after nitriding.

4.3.3 Fatigue Tests

As presented in the experimental section, the effect of heat treatment and surface treatment on the fatigue life of the alloys was determined by applying stress amplitudes between 610-650 MPa.

The first test was started with a stress of 620 MPa, below the yield strength of the alloy, they continued using stress values at approximately 10 MPa intervals to examine the effects of different stress levels. Fifteen tests were carried out to determine the initial fatigue life of the as-received samples, as seen in Table 11. Afterward, the effect of surface processing and heat treatment on fatigue life was determined at a single stress amplitude of 650 MPa.

Considering the capacity of the axial fatigue testing device, it has been determined that it will take approximately 29 days to complete a single test if continuous 10,000,000 cycles were used. Therefore, in this study, it was decided to use 1,000,000 cycles corresponding to fatigue strength. According to axial fatigue test results, the fatigue strength of the specimen was determined as 610 MPa at 10^6 cycles (Table 11 and Figure 4.32). Altenberger et al. [73] used a wrought titanium alloy with a microstructure similar to that of in the present thesis, which had a tensile strength of 1030 MPa. The fatigue strength of the alloy at R=-1 and 10^7 cycles was about 500 MPa at R =-1). In the present study, fatigue strength (610 MPa) found at 10^6 cycles is compatible with the S-N curve trend literature given in the literature.

Table 11. Fatigue test results of an as-received specimen.

Stress (MPa)	**Cycles**
650	69,145
650	98,871
650	72,055
640	116,401
640	123,463
640	186,978
630	234,351
630	113,891
630	213,746
620	472,656
620	590,537
620	681,873
610	1,000,000
610	1,000,000
610	1,000,000

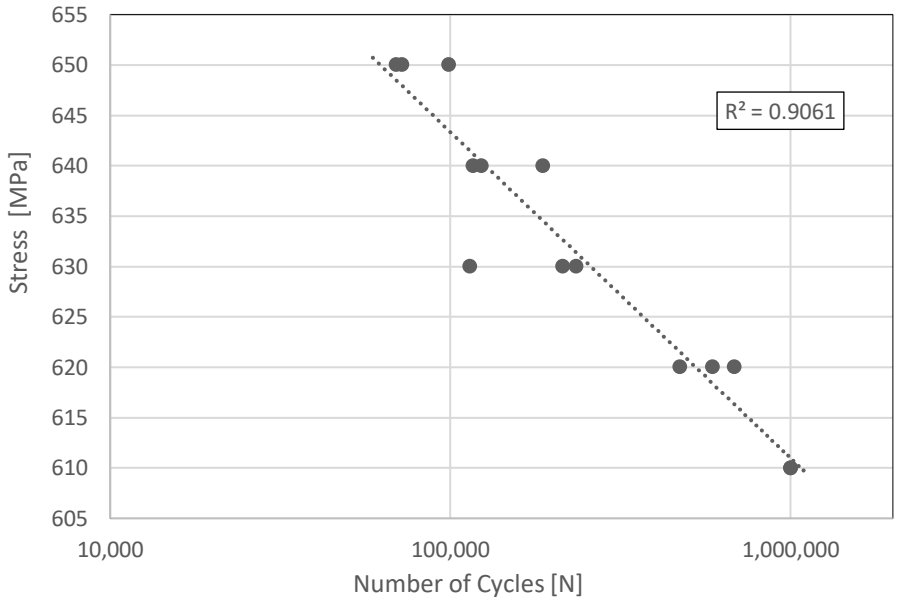

Figure 4.32 S-N curve for as-received samples.

Fatigue failure typically occurs in three distinct stages: crack initiation, crack propagation, and final failure attributed to rapid fracture. The fatigue life of an alloy is the sum of the life spent for crack initiation and the life spent for crack propagation. Depending on the magnitude of the stress amplitude and fatigue life, fatigue is classified as high cycle fatigue (elastic deformation and $N_f > 10^4$ cycles) and low cycle fatigue (elastic + plastic deformation, $N_f < 10^4$ cycles). In high cycle fatigue, the life spent for crack initiation is higher than the life spent for crack propagation. Accordingly, crack propagation is generally regarded as more significant than crack initiation. and propagation life should be increased. On the other hand, in low cycle fatigue, occurring at relatively higher stress levels, the life spent for crack propagation is higher; therefore, crack initiation life should be increased. There are several factors that affect crack initiation and crack propagation in titanium alloy. For example, the surface condition of the part influences the crack initiation, while the internal structure (globular, equiaxed, and lamellar) determines the crack growth behavior of the alloy.

It is known that globular microstructure in Ti-6Al-4V alloy shows more resistance crack propagation with respect to lamellar microstructure. For the as-received sample, the stress amplitudes utilized in the fatigue tests (610-650 MPa) were lower than the yield strength of the alloy (1015 MPa), thereby, inducing elastic deformation only. Additionally, measured fatigue life was above 10^4 cycles which may be classified as high cycle fatigue which means that the crack propagation life should be improved. In the present study, fatigue life of the parts was tried to be increased by surface processing and microstructural refinement heat treatment. In the present study, the effect of surface process (nitriding) and heat treatment (THP) was evaluated at a stress level of 650 MPa, which was still below the yield strength of the alloy. Gas and plasma nitriding surface processes are typically conducted within the temperature range of 750 to 1100ºC. Although nitriding yields a hard coating layer, numerous studies have demonstrated that utilizing high temperatures in these processes results in the deterioration of fatigue properties due to both grain growth and microstructural coarsening [39, 40, 41]. Farokhzadeh and Edrisy [54, 74] investigated the influence of plasma nitriding on the fatigue behavior of Ti-6Al-4V alloy at two different temperatures. At 600 °C, plasma nitriding exhibited an endurance limit of 552 MPa, surpassing the fatigue strength achieved through conventional nitriding processes conducted at 750–1100 °C. Conversely, nitriding at 900 °C reduced the fatigue life compared to the 600 °C process, accompanied by a 13% reduction in tensile strength and a 78% decrease in ductility. The deterioration in mechanical properties observed at elevated temperatures has been attributed to an α-case layer (~20 mm) formation, development of a thick compound layer (~6 mm) on the surface, and transformation of microstructure to coarser bimodal structure from fully finer equiaxed structure. Likewise, nitriding at 950 °C for 1 h caused grain growth. In addition to grain coarsening, formation of an α-case is known to affect fracture toughness and fatigue properties of the alloy negatively. Bell et al.'s research [43] conducted on the plasma-nitrided Ti–6Al–4V alloy at various temperatures (750–1050 °C) revealed reduction of fatigue limit with the increased α-Case layer (rich in Al) thickness.

Similarly, in the study of Tokaji et al. [63], it was observed that the nitriding process conducted at elevated temperatures revealed that further improvement in fatigue life can be achieved by removing the compound layer and partial removal of the diffusion zone. These results indicated that the diffusion zone and compound layer of the sample played a role in determination of fatigue properties. In the current study, the fatigue of the alloy decreased from ~10^5 cycles to ~$2x10^4$ cycles (Figure 4.33) as a result of gas nitriding at 950^{o}C for 1 h, which caused grain coarsening in addition to formation of hard compound layer, α-Case and a diffusion zone (Figure 4.13). Although nitriding increased the surface hardness of the alloy, coarsened grains became dominant in determination of the the fatigue of the alloy. On the other hand, THP, which was applied for microstructural refinement (refining α-phase especially), also yielded fatigue life around $2x10^4$ cycles at stress amplitude of 650 MPa. Although, THP refined the α-phase it increased the grain size of the alloy as well due to prolonged high temperature exposure of the alloy. The process, which aimed obtaining of nitride layer and microstructural refinement (THPing after gas nitriding) was applied to increase the resistance for crack initiation and crack propagation of the alloy. However, it also ended with an alloy having fatigue life similar to nitrided and THPed alloys. It was concluded that nitriding process applied before THP was the decisive processing step which caused grain growth, dominant factor in fatigue life.

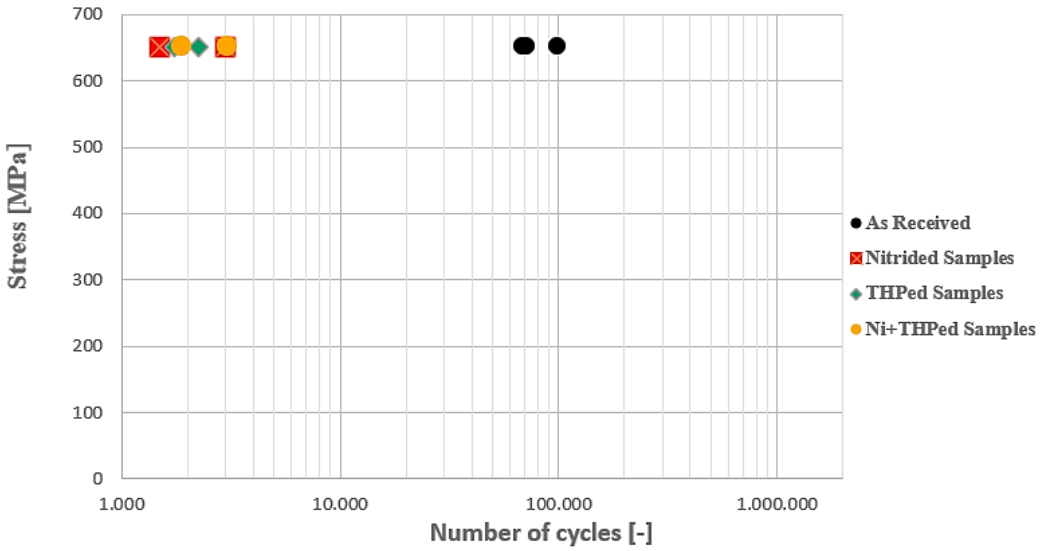

Figure 4.33 The S-N curve of samples treated with different parameters under 650 MPa loading.

Figure 4.34 presents the collected fatigue data of wrought and additive manufactured (AM) Ti6Al4V alloys at high and low cycle fatigue regimes when loaded using reversed stress cycles at R = -1. Both the endurance limit of the wrought alloys and the fatigue life at any stress level are higher than that of AM alloys for similar microstructures. The presence of process-related residual porosity in AM alloys reduces the fatigue strength and fatigue life (N_f) of the alloy. At 650 MPa (stress amplitude used in the present study), the wrought alloys display a fatigue life as high as ~10^5 cycles as in the present study, while the fatigue life of AM parts was around $8x10^3$ cycles, which was lower than nitrided and THPed samples in which N_f was around $2x10^4$ cycles.

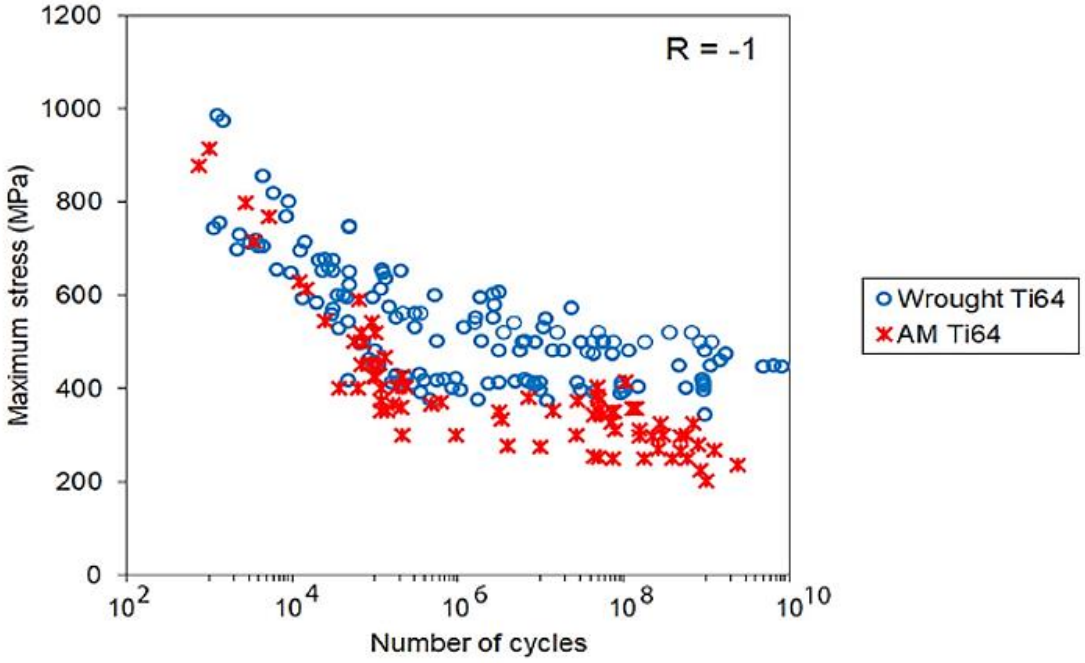

Figure 4.34 Tension-compression (R = -1) fatigue properties of both wrought and additively manufactured Ti-6Al-4V alloy samples summarized by various researchers [75–86].

The fatigue fracture surfaces of the samples are presented in Figures 4.35-4.38. The fracture surfaces consist of a crack initiation point, crack propagation and the final fracture region. As-received alloy tested at 650 MPa showed distinct features on the fatigue fracture surface. The fatigue crack initiation site in as-received alloy depicted as point b in Figure 4.35. The crack initiation site at higher magnification (Figure 4.35 (b)) revealed extensive plastic deformation at the fatigue crack initiation site. On the other hand, striations formed in crack propagation region are clearly visible in Figure 4.35 (c). Fatigue fracture surface of the THPed Ti-6Al-4V alloy tested at 650 MPa is given in Figure 4.36. In addition to crack initiation region, the dimpled morphology was observed prior to the final rupture (Figure 36 (c)). On the other hand, in fracture surface of nitrided alloy (Figure 4.37) crack initiation sites formed at more than one point, point b in Figure 4.37 (a), revealed surface fragmentation and

crack formation within the compound layer. Fatigue crack propagation exhibited a relatively smooth surface with striations and microcracks perpendicular to the crack propagation direction. The starting point of fatigue cracks on the surface is associated with the fragmentation of the compound layer and crack formation. The initial stage of crack propagation appeared as a distinct smooth area with radial marks on a macroscopic scale. Upon closer inspection at higher magnifications, there were striations and microcracks perpendicular to the crack propagation direction. The second crack propagation stage exhibited a rippled appearance composed of dimples. In the fracture surface of THPed alloy after the nitriding process (Figure 4.38), a crack initiation site formed at more than one point, point b in Figure 38 (b), revealed surface fragmentation and crack formation within the compound layer as same as nitrided alloy. There were striations upon closer inspection at higher magnifications (Figure 4.38 (c)). In addition to the crack initiation region, the dimpled morphology was observed prior to the final rupture (Figure 4.38 (d)), the same as the THPed alloy (Figure 4.36 (a)).

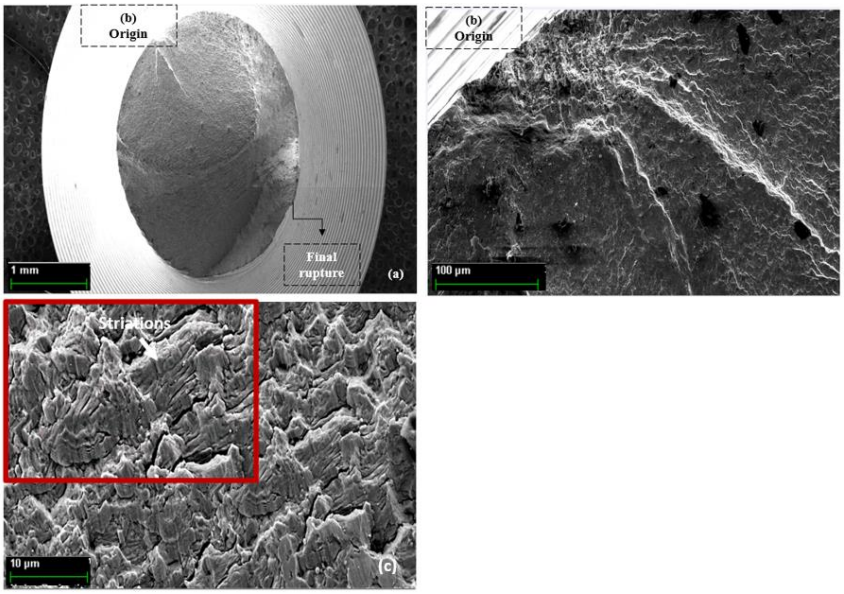

Figure 4.35 Fracture surface analysis of as-received specimen, (a) General morphology of failure. (b) crack initiation site at higher magnification (c) striations formed in crack propagation region.

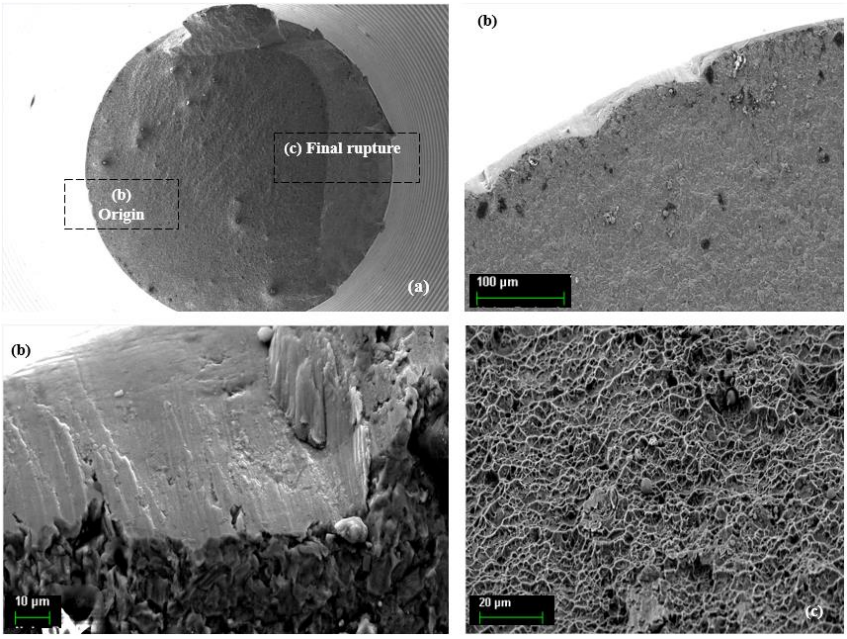

Figure 4.36 Fracture surfaces of THPed specimen, (a) General morphology of failure. (b) crack initiation site at higher magnification (c) the dimpled morphology at final rupture.

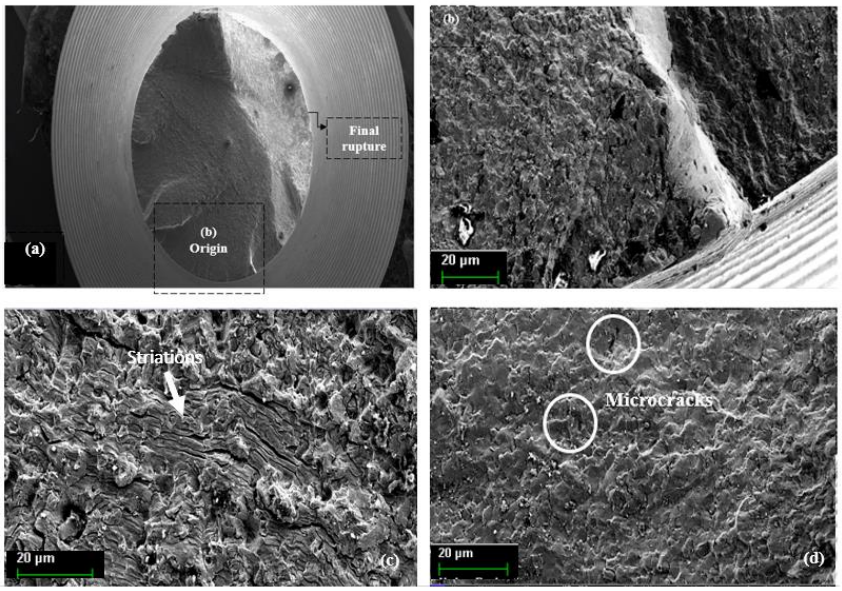

Figure 4.37 Fracture surfaces of Nitrided specimen, (a) General morphology of failure. (b) multi crack initiation site at higher magnification, (c) striations formed in crack propagation region perpendicular to the crack propagation direction, (d) microcracks formation.

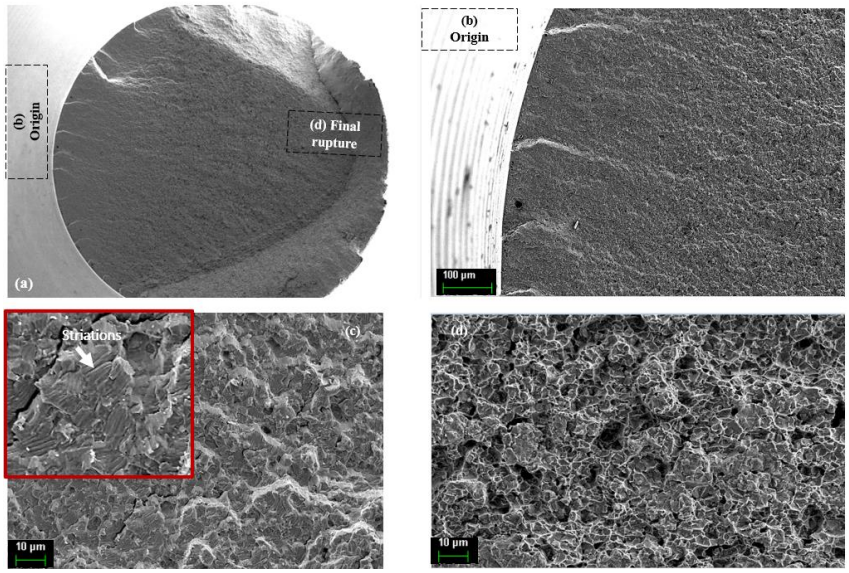

Figure 4.38 Fracture surfaces of THPed specimen after nitriding (a) General morphology of ductile failure. (b) multi crack initiation site at higher magnification, (c) striations formed in the crack propagation region perpendicular to the crack propagation direction, (d) the dimpled morphology at final rupture.

CHAPTER 5

CONCLUSIONS

The effect of nitriding, thermo-hydrogen processing, and the combination of these two processes on the microstructure and mechanical properties of the wrought Ti-6Al-4V have been studied. The effect of starting material, applied heat treatments, and selected process parameters on the fatigue properties of wrought Ti-6Al-4V alloys have been investigated systematically. The following conclusions have been drawn based on the results of this study.

1. Samples subjected to hydrogenation at 650 °C for 1 h under a high-purity hydrogen atmosphere were found to have a hydrogen content of 1.81 wt.% and exhibited the presence of the δ (TiH_2) phase as revealed by XRD patterns.

2. THP enabled microstructural refinement of the α-phase by transformation of δ-phase to fine α-phase, where high process temperature coarsened the overall structure. While the average grain size of the starting sample was 0.85 ± 0.24 μm, it increased to 2.83 ± 0.93 μm after THP process. In samples with an average grain size of 3.21± 1.17 obtained after high temperature nitriding, subsequent THP process reduced the average grain size by approximately 13%. Similar to the literature results, in this study THP process was not found to be effective on fine initial grain sizes.

3. Hydrogenation process increased the hardness of the alloy due to formation of harder δ-phase in the α+β microstructure. The hardness value of the hydrogenated sample increased by approximately 35-40% compared to the as-received sample.

Despite the observed decrease in hardness during subsequent dehydrogenation due to disappearance of the δ-phase, hardness of the THPed alloy was higher (~5%) than that of the as-received sample possibly due to refined α-phase.

4. Nitrided samples revealed higher compound layer hardness with respected to as-received, hydrogenated and THPed samples due to formation of outermost compound layer (containing TiN + TiN_2 phases) and α-case with the diffusion layer. THP process applied after nitriding further increased the alloy's hardness due to refined underlying microstructure and mainly because of surface oxidation of the samples caused by prolonged exposure to high temperature.

5. Grain orientation maps obtained from EBSD analysis revealed that THP and nitriding processes applied to the as-received sample caused nearly complete recrystallization and decreased dislocation density. When the GOS maps of the THPed and THPed after nitriding samples were compared with the as-received sample, it was observed that recrystallization occurred and the dislocation density decreased by approximately 35-40%.

6. THP slightly increased the UTS values of the as-received specimens up to 1050 MPa by the refinement of the α-phase, while nitriding ended up with alloys having lower strength due to grain coarsening and formation of non-uniform compound layer which acted as stress concentration sites.

7. Application of THP after nitriding slightly increased the strength, while the ductility remained constant. Although THP refined the α-phase after nitriding, the coarse-grained structure formed during nitriding could not be eliminated completely.

8. Among all of the samples, as-received sample with very fine globular microstructure revealed the highest fatigue life of 10^5 cycles at a stress amplitude of 650 MPa similar to wrought Ti6Al4V alloys tested under the same conditions. On the other hand, the nitrided, THPed and nitrided + THPed alloys displayed lower fatigue life (~$2x10^3$ cycles) compared to as-received alloy.

9. Although the nitriding process provided the formation of a hardened layer, it caused grain growth, which was responsible for reduced fatigue life. THP applied subsequent to nitriding did not change the fatigue life considerably since coarsened grains formed during nitriding could not be eliminated.

Future studies

In similar studies, the 2-step THP process was found to be more effective on samples with grain sizes above 10 µm. Contrary to the starting sample used in the present study, the effect of THP and nitriding processes should be investigated using alloys containing coarser globular or lamellar microstructure.

Since during gas nitriding oxidation could not be eliminated, the hardened layer was mainly formed as a porous layer. Therefore, plasma nitriding at lower processing temperatures may be used. Additionally, the use of Transmission Electron Microscopy (TEM) is recommended to understand the microstructural refinement mechanism formed by the δ to α phase transformation during THP.

REFERENCES

[1] Andrea La Monaca et al. “Surface integrity in metal machining-Part II: Functional performance”. In: *International Journal of Machine Tools and Manufacture* 164 (2021), p. 103718.

[2] Ramadan N Elshaer et al. “Effect of heat treatment processes on microstructure and mechanical behavior of TC21 titanium alloy”. In: *Open Journal of Metal* 7.03 (2017), p. 39.

[3] L Wagner. “Mechanical surface treatments on titanium, aluminum, and magnesium alloys.” In: *Materials Science and Engineering: A* 263.2 (1999), pp. 210– 216.

[4] Hans Albert Richard and M Ermüdungsrisse Sander. “Erkennen, sicher beurteilen, vermeiden”. In: *Vieweg+ Teubner Verlag* (2009).

[5] T Tanaka. “Fatigue Strength: Improving by Surface Treatment”. In: *Encyclopedia of Materials: Science and Technology* (2001), pp. 2990–2994.

[6] Güney Mert Bilgin et al. “Optimization of the mechanical properties of Ti-6Al- 4V alloy fabricated by selective laser melting using thermohydrogen processes”. In: Materials Science and Engineering: A 700 (2017), pp. 574–582.

[7] Ani Zhecheva et al. “Enhancing the microstructure and properties of titanium alloys through nitriding and other surface engineering methods”. In: Surface and Coatings Technology 200.7 (2005), pp. 2192–2207.

[8] Alokesh Pramanik and Guy Littlefair. “Machining of titanium alloy (Ti-6Al- 4V)—theory to application”. In: *Machining science and technology* 19.1 (2015), pp. 1–49.

[9] Christoph Leyens and Manfred Peters. *Titanium and titanium alloys: fundamentals and applications*. Wiley Online Library, 2006.

[10] N Valentin Moiseyev. *Titanium Alloys. Russian Aircraft and Aerospace Application*. 2006.

[11] G Lütjering, JC Williams, and A Gysler. “Microstructure and mechanical properties of titanium alloys”. In: *Microstructure And Properties Of Materials: (Volume 2)*. 2000, pp. 1–77.

[12] EO Ezugwu and ZM Wang. “Titanium alloys and their machinability—a review”. In: *Journal of materials processing technology* 68.3 (1997), pp. 262–274.

[13] K Tanrıöven and A Tasçı. “Titanyum Alasımlarının Isıl İşlemi”. In: *Makine Magazin* 58 (1997).

[14] MV Ribeiro, MRV Moreira, and JR Ferreira. “Optimization of titanium alloy (6Al–4V) machining”. In: *Journal of Materials Processing Technology* 143 (2003), pp. 458–463.

[15] Valentin N Moiseyev. *Titanium alloys: Russian aircraft and aerospace applications*. CRC Press, 2005.

[16] RTI, Titanium Alloy Guide, (2013) 43–74. www.smt.sandvik.com.

[17] J Donachie Matthew Jr. “Heat treating titanium and its alloys”. In: *Heat Treat. Prog* 47 (2001), pp. 47–57.

[18] Alptekin İşler. “Titanyum Alaşımlarının Isıl Isıl İşlem ve Mekanik Özellikleri”. PhD thesis. Fen Bilimleri Enstitüsü, 1999.

[19] M Göbel, VAC Haanappel, and MF Stroosnijder. “On the determination of diffusion coefficients of oxygen in one-phase Ti (α-Ti) and two-phase Ti–4Nb (α- and β-Ti) by micro-hardness measurements”. In: *Oxidation of metals* 55 (2001), pp. 137–151.

[20] R Boyer. “Materials Properties Handbook. Titanium Alloys/Ed. by R. Boyer, G. Welsch, EW Colling.-ASM International”. In: (1994).

[21] Nikolas Hrabe, Thomas Gnäupel-Herold, and Timothy Quinn. “Fatigue properties of a titanium alloy (Ti–6Al–4V) fabricated via electron beam melting (EBM): Effects of internal defects and residual stress”. In: *International Journal of Fatigue* 94 (2017), pp. 202–210.

[22] OM Ivasishin and PE Markovsky. “Enhancing the mechanical properties of titanium alloys with rapid heat treatment”. In: *Jom* 48 (1996), pp. 48–52.

[23] Matthew J Donachie. Titanium: a technical guide. ASM international, 2000.

[24] Cihat ENSARİOĞLU and M Cemal ÇAKIR. “Titanyum ve alaşımlarının işlenebilirlik etüdü-Bölüm II”. In: *Mühendis ve Makina* 46.547 (2005), pp. 21–27.

[25] ON Senkov, JJ Jonas, and FH Froes. “Recent advances in the thermohydrogen processing of titanium alloys”. In: *Jom* 48 (1996), pp. 42–47.

[26] C Ohkubo et al. “The machinability of cast titanium and Ti–6Al–4V”. In: *Biomaterials* 21.4 (2000), pp. 421–428.

[27] Sara M Gaytan et al. “Advanced metal powder based manufacturing of complex components by electron beam melting”. In: *Materials Technology* 24.3 (2009), pp. 180–190.

[28] Denis Cormier, Ola Harrysson, and Harvey West. “Characterization of H13 steel produced via electron beam melting”. In: Rapid prototyping journal 10.1 (2004), pp. 35–41.

[29] Manuela Galati and Luca Iuliano. “A literature review of powder-based electron beam melting focusing on numerical simulations”. In: *Additive Manufacturing* 19 (2018), pp. 1–20.

[30] LE Murr et al. “Microstructures and mechanical properties of electron beam-rapid manufactured Ti–6Al–4V biomedical prototypes compared to wrought Ti– 6Al–4V”. In: *Materials characterization* 60.2 (2009), pp. 96–105.

[31] Adnan Safdar et al. “Evaluation of microstructural development in electron beam melted Ti-6Al-4V”. In: *Materials Characterization* 65 (2012), pp. 8–15.

[32] Ian Polmear et al. *Light alloys: metallurgy of the light metals*. Butterworth-Heinemann, 2017.

[33] Shunyu Liu and Yung C Shin. “Additive manufacturing of Ti6Al4V alloy: A review”. In: *Materials & Design* 164 (2019), p. 107552.

[34] Merve Nur Doğu. “Production of Ti-6Al-4V alloy by 3D electron beam melting technique and development of its post treatments”. MA thesis. Middle East Technical University, 2019.

[35] Bloyce, A., Morton, P.H., Bell, T., 1994. Surface Engineering of Titanium and Titanium Alloys, ASM Handbook Vol 5: Surface engineering, tenth edition. ASM International. 2253.

[36] Tkachuk, O., et al. "Diffusion of Nitrogen and Phase—Structural Transformations in Titanium." Металлофизика и новейшие технологии (2014).

[37] Fromm, Eckehard, and Erich Gebhardt. "Gase und kohlenstoff in metallen." (No Title) (1976).

[38] Korwin, M.J., Morawski, C.D., Tymowski, G.J., Liliental, W.K., 2004. Design of Nitrided and Nitrocarburized Materials, Handbook of Metallurgical Process Design. Marcel Dekker, New York, USA. 548 578.

[39] T.Bell,H.W.Bergmann,J.Lanagan,P.H.Morton,A.M.Staines,Surf.Eng.2 (1986)133–143.

[40] H.-J. Spies, Surf. Eng. 26 (2010) 126–134.

[41] H.-J.Spies, B.Reinhold, K.Wilsdorf, Surf. Eng. 17(2001)41–54.

[42] Knerr, C.H., Rose, T.C., Filkowski, J.H., O'Brien, J.M., Goodman, D., 1991. Gas nitriding of Steels, Liquid Nitriding of Steels, Plasma (Ion) Nitriding of Steels, ASM Handbook Vol 4: Heat Treating, tenth edition. ASM International. 903-923, 953, 2149.

[43] T Bell et al. "Surface engineering of titanium with nitrogen". In: Surface engineering 2.2 (1986), pp. 133–143.

[44] B Sarma and KS Ravi Chandran. "Recent advances in surface hardening of titanium". In: *Jom* 63 (2011), pp. 85–92.

[45] Peter Schaaf. "Laser nitriding of metals". In: *Progress in materials science* 47.1 (2002), pp. 1–161.

[46] H-J Spies. "Surface engineering of aluminum and titanium alloys: an overview." In: *Surface Engineering* 26 (2010), pp. 126–134.

[47] H Dong and T Bell. "Surface engineering of titanium: an-overview". In: Ti-2003 Science and Technology, Proc. of the 10th World Conf. on Titanium Held at the CCH-Congress Center. 2003, pp. 13–18.

[48] Hubert Gräfen et al. *Lexikon Werkstofftechnik: Berichtigter Nachdruck.* Springer- Verlag, 2013.

[49] Edson Costa Santos et al. "Laser gas nitriding of pure titanium using CW and pulsed Nd: YAG lasers". In: *Surface and Coatings Technology* 201.3-4 (2006), pp. 1635–1642.

[50] Ettore Carpene, Michelle Shinn, and Peter Schaaf. "Free-electron laser surface processing of titanium in nitrogen atmosphere". In: Applied surface science 247.1- 4 (2005), pp. 307–312.

[51] Peter Schaaf, M Kahle, and Ettore Carpene. "Reactive laser synthesis of carbides and nitrides". In: *Applied surface science* 247.1-4 (2005), pp. 607–615.

[52] Daniel Höche et al. “Free electron laser nitriding of metals: From basis physics to industrial applications”. In: *Applied surface science* 253.19 (2007), pp. 8041– 8044.

[53] Mauro Satta et al. “Time-resolved studies of electron–phonon relaxation in metals using a free-electron laser”. In: *Applied surface science* 154 (2000), pp. 172–178.

[54] Farokhzadeh, K., and A. Edrisy. "Fatigue improvement in low temperature plasma nitrided Ti–6Al–4V alloy." Materials Science and Engineering: A 620 (2015): 435-444.

[55] Oleksandr Tisov et al. “Duplex aging and gas nitriding process as a method of surface modification of titanium alloys for aircraft applications”. In: *Metals* 12.1 (2022), p. 100.

[56] Adolf Fry. “Stickstoff in Eisen, Stahl und Sonderstahl. Ein neues Oberflachen- hartungsverfahren”. In: *Stahl und Eisen* 43 (1923), p. 1271.

[57] M Łępicka and M Gradzka-Dahlke. “Surface Modification of Ti64 Titanium alloy for biomedical applications and its effect on tribological performance - A review.” In: *Reviews on Advanced Materials Science* 46.1 (2016).

[58] A Bloyce, PH Morton, and T Bell. “Surface engineering of titanium and titanium alloys”. In: ASM handbook 5 (1994), pp. 835–851.

[59] Afsaneh Edrisy and Khorameh Farokhzadeh. “Plasma nitriding of titanium alloys”. In: *Plasma Science and Technology–Progress in Physical States and Chemical Reactions* (2016).

[60] Gloria P Rodriguez, Gemma Herranz, and Ana Romero. “Solar gas nitriding of Ti6Al4V alloy”. In: *Applied surface science* 283 (2013), pp. 445–452.

[61] S Kikuchi et al. “Formation of nitrided layer using atmospheric-controlled IH- FPP and its effect on the fatigue properties of Ti-6Al-4V alloy under four-point bending”. In: *Procedia Structural Integrity* 2 (2016), pp. 3432–3438.

[62] Keiro Tokaji, Takeshi Ogawa, and Hideaki Shibata. “The effect of gas nitriding on fatigue behavior in pure titanium.” In: *International Journal of fatigue* 16.5 (1994), pp. 331–336.

[63] K Tokaji, T Ogawa, and H Shibata. “The effects of gas nitriding on fatigue behavior in titanium and titanium alloys”. In: *Journal of Materials Engineering and Performance* 8 (1999), pp. 159–167.

[64] Aamir Mukhtar et al. “Effects of gas nitriding on fatigue and crack initiation of Ti6Al4V produced by selective laser melting”. In: *Materials Research* 22 (2019).

[65] T.Morita, H.Takahashi, M.Shimizu, K.Kawasaki, Fatigue Fract. Eng. Mater. 20 (1997)85–92.

[66] FH Froes, ON Senkov, and JI Qazi. “Hydrogen as a temporary alloying element in titanium alloys: thermohydrogen processing”. In: *International Materials Reviews* 49.3-4 (2004), pp. 227–245.

[67] Wei Sha, Haji Muhd Syamaizar Haji Mat Daud, and Xiaomin Wu. “Gas Nitriding of High Strength Titanium Alloy b21s and Its Microstructure”. In: *Microscopy and Analysis-UK* 129 (2009), p. 5.

[68] O. Senkov, Thermohydrogen processing of titanium alloys, Int. J. Hydrogen Energy. 24 (1999) 565–576. doi:10.1016/s0360-3199(98)00112-8.

[69] JI Qazi et al. “Phase transformations in Ti-6Al-4V-x H alloys”. In: *Metallurgical and Materials Transactions A* 32 (2001), pp. 2453–2463.

[70] Lee, Dong Bok, et al. "Gas nitriding and subsequent oxidation of Ti-6Al-4V alloys." Nanoscale research letters 7 (2012): 1-5.

[71] Chakrabarty, Shanta, et al. "Surface Gas Nitriding of Titanium (Ti–6Al–4V) Alloy." Advances in Mechanical Processing and Design: Select Proceedings of ICAMPD 2019. Springer Singapore, 2021.

[72] A. Safdar, L.Y. Wei, A. Snis, Z. Lai, Evaluation of microstructural development in electron beam melted Ti-6Al-4V, Mater. Charact. 65 (2012) 8–15, https://doi.org/ 10.1016/j.matchar.2011.12.008.

[73] Fatigue improvement in low temperature plasma nitrided Ti–6Al–4V alloy

[74] Long M, Rack HJ. Titanium alloys in total joint replacement—a materials science perspective. Biomaterials 1998;19:1621–39. https://doi.org/10.1016/S0142- 9612(97)00146-4.

[75] L. Saitova, H. Höppel, M. Göken, I. Semenova, R. Valiev, Int. J. Fatigue 31 (2) (2009) 322–331.

[76] R.J. Morrissey, T. Nicholas, Int. J. Fatigue 27 (10–12) (2005) 1608–1612.

[77] P.E. Carrion, N. Shamsaei, S.R. Daniewicz, R.D. Moser, Int. J. Fatigue 99 (2017) 87–100.

[78] M. Janecˇek, F. Novy´ , J. Strásky´ , P. Harcuba, L. Wagner, J. Mech. Behav. Biomed. Mater. 4 (3) (2011) 417–422.

[79] J. Peters, G. Lütjering, Metallur. Mater. Trans. A 32 (11) (2001) 2805–2818.

[80] J. Zuo, Z. Wang, E. Han, Mater. Sci. Eng., A 473 (1–2) (2008) 147–152.

[81] X. Liu, C. Sun, Y. Hong, Mater. Sci. Eng., A 622 (2015) 228–235.

[82] A.J. Sterling, B. Torries, N. Shamsaei, S.M. Thompson, D.W. Seely, Mater. Sci. Eng., A 655 (2016) 100–112.

[83] M. Benedetti, V. Fontanari, M. Bandini, F. Zanini, S. Carmignato, Int. J. Fatigue 107 (2018) 96–109.

[84] J. Günther, D. Krewerth, T. Lippmann, S. Leuders, T. Tröster, A. Weidner, H. Biermann, T. Niendorf, Int. J. Fatigue 94 (2017) 236–245.

[85] E. Wycisk, S. Siddique, D. Herzog, F. Walther, C. Emmelmann, Front. Mater. 2 (2015)72.

[86] M. Benedetti, E. Torresani, M. Leoni, V. Fontanari, M. Bandini, C. Pederzolli, C. Potrich, J. Mech. Behav. Biomed. Mater. 71 (2017) 295–306.

[87] Merve Nur Doğu et al. “Microstructural and texture evolution during thermo-hydrogen processing of Ti6Al4V alloys produced by electron beam melting”. In: Materials Characterization 168 (2020), p. 110549.

[88] Altenberger, Igor, Ravi K. Nalla, Yuji Sano, Lothar Wagner, and Robert O. Ritchie. "On the effect of deep-rolling and laser-peening on the stress-controlled low-and high-cycle fatigue behavior of Ti–6Al–4V at elevated temperatures up to 550 C." International Journal of Fatigue 44 (2012): 292-302

[89] Murakami Y, Endo M. Effects of defects, inclusions and inhomogeneities on fatiguestrength. Int J Fatigue 1996;16:163–82. https://doi.org/10.1016/0142-1123(94) 90001-9.

[90] Nakai Y, Kubo S. Fracture mechanics. Asakura Publishing Co., Ltd.; 2014. p. 32. ISBN978-4-254-23793-1 C3353.

[91] J.L. Murray, Phase Diagrams in Binary Titanium Alloys, ASM International, Materials Park, OH, 1990, p. 176.